This is to certify that the

dissertation entitled

presented by

Fida Muhammad Khan

has been accepted towards fulfillment
of the requirements for

Doctor of Philosophy degree in Electrical & Computer Engineering

Elias G. Strangas
Major professor

Date 30 Sep 1999

PLACE IN RETURN BOX to remove this checkout from your record.
TO AVOID FINES return on or before date due.
MAY BE RECALLED with earlier due date if requested.

DATE DUE	DATE DUE	DATE DUE

SENSOR-LESS FLUX DETERMINATION IN INDUCTION MOTOR BASED UPON SATURATION EFFECTS USING HIGH-FREQUENCY MAGNETIZING CURRENT

By

Fida Muhammad Khan

A DISSERTATION

Submitted to
Michigan State University
in partial fulfillment of the requirements
for the degree of

DOCTOR OF PHILOSOPHY

Electrical and Computer Engineering

1999

ABSTRACT

SENSOR-LESS FLUX DETERMINATION BASED UPON SATURATION EFFECTS USING HIGH FREQUENCY MAGNETIZING CURRENT

By

Fida Muhammad Khan

As real-time computation costs continually decline, both mechanical robustness and economic considerations increasingly favor the replacement of mechanical sensors and transducers by software-based state estimation methods. The elimination of encoders or resolves on induction machine drives is a prime example. For high performance induction motor drives based on 'field-orientation', it is necessary to determine the angle of a magnetic flux vector inside the induction machine (rotor, stator, air-gap) with respect to a stator frame. When this is done without a flux sensor and without a rotor speed/position sensor, the voltage/current, or v/i-model, is the means of determining this flux angle. The v/i-model has drift problems, especially at low flux frequencies. By analyzing the v/i-model in the magnetic field coordinates instead of the fixed stator coordinates, the drift problem becomes a stability problem. Internal feedback methods still leave an operation area where such sensor-less control performance is low: the area around zero flux frequency [1]. In this frequency range the high frequency magnetizing current injection method can provide a way of determining the flux angle, even at zero flux frequency. This method is based upon saturation effects inside the induction machine and its structure is the basis of this proposal.

Prior to this work, existing control methods by injecting high frequency estimation techniques for machines were design dependent [1,2-7]. Furthermore, the limitations of these existing and also newly emerging observer-based estimation techniques were not well understood nor well applied. This work first focuses on evaluating and improving the rotor flux estimation from stator voltage and currents for standard induction machines, without modification to rotor design. In this work, recent developments in the saturated model of induction machines and their use for obtaining the correct location of the rotor magnetic flux for the induction motor are considered. In particular, the motion of stator current vector is transformed to the motion of the rotor current vector through a transformation ratio obtained from the motor magnetic saturation and the motion of the rotor current vector information is extracted from the motor voltage equations [3]. The method is based upon an effect that appears in the region of magnetic saturation. The transfer properties are derived from the equations of current fed (current regulated) induction machines taking saturation into account. Simulation results are presented to show that the algorithm combined with the saturated effect has promising results and would be able to achieve the zero speed control of sensor less induction motor.

To My Parents

ACKNOWLEDGMENTS

I would like to express my thanks and gratitude to Professor Elias Strangas for being my principal advisor and for his encouragement, support and guidance. I would also like to thank Professor Hassan K. Khalil, Professor Robert Schlueter and Professor Jerry D. Schuur for their time and effort in being on my committee.

A special words of thanks are directed to my lab colleagues: ,Bader Aloliwi, Zanardelli Wes, Ali Khurram, Andras Diaz, Shanelle Hogan and John Kelly who provided me with friendship, and fruitful discussions. Many thanks to Marilyn, Roxanne and Brian for their assistance in the Department office and Laboratory matters. Also, I wish to thank all other members of the Electrical Engineering Department for their support, be it scientific, technical or other.

Finally, I owe a special thanks to my Parents, my wife Shahnaz Khan and my kids for their encouragement, support and patience.

TABLE OF CONTENTS

LIST OF TABLES

LIST OF FIGURES

LIST OF ABBREVIATIONS

Subscripts

s	Stator
r	rotor
A,B,C	three phase system
a,b	stator reference frame
d,q	rotor flux reference frame
α,β	rotor reference frame
l	Leakage
m	magnetizing
g	general reference

Superscript

^	estimated
*	command

Quantities

i_{sA}, i_{sB}, i_{sC}	stator three phase currents,
i_{rA}, i_{rB}, i_{rC}	rotor three phase currents
i_{sa}, i_{sb}	stator currents in the stator reference frame (RF)
$\bar{i}_{ra}, \bar{i}_{rb}$	rotor currents in the stator (RF)
$i_{s\alpha}, i_{s\beta}$	stator currents in the rotor (RF)
i_{ra}, i_{rb}	rotor currents in the stator (RF)
$\Delta\bar{i}_s$	test stator current vector
$\Delta\bar{i}_r$	test rotor current vector
$\Delta i_{rd}, \Delta i_{rq}$	component of the test rotor current ($\Delta\bar{i}_r$), in the rotor flux-RF
$\Delta i_{sd}, \Delta i_{sq}$	component of the test stator current ($\Delta\bar{i}_s$), in the rotor flux-RF
$\Delta i_{s\hat{d}\hat{q}}$	stator test current vector in the test current coordinates.

$\lvert \bar{i}_{mr} \rvert$	rotor magnetization current
K_1, K_2	test current transfer factors
$L = \frac{d\lvert \psi_r \rvert}{d\lvert \bar{i}_{mr} \rvert}$	tangent or dynamic (tangent-slope or incremental) inductance
$L_m = \frac{\lvert \psi_r \rvert}{\lvert \bar{i}_{mr} \rvert}$	static (chord slope or amplitude) or chord inductance
$\bar{L}_{rm}$	magnetizing inductance
L_{sl}	stator leakage inductance
L_{rl}	rotor leakage inductance
$\bar{L}_s$	stator self-inductance of one stator phase winding
L_s	total three-phase stator inductance
L_r	total three-phase rotor inductance
$\bar{L}_r$	rotor self-inductance of one stator phase winding
L_m	resultant three phase magnetizing inductance
$\bar{M}_s$	mutual inductance between two stator windings
$\bar{M}_r$	mutual inductance between two rotor windings
$\bar{M}_{sr}$	maximum mutual inductance between the stator and rotor
N_r, N_s	are the effective number of rotor and stator turns
RF	refrence frame
R_s, R_r	stator and rotor resistance of phase windings
s	motor slip
T_r^*	modified rotor time constant including saturation effect
T_r	rotor time constant
$U_{sA}, U_{sB}, U_{sC},$	stator instantaneous three phase voltages
$U_{rA}, U_{rB}, U_{rC},$	rotor instantaneous three phase voltages
V_{so}, V_{ro}	stator, rotor zero-sequence component
V_{sa}, V_{sb}	stator voltages in an equivalent two-phase stator winding
$V_{r\alpha}, V_{r\beta}$	rotor voltages in an equivalent two-phase rotor winding

$\overline{V}_{r(ab)}, \bar{i}_{r(ab)}$ rotor voltages and currents in the stator reference frame

$\overline{\Psi}_{s(ab)}$ stator and rotor space phasor flux linkages

$\overline{\Psi}_{s(ab)}$ stator and rotor space phasor flux linkages

ψ_r actual rotor flux

$\hat{\psi}_r$ estimated rotor flux

θ_r the rotor angle

ω_s stator flux speed called synchronous speed

ω_g speed of general reference frame

ω_r rotor speed

ω_{sm} rotor flux speed

$\hat{\rho}$ estimated rotor flux angle

ρ actual rotor flux angle

β angle of the tangent in the operating point

σ angle with respect to the origin of the curve

angle difference between the rotor test current vector and the stator test current vector

test angle in the estimated flux of reference.

difference angle between the estimated and the actual flux.

Mathematical symbols

$P = \frac{d}{dt}$

Miscellaneous

DFO Direct Filed orientation

IDFO Indirect Filed orientation

HPF High Pass Filter

LPF Low Pass Filter

RT Real Time

Chapter 1

INTRODUCTION

Induction motors constitute a theoretically interesting and practically important class of nonlinear systems, which are evolving into a benchmark example for nonlinear control. They are described by a fifth order nonlinear differential equation with two inputs and only three states available for measurement. Control objectives are complicated by the fact that the operation of induction motors is subject to unknown (load) disturbances and the parameters are highly uncertain and subject to variation. The machines/control engineers are faced with the challenging problem of controlling a highly nonlinear system, with time varying parameters, where the regulated outputs, besides being not measurable, are perturbed by unknown additive signals. Existing solutions to this problem, in particular the de-facto industry standard field-oriented control, suffer from some drawbacks, both in commissioning and in high performance applications [4].

These factors, together with recent developments of powerful theoretical tools for analysis and synthesis of nonlinear systems, have compelled machine/control researchers to tackle this problem. Moreover, due to decline in the computational cost at real time, nowadays field orientation of the three-phase ac induction machine is carried out without using flux sensors, but only using easily measurable stator voltages and stator currents. High performance induction machine drives in use today exist as the result of the simultaneous development of the two key technologies: electronics including both power electronics and microelectronics, and machine/drives control theory. Implicit within these two are sensor and state estimation technologies. Induction machine design has played a lessor role.

Beyond becoming more efficient and compact, the induction machine has not changed substantially over the last half century. The theory of space vectors developed in the late 50's is credited with providing the necessary foundation for the analysis of AC machine dynamics. New control methods based upon moving frames of reference aligned with flux vectors were introduced in the early 70's. These methods greatly simplified the analysis of AC machines dynamics by enabling the de-coupling of the flux and armature axes inherent in DC machines. Field orientation did not gain wide industrial acceptance until the advent of digital implementation means, especially microprocessor and Digital Signal Processor (DSP), in 80's. By enabling the implementation of complex control functions in the software, the hardware requirements are becoming more economical.

Self-tuning and online adaptation of the plant and mechanical sensors [5,6] and internal sensors for measuring flux are generally regarded as unacceptable for all but very low power systems. The inherent flexibility of software implementation enabled control schemes to be extended and improved upon as DSP computational power increased. Thus direct and indirect field oriented flux techniques based upon machine models have evolved. The limited accuracy of existing estimation techniques and the requirement of rotor position/velocity feedback for torque control at zero and low speeds have been two significant factors forestalling the complete replacement of DC drives. The functional integration of machine design with state estimation, control and drive technologies has the potential of overcoming these limitations [4,7]. But the motor design changes requires additional process stages during manufacturing and will add cost and inventory burden to a low margin production.

1.1 PROBLEM STATEMENT

1. The major contributions of this work include the development of the saturated induction machine theory in order to use it to sense the position of the rotor flux. This scheme is in relation to the demand of a high performance at very low frequencies. In particular, the following are presented here for the saturated motor:

 1.1 Analyze the relationship between the stator and rotor currents and fluxes.

 1.2 Simplify the relationships described in 1.1 above, and develop a similarity and simplified relationship for the stator voltages that can be implemented in a controller.

2. Find the limits of the proposed method in terms of initial errors in the estimation of flux the position, effects of test and power frequency etc.

3. Develop a smooth way to transition between low-speed operation using of saturated induction motor with injection of high frequency

magnetizing test current and higher speed operation with direct field orientation (DFO).

1.2 OVERVIEW OF CHAPTERS

Chapter 1 provides a literature review of the main techniques of sensor-less control of induction motor for high-performance applications including state estimation and control Strategies of the Induction Motor.

Chapter 2 outlines the main techniques of sensor-less control of the induction Motor for high-performance applications, including state estimation and control Strategies. Open-loop and closed-loop rotor flux observers are evaluated with particular emphasis on estimation accuracy. Further, the limitations of the transducer-less direct field orientation (DFO) and the indirect field orientation (IDFO) are investigated using voltage and flux models. An improved system is proposed

Chapter 3 gives the derivation of the unsaturated induction motor model and then derives the saturated induction model. There a method is developed for calculating the inductance parameter from the motor magnetization curve.

Chapter 4 and Chapter 5 are experimental verifications. The improvements are incremental and very optimistic, however, they do not overcome certain fundamental limitations. To overcome the limitations, more active to flux estimation at zero frequency is developed in Chapter 4 and Chapter 5 without integration. A new closed system is presented based upon the injected high frequency technique. These chapters also focus on the different derivation of saturated induction motor voltage equations used for simulation. These equations and their derivations are based on the saturated effect.

Chapter 6 presents the behavior of induction motor parameters in saturated conditions under dynamic and steady state conditions.

Rotor flux direct field orientation (DFO) approaches based upon the new methods are analyzed and developed chapter 7 to be used in conjunction with the proposed technique for high speed operation.

Chapter 9 describes the experimental setup and the use of Real Time Linux(RT-Lunix) for this thesis. Chapter 9 ends with conclusion and further research to be carried out on this thesis.

Chapter 2

CONTROL STRATEGIES OF THE INDUCTION MOTOR

2.1 INTRODUCTION

The present state of the art in the field-oriented (or vector control) technique was introduced by Blaschke [8]. This method consists of rewriting the dynamic equations of the induction motor in a reference frame that rotates synchronously with the magnetic flux inside the machine. This can be the stator flux, the rotor flux or the air gap fluxes, figure 2.1.

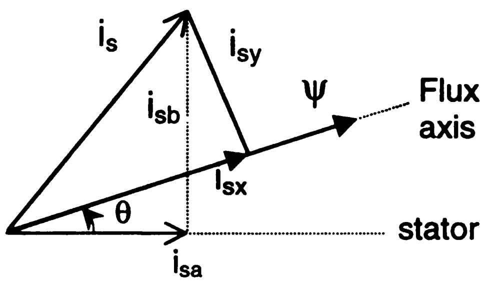

Fugure 2.1 Vector diagram: Field orientation of the induction machine

In the rotor field coordinate system, one observes that by holding the rotor flux constant using one input (i_x) , there is a linear relationship between the second input, (i_y) and the torque. For the other two coordinate systems, the relationships are also relatively simple. For field orientation, the flux vector in the induction machine, especially its angle, has to be known. This flux angle can be found in the three different ways:

a). By a measuring the magnetic field inside the machine with Hall sensors or sense coils. These sensors are mechanically vulnerable and costly to install.

b) By using a machine model, the so-called current model, fed by the stator current and the rotor speed or angle model. This requires a shaft encoder that is often undesired, because it is an extra mechanical component with separate wiring.

c) By using a machine model that needs only the stator voltage and current as its inputs. This is the voltage/current model and enables a sensor-less field-oriented control, because no additional flux or speed/position sensors are necessary.

The sensor-less field-oriented control by means of the voltage/current model is the preferred way of highly dynamic induction machine control, and is the basis of this proposal. Field orientation enables a simple decoupling control similar to DC machine control and serves three purposes: i) to maintain a constant flux level; ii) to limit the current; iii) to stabilize the ac machine. Electric and hybrid electric vehicles and industrial speed controlled drives are usually controlled by the preferred method of indirect vector control. However, this method requires a speed encoder on the machine shaft and feed-forward slip frequency signals for the generation of the vectors. The encoder provides the speed feedback signals, which are used in the generation of the unit vectors and for speed control. Typically, the speed encoder is undesirable because it is expensive, fragile and requires an additional wire harness and connectors which can be unreliable in the drive system. The direct vector method generates the flux vector from the machine terminal voltages and currents, without the need of a speed encoder.

Relating to the process of calculating the flux space phasor position, θ, the direct and indirect methods use estimators for the stator voltages, currents and speed measured, and known motor parameters. At low speeds (and low frequencies) direct methods are susceptible to noise, and DC offset and are better suited for high speed applications. Indirect methods based on current models are sensitive to changes in the rotor time constant, and otherwise are appropriate at low speeds. Boldea and Nasar [9] summarize the most appropriate strategies for the vector control of induction motors in table 2.1.

Table 2.1 Vector Control Strategies of Induction Motor

Flux Orientation	Current Control	Voltage Control	Combined Voltage and Current	Indirect Method	Direct Method
Rotor Flux Orientation	Most Appropriate	*Feasible*	Most Appropriate	Most Appropriate	*Feasible*
Stator Flux Orientation	*Feasible*	Most Appropriate	*Feasible*	*Feasible*	Most Appropriate
Airgap Flux Orientation	Most Appropriate	*Feasible*	*Feasible*	*Feasible*	Most Appropriate

2.2 MAIN TECHNIQUES OF SENSOR-LESS CONTROL OF INDUCTION MOTOR.

Since the end of 1980s the estimation of the rotor position, or the position of the rotor flux, has been the subject of intensive research. The methods utilized include a variety of control theory approaches, and the state of the art is detailed in [10-11,1]. Estimators using intelligence (neural networks, fuzzy-logic-based systems, fuzzy-neural networks and genetic algorithms) have also shown some promising results. Various techniques used in high performance drives for the estimation of the slip, rotor, speed, rotor angle, and various flux linkages are discussed in section 2.3.

Most methods of transducer-less velocity estimation of the induction motor utilize the back emf based upon the fundamental component model of the machine. To evaluate such approaches, two basic facts should be recognized; 1) Rotor flux is not fixed in magnitude or position relative to the rotor, thus, velocity estimation via back emf is more difficult and parameter sensitive in induction machines than in DC or synchronous machines and 2) Spatial dependencies are not intrinsically within the fundamental design of symmetrical induction machines, so that when needed artificial saliencies must be introduced.

2.3 ESTIMATORS USING BACK EMF

2.3.1 Open-loop estimator using monitored stator voltages/currents

In open loop estimators, especially at low speeds, parameter deviations have significant influence on the performance of the drive both in the steady state and transient state. The stator resistance (R_s) has important effects on the stator flux linkages, especially at low speeds. In some schemes, the rotor flux-linkage estimation requires the knowledge of the rotor time constant (T_r=L_m/R_r). The rotor resistance can vary due to temperature and skin effects, and L_m can vary due to skin and saturation effects. The thermal model of the induction machine or adaptive control and self commissioning schemes are used to minimize the effect of parameter deviation[10,12 ,13, 14].

2.3.2 Model reference adaptive systems (MRAS)

As stated above, the open loop estimators strongly depend on the machine parameters. In MRAS system some state variables, e.g. rotor flux and the back e.m.f are estimated from the stator voltage and currents in the estimated model and then are compared with the state variables estimated by using an adaptive model [10,14,1, 15, 16]. The difference between these state variables is then used in an adaptation mechanism, which outputs the estimated value of the rotor speed and adjusts the adaptive model until satisfactory performance is obtained. Using Popov's criterion of hyperstability the adaptation mechanism is derived. The MRAS technique can be robust with respect to the stator and rotor resistance, which can be used at low speeds, e.g. 0.3Hz, [8]. Problems arise at extremely low frequencies, due to incorrect flux estimation.

2.3.3 Observer (General, Kalman, Luenberger)

A closed-loop estimator is referred to as an observer. It is possible to improve the robustness against parameter mismatch and also additive noise by using closed loop observers. The Kalman filter (KF) observer is of the stochastic type and Luenberger observer (LO) is of the deterministic type[6,16]. Both types the KF and LO can be applied to linear and non-linear systems. Various industrial a.c. drives already incorporate observers [17]. However, when the stator frequency is very low, its non-linear observability becomes weak for both flux linkage and speed estimation and it can not operate at zero speed.

Accuracy Limitations: the entire above estimator algorithms used for sensor-less operation fail to operate at zero stator frequency region [5]. At zero no signal frequency is available from which rotor dynamics can be measured. Performance of sensor-less drives is inferior to that of the sensor-based drives at low frequency. For applications where very low-speed operation is less important than the high speed, direct field orientation gives satisfactory torque control performance.

2.4 ESTIMATION USING SPATIAL PHENOMENA

An example of velocity estimation based upon spatial phenomena inherent within the machine is using the tracking of induced voltage or current ripple due to rotor slotting. Viable estimation has been demonstrated under steady state, medium-high speed, medium-high speed load operating conditions, but not at low and zero speeds and/or light loads [4 5 7]. Other forms of potentially useful phenomena occurring within the induction machine include rotor/stator eccentricities and winding/cage asymmetries. Because such phenomena relate directly to rotor position, tracking of spatial phenomena offers higher potential in terms of position and velocity estimation accuracy than the back-emf-based approaches. Unfortunately intrinsic spatial phenomena are often inadequate for robust tracking. Furthermore existing approaches lack the capabilities of dynamic estimation of position, or even velocity.

Real-time fast Fourier transformation were utilized by Ferrah, [18] to identify the speed-dependent slot ripple harmonics in the measured stator currents. A search scheme based upon a peak-picking algorithm was used to isolate the slot harmonic. Successful operation was claimed under different load levels and velocities. The amplitude of the rotor slot harmonics were shown to vary with load. However, under light loading, the amplitude of third harmonics was insufficient for tracking.

Hurst [19] proposed a velocity estimation scheme based upon the isolation of a particular rotor slot harmonic in the stator currents, followed by pulse counting to obtain velocity. Although measured current spectra are provided, experimental verification of velocity estimation is not provided, this approach lacks the capability of tracking the flux at zero speed

Another group of sensor-less algorithms uses the non-ideal machine characteristics such as eccentricity of rotor, rotor slots harmonics, and rotor unbalance. These algorithms requires frequency spectrum analysis, and they are time consuming and need some machine construction data such as number of rotor slots and stator slots, which can not be easily obtained for off-the-shelf motor. Rather than tracking slot harmonics in the stator currents, in a much earlier approach Ishida and Iwata [20] tracked slot harmonics in the stator voltage. The three phase voltages were summed to isolate harmonics. By sampling the assumed voltage at a multiple of the excitation frequency, a signal with a multiple of the slip frequency was obtained. A zero crossing detector generated pulses of constant area that were smoothed through a low-pass filter to obtain the estimated slip frequency. Good results were claimed in the speed range of -50% to +30% of the stator frequency, but the method has limitations especially under dynamic conditions or low speeds. Even with the modem digital signal processing algorithms, still the performance of the speed control bandwidth of the drive appears like unsatisfactory.

Zinger, Lipo, and Novotny [21] implemented a field oriented drive that utilized the voltage measured across tapped stator windings for flux and rotor speed sensing. The speed was estimated by detecting the rotor slot ripple voltage harmonic. To isolate the slot ripple, the voltages of three coils displaced by 120^0 were summed, leaving primarily a 3^{rd} harmonic due to saturation and a slot ripple. A switched-capacitor band-pass filter with a center frequency that tracked the slot ripple provided further isolation. A phase locked loop was used to track the slot ripple frequency and yield rotor speed. The steady state performance was good at high speeds, but at low speeds, below 5Hz, the slot harmonic signal became too small to track.

Cuzner, Lorenz and Novotny [22] demonstrated the principle and operation of velocity and position control sensing approach for an induction machine using the motor terminal properties and torque command (assuming Field Orientation) [23]. A closed loop non-linear observer was proposed to calculate (in real time) the rotor position and speed based upon an analytical model of the machine magnetic saliencies and winding asymmetries. The observer calculates the harmonic spatial components in the emf. After comparing then to the measured emf they are used to drive the observer to accurate position and speed estimates. An important conclusion was reached, that machine designers should consider intentionally incorporating magnetic saliencies and winding asymmetries into future machines. This method can not be reliably applied to the existing standard induction machines.

Another category of algorithms is the heterodyne method that requires injecting a signal to the motor terminals and checking the response of the motor to this injected signal [7]. This algorithm gives reasonably satisfactory performance for the induction motor with open slot rotor. But in the case of closed rotor slots, as is the case with most of small and medium power squirrel cage induction machines, this algorithm does not work well, especially at loaded conditions. This is because of saturation effects on the leakage inductance with load current flowing in the rotor circuit. The torque controllability in the low and zero frequency region is not adequate for off-the-shelf general purpose inverter fed conventional squirrel cage induction motors. So far, most algorithms do not work well with the mass-produced closed rotor slot motor in the zero or low stator frequency region under heavily loaded conditions.

2.5 ESTIMATION USING SATURATION EFFECTS

The flux estimation schemes in the previous sections were not based upon the fundamental induction machine equations. Alternative approaches were developed based upon secondary effects such as saturation. An obvious limitation of saturation-based approaches is their incapacity of field-weakened operation.

Operation of a machine in a saturated state creates a third harmonic spatial component in the air gap flux and phase voltages. Kreindler [24] developed and demonstrated a direct field oriented controller using third harmonic component. By summing the phase voltages of the wye-connected machine, the third harmonic was isolated, in addition to rotor slot ripple components. Since the third harmonic is fixed relative to the air gap flux, the relative flux angle could be directly determined. The rotor flux angle is obtained upon compensation for rotor leakage inductance, position feedback is not required. Furthermore, the low speed limitations of the voltage model involving integration and sensitivity to stator resistance are absent. However, because the third harmonic amplitude is speed dependent, the method still fails at zero and low speeds.

Chapter 3

MATHEMATICAL MODEL OF INDUCTION MACHINE

3.1 INTRODUCTION

For the purpose of understanding and designing vector controlled drives, it is necessary to know the dynamic model of the induction machine. Such a model, valid for any instantaneous value of voltage and current, and adequately describing the performance of the machine under both steady state and transient operation, can be obtained by utilizing the space phasor theory.

In the stationary reference frame the stator voltage equation can be expressed as:

$$\overline{U}_{s(ABC)} = R_s.\bar{i}_{s(ABC)} + \frac{d\overline{\Psi}_{s(ABC)}}{dt} \tag{3.1}$$

$$\overline{U}_{r(ABC)} = R_r.\bar{i}_{r(ABC)} + \frac{d\overline{\Psi}_{r(ABC)}}{dt} \tag{3.2}$$

A similar expression holds for the rotor voltage equations expressed in the reference frame fixed to the rotor:

Where the $U_{sA,} U_{sB,} U_{sC,}$ and $U_{rA,} U_{rB,} U_{rC,}$ are the stator and rotor instantaneous phase voltages; similarly i_{sA}, i_{sB}, i_{sC} and i_{rA}, i_{rB}, i_{rC} are the stator and rotor three phase currents, R_s and R_r are the resistance of stator and rotor phase windings. The instantaneous values of the stator and rotor flux linkages components, can be expressed as:

$$
\begin{aligned}
\psi_{sA} &= \overline{L}_s i_{sB} + \overline{M}_s i_{sB} + \overline{M}_s i_{sC} + \overline{M}_{sr}\cos\theta_r i_{rA} + \overline{M}_{sr}\cos(\theta_r + 2\pi/3) i_{rB} + \overline{M}_{sr}\cos(\theta_r + 4\pi/3) i_{rC} \\
\psi_{sB} &= \overline{L}_s i_{sB} + \overline{M}_s i_{sA} + \overline{M}_s i_{sC} + \overline{M}_{sr}\cos(\theta_r + 4\pi/3) i_{rA} + \overline{M}_{sr}\cos\theta_r i_{rB} + \overline{M}_{sr}\cos(\theta_r + 2\pi/3) i_{rC} \\
\psi_{sC} &= \overline{L}_s i_{sC} + \overline{M}_s i_{sB} + \overline{M}_s i_{sA} + \overline{M}_{sr}\cos(\theta_r + 2\pi/3) i_{rA} + \overline{M}_{sr}\cos(\theta_r + 4\pi/3) i_{rB} + \overline{M}_{sr}\cos\theta_r i_{rC} \\
\psi_{rA} &= \overline{L}_r i_{rA} + \overline{M}_r i_{rB} + \overline{M}_r i_{rC} + \overline{M}_{sr}\cos\theta_r i_{sA} + \overline{M}_{sr}\cos(\theta_r + 4\pi/3) i_{sB} + \overline{M}_{sr}\cos(\theta_r + 2\pi/3) i_{sC} \\
\psi_{rB} &= \overline{L}_r i_{rB} + \overline{M}_r i_{rA} + \overline{M}_r i_{rC} + \overline{M}_{sr}\cos(\theta_r + 2\pi/3) i_{sA} + \overline{M}_{sr}\cos\theta_r i_{sB} + \overline{M}_{sr}\cos(\theta_r + 4\pi/3) i_{sC} \\
\psi_{rC} &= \overline{L}_r i_{rC} + \overline{M}_r i_{rA} + \overline{M}_r i_{rB} + \overline{M}_{sr}\cos(\theta_r + 4\pi/3) i_{sA} + \overline{M}_{sr}\cos(\theta_r + 2\pi/3) i_{sB} + \overline{M}_{sr}\cos\theta_r i_{sC}
\end{aligned}
$$

where θ_r is the rotor angle i.e between the rotor axis and the stationary axis. The stator self-inductance of one stator phase winding $\overline{L}_s$ can be expressed as the sum of the stator leakage inductance L_{sl} and the stator magnetizing inductance L_{sm}, ($\overline{L}_s = L_{sl} + L_{sm}$,), where $L_{sm} = (N_r / N_s)\overline{M}_{sr}$, N_r and N_s.are the effective number of rotor and stator turns. The mutual inductance between two stator windings $\overline{M}_s = L_{sm}\cos(2\pi/3) = -\frac{L_{sm}}{2}$. Similarly, the rotor self-inductance $\overline{L}_r = L_{rl} + L_{rm}$, where $L_{rm} = (N_r / N_s)\overline{M}_{sr}$, and the mutual inductance between two rotor windings $\overline{M}_r = L_{rm}\cos(2\pi/3) = -\frac{L_{rm}}{2}$. The maximum value of mutual inductance between the stator and rotor, $\overline{M}_{sr} = \sqrt{L_{sm}L_{rm}}$. The resultant three phase magnetizing inductance can be written as $L_m = \frac{3}{2}\overline{M}_{sr}$, then it follows from above that the total three-phase stator inductance L_s takes the form

$L_s = \overline{L}_s - \overline{M}_s = L_{sl} + L_{sm} + \frac{1}{2} L_{sm} = L_{sl} + \frac{3}{2} L_{sm}$, Similarly, the total three-phase rotor inductance L_r takes the form $L_r = \overline{L}_r - \overline{M}_r = L_{rl} + L_{rm} + \frac{1}{2} L_{rm} = L_{rl} + \frac{3}{2} L_{rm}$

3.2 THREE PHASE VOLTAGE MODEL

Substituting, the above instantaneous values of the stator and rotor phase-variable flux linkages components into equations (3.1) and (3.2) of the three-phase machine can be combined into single matrix equation.

$$
\begin{bmatrix} U_{sA} \\ U_{sB} \\ U_{sC} \\ U_{rA} \\ U_{rB} \\ U_{rC} \end{bmatrix} =
\begin{bmatrix}
R_s + P\overline{L}_s & P\overline{M}_s & P\overline{M}_s & P\overline{M}_{sr}\cos\theta & P\overline{M}_{sr}\cos\theta_1 & P\overline{M}_{sr}\cos\theta_2 \\
P\overline{M}_s & R_s + P\overline{L}_s & P\overline{M}_s & P\overline{M}_{sr}\cos\theta_2 & P\overline{M}_{sr}\cos\theta & P\overline{M}_{sr}\cos\theta_1 \\
P\overline{M}_s & P\overline{M}_s & R_s + P\overline{L}_s & P\overline{M}_{sr}\cos\theta_1 & P\overline{M}_{sr}\cos\theta_2 & P\overline{M}_{sr}\cos\theta \\
P\overline{M}_{sr}\cos\theta & P\overline{M}_{sr}\cos\theta_2 & P\overline{M}_{sr}\cos\theta_1 & R_r + P\overline{L}_r & P\overline{M}_r & P\overline{M}_r \\
P\overline{M}_{sr}\cos\theta_1 & P\overline{M}_{sr}\cos\theta & P\overline{M}_{sr}\cos\theta_2 & P\overline{M}_r & R_r + P\overline{L}_r & P\overline{M}_r \\
P\overline{M}_{sr}\cos\theta_2 & P\overline{M}_{sr}\cos\theta_1 & P\overline{M}_{sr}\cos\theta & P\overline{M}_r & P\overline{M}_r & R_r + P\overline{L}_r
\end{bmatrix}
\begin{bmatrix} i_{sA} \\ i_{sB} \\ i_{sC} \\ i_{rA} \\ i_{rB} \\ i_{rC} \end{bmatrix}
\tag{3.3}
$$

Where $P = \frac{d}{dt}$, which operates also on the inductances, since in general they can vary with current. The angle θ_r is the rotor angle, between the rotor axis and the stationary axis; angles θ, θ_1 and θ_2 are defined as $\theta=\theta_r$, $\theta_1=\theta_r+2\pi/3$, and $\theta_2=\theta_r+4\pi/3$.

3.2.1 Transformation From Three Phase to Two Phase Model

The above matrix is the impedance matrix of the three-phase model, which contains 36 non-zero elements. It is possible to achieve reduction in the elements in a balanced three-phase induction motor, which can be described as an equivalent two-phase machine with a simpler mathematical model, containing 12 elements. Considering the equation 3.3 and using a transformation equation:

$$\begin{bmatrix} V_o \\ V_{a(\alpha)} \\ V_{b(\beta)} \end{bmatrix} = \frac{2}{6}\begin{bmatrix} 1 & 1 & 1 \\ 2 & -1 & -1 \\ 0 & \sqrt{3} & -\sqrt{3} \end{bmatrix} \cdot \begin{bmatrix} U_{(s,r)A} \\ U_{(s,r)B} \\ U_{(s,r)C} \end{bmatrix}$$

Both stator and rotor equations can be transformed to 2-axis, 12 elements, simple voltage model. The zero-sequence component, V_{so} and V_{ro} in the above equations are zero, provided the power invertor do not contain a dc offsets. Due to symmetrical sinusoidal winding in the induction machine, it is assumed that there is no zero-sequence voltages and currents in the stator and rotor windings. The components V_{sa} and V_{sb} are the stator voltages in an equivalent two-phase stator winding that establishes the same result as the three-phase rotor winding. Similarly $V_{r\alpha}$ and $V_{r\beta}$ are the rotor voltages in an equivalent two-phase rotor winding. The same transformation technique can be applied for current transformation, for more detail refer to [25,8]. This corresponds to using a quadrature-phase machine model instead of the three-phase model. The transformation equation results in the two-phase voltage equations of induction motor in the natural reference frames:

3.2.2 Natural Reference Frame-Voltage Model (Unsaturated Model)

$$\begin{bmatrix} V_{sa} \\ V_{sb} \\ V_{r\alpha} \\ V_{r\beta} \end{bmatrix} = \begin{bmatrix} R_s + PL_s & 0 & PL_m \cos\theta_r & -PL_m \sin\theta_r \\ 0 & R_s + PL_s & PL_m \sin\theta_r & PL_m \cos\theta_r \\ PL_m \cos\theta_r & PL_m \sin\theta_r & R_r + PL_r & 0 \\ -PL_m \sin\theta_r & PL_m \cos\theta_r & 0 & R_r + PL_r \end{bmatrix} \cdot \begin{bmatrix} i_{sa} \\ i_{sb} \\ i_{r\alpha} \\ i_{r\beta} \end{bmatrix} \quad (3.4)$$

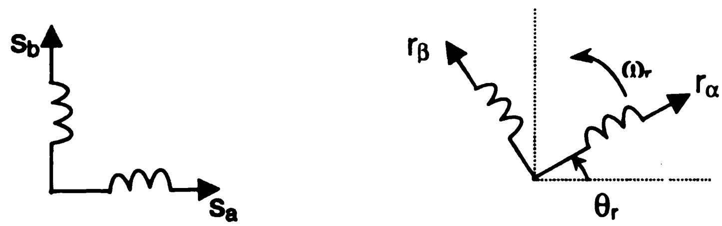

Figure 3.1 Schematic of the quadrature-phase model
(Natural reference frame)

The equation (3.4) can be put into the following space-phasor form

$$\overline{V}_{s(ab)} = R_s.\bar{i}_{s(ab)} + \frac{d\overline{\Psi}_{s(ab)}}{dt}$$

$$\overline{V}_{r(\alpha\beta)} = 0 = R_r.\bar{i}_{r(\alpha\beta)} + \frac{d\overline{\Psi}_{r(\alpha\beta)}}{dt}$$

The stator and rotor space phasor flux linkages are given by $\overline{\Psi}_{s(ab)} = L_s\bar{i}_{s(ab)} + L_m\bar{i}_{r(ab)}$ and $\overline{\Psi}_{r(\alpha\beta)} = L_s i_{r(\alpha\beta)} + L_m i_{s(\alpha\beta)}$ where $i_{s\alpha}$ and $i_{s\beta}$ are the stator currents in the rotor reference frame, and, i_{ra} , i_{rb} are the rotor currents in the stator reference frame, (the transformation matrix are explained below). It follows from the equation (3.4) that as a consequence of the phase transformation, the machine model contains only 12 elements. The stator and rotor variables are in their natural reference frame, figure 3.2; and even if the machine parameters are constant, the system of voltage differential equations is time dependent, since the equations contain the rotor angle θ_r, which changes with the time. If the inductances are independent of i_{mr} (unsaturated condition), the differential operator can be moved after the inductance element. However, by transforming the rotor voltages and currents from the rotor reference frame to the stator reference frame, it is possible to achieve further reduction in the elements of the impedance matrix, i.e. eliminating the angles.

The rotor current and flux linkages in the stator reference frame are related to the rotor current and flux linkages in the rotor reference frame by the following transformation:

$$\bar{i}_{r(ab)} = \bar{i}_{r(\alpha\beta)} e^{j\theta_r} = (i_{r\alpha} + i_{r\beta}) e^{j\theta_r}$$

$$\begin{bmatrix} i_{ra} \\ i_{rb} \end{bmatrix} = \begin{bmatrix} \cos\theta_r & -\sin\theta_r \\ \sin\theta_r & \cos\theta_r \end{bmatrix} \begin{bmatrix} i_{r\alpha} \\ i_{r\beta} \end{bmatrix}$$

Similarly the rotor flux linkages can be expressed in the stator reference frame as:

$$\bar{\psi}_{r(ab)} = \bar{\psi}_{r(\alpha\beta)} e^{j\theta_r} = (\psi_{r\alpha} + \psi_{r\beta})\, e^{j\theta_r}$$

$$\begin{bmatrix} \psi_{ra} \\ \psi_{rb} \end{bmatrix} = \begin{bmatrix} \cos\theta_r & -\sin\theta_r \\ \sin\theta_r & \cos\theta_r \end{bmatrix} \begin{bmatrix} \psi_{r\alpha} \\ \psi_{r\beta} \end{bmatrix}$$

Thus by considering the transformation equations, the transformed set of stator and rotor voltages can be expressed in the frame of reference fixed to the stator:

3.2.3 Stator Reference Frame-Voltage Model (Unsaturated Model)

$$\begin{bmatrix} V_{sa} \\ V_{sb} \\ V_{ra} \\ V_{rb} \end{bmatrix} = \begin{bmatrix} R_s + pL_s & 0 & pL_m & 0 \\ 0 & R_s + pL_s & 0 & pL_m \\ pL_m & \omega_r L_m & R_r + pL_r & \omega_r L_r \\ -\omega_r L_m & pL_m & -\omega_r L_r & R_r + pL_r \end{bmatrix} \begin{bmatrix} i_{sa} \\ i_{sb} \\ i_{ra} \\ i_{rb} \end{bmatrix} \tag{3.5}$$

Figure 3.2 Schematic of the quadrature-phase model

The above equation can be put into the following space-phasor form

$$\overline{V}_{s(ab)} = R_s.\bar{i}_{s(ab)} + \frac{d\overline{\Psi}_{s(ab)}}{dt} \tag{3.6}$$

$$\overline{V}_{r(ab)} = 0 = R_r.\bar{i}_{r(ab)} + \frac{d\overline{\Psi}_{r(ab)}}{dt} \tag{3.7}$$

Hence, the stationary-axis stator quantities are unchanged, but the rotor voltage and currents are transformed. The schematic of this machine is shown in figure 3.2; on the stator there are direct and quadrature-axis windings denoted by s_a, s_b and on the rotor there are windings denoted by r_a, r_b respectively. $\overline{V}_{r(ab)}$ and $\bar{i}_{r(ab)}$ are the rotor voltages and currents in the stator reference frame. Moreover, in the direct-axis rotor windings, the term $P(L_m.i_{sa} + L_r i_{ra})$ describes induces voltages by transformer effects, and $\omega_r(L_m.i_{sb} + L_r i_{rb})$ produces voltages due to the rotation. Under unsaturated magnetic condition, the differential operator can be moved after the inductance, and when the motor is saturated, the differential operator can be moved before the inductance; this is discussed in the next section.

However, instead of a reference frame fixed to the stator or rotor, a general reference frame is used, with direct and quadrature axes x,y, rotating at a general instantaneous speed $\omega_g = d\theta_g/dt$, where θ_g is the angle between the direct-axes of the stationary reference frame s_a fixed to the stator and the real axis(x) of the general reference frame, hence the equations (3.6) and (3.7) can be written:

$$\overline{V}_{s(xy)} = R_s.\bar{i}_{s(xy)} + \frac{d\overline{\Psi}_{s(xy)}}{dt} + j\omega_g\overline{\Psi}_{s(xy)}$$

$$\overline{V}_{r(xy)} = 0 = R_r.\bar{i}_{r(xy)} + \frac{d\overline{\Psi}_{r(xy)}}{dt} + j(\omega_g - \omega_r)\overline{\Psi}_{r(xy)}$$

where $\overline{\Psi}_{s(xy)} = L_s\bar{i}_{s(xy)} + L_m\bar{i}_{r(xy)}$ and $\overline{\Psi}_{r(xy)} = L_s i_{r(xy)} + L_m i_{s(xy)}$, hence equation (3.5) can be put in the general reference frame voltage model:

3.2.4 General Reference Frame-Voltage Model (Unsaturated Model)

$$\begin{bmatrix} V_{sx} \\ V_{sy} \\ V_{rx} \\ V_{ry} \end{bmatrix} = \begin{bmatrix} R_s + PL_s & -\omega_g L_s & PL_m & -\omega_g L_m \\ \omega_g L_s & R_s + PL_s & \omega_g L_m & PL_m \\ PL_m & -(\omega_g - \omega_r).L_m & R_r + PL_r & -(\omega_g - \omega_r).L_r \\ (\omega_g - \omega_r)L_m & PL_m & (\omega_g - \omega_r).L_r & R_r + PL_r \end{bmatrix} \begin{bmatrix} i_{sx} \\ i_{sy} \\ i_{rx} \\ i_{ry} \end{bmatrix} \quad (3.8)$$

If $\omega_g = 0$, equation (3.8) yields equation (3.5), which corresponds to the set of stator voltages and rotor voltage expressed in the fixed to the stator.

Equation (3.8) can be transformed to the synchronous reference frame aligned to the rotor flux frame by replacing ω_g with the synchronous speed, rotor flux ω_{mr}. For an induction machine, $\omega_{mr}-\omega_r = s\omega_{mr}$ is the slip speed and *s* is the slip.

3.3 SATURATED MODEL

In this section the stator and the rotor voltage equations are obtained. They contain the effects of main flux saturation and are formulated in the reference frame fixed to the rotor-flux linkage space phasor. The method followed here is similar to that used in the previous section. By considering the equations (3.8), which are the stator space-phasor voltage and the stator flux space-phasor equations in the general reference frame, the stator-voltage space phasor equation (3.9) is obtained in the reference frame fixed to the rotor flux-linkages space phasor. It rotates at the speed ω_{mr}. This speed is the first derivative of the space angle ρ of the rotor magnetization-current space phasor with respect to the direct axis of the stationary reference frame. By substituting the general reference equation of stator flux space-phasor and rotor flux space-phasor into equation (3.8), the model can be oriented to the rotor flux reference frame:

$$\overline{V}_{s(dq)} = R_s \cdot \bar{i}_{s(dq)} + \frac{d(L_s \bar{i}_{s(dq)})}{dt} + \frac{d(L_m \bar{i}_{r(dq)})}{dt} + j\omega_{mr}(L_s \bar{i}_{s(dq)} + L_m \bar{i}_{r(dq)}) \quad (3.9)$$

$$\bar{\Psi}_{r(dq)} = L_m |\bar{i}_{mr}|$$

$$0 = R_r . \bar{i}_{r(dq)} + \frac{d\bar{\Psi}_{r(dq)}}{dt} + j(\omega_g - \omega_r)\bar{\Psi}_{r(qd)}$$

where, i_{mr} is the rotor magnetization current: Later it will be shown that i_{mr} is a function of L_m.

$$0 = R_r . \bar{i}_{r(dq)} + L_m \frac{d|\bar{i}_{(mr)}|}{dt} + j(\omega_{mr} - \omega_r) L_m |\bar{i}_{(mr)}|$$

$$\frac{(dL_m|\bar{i}_{mr}|)}{dt} = \frac{d|\bar{\Psi}_r|}{dt} = \frac{d|\bar{\Psi}_r|}{d|\bar{i}_{mr}|}\frac{d|\bar{i}_{mr}|}{dt} = L\frac{d|\bar{i}_{mr}|}{dt}$$

$$\text{where,} \quad \bar{i}_{r(dq)} = \frac{|\bar{i}_{mr}| - is_{(dq)}}{1+\sigma_r} = \frac{(|\bar{i}_{mr}| - \bar{i}_{s(dq)})L_m}{L_r}$$

$$0 = R_r . L_m \frac{|\bar{i}_{(mr)}| - \bar{i}_{s(dq)}}{L_r} + \frac{d(L_m|\bar{i}_{(mr)}|)}{dt} + j(\omega_{mr} - \omega_r) L_m |\bar{i}_{(mr)}|$$

$$T_r(\frac{L}{L_m})\frac{d|\bar{i}_{mr}|}{dt} + |\bar{i}_{mr}| = is_{dq} - j(w_{mr} - w_r)T_r|\bar{i}_{mr}| \qquad (3.10)$$

$$T_r^* = Tr(\frac{L}{Lm}) = L(\frac{L_{rl} + L_m}{L_m R_r})$$

$$T_r = (\frac{L_r}{R_r}) = (\frac{L_{rl} + L_m}{R_r})$$

where, L is a dynamic (tangent-slope or incremental) inductance, and it is equal to the derivative of the modulus of the rotor magnetization-flux space phasor with respect to the modulus of the rotor magnetization current space phasor, $L = \frac{d|\bar{\psi}_r|}{d|\bar{i}_{mr}|}$. It should be noted that in contrast to this, $L_m = \frac{|\bar{\psi}_r|}{|\bar{i}_{mr}|}$ is the static (chord slope) or amplitude inductance. Moreover, T_r is the rotor time constant, which because of saturation is not constant. In this expression, L_{rl} is the leakage inductance of the rotor, which has been assumed to be constant. Under linear magnetic condition $L=L_m$. It must be mentioned that because of saturation, the modified time constant T_r^*, has chord and tangent inductance effects as a result of saturation. Hence, it is important to note that because of saturation, both T_r^* and T_r are varying parameters and depend on the magnetization inductance, which changes with $|\bar{i}_{mr}|$. When equation (3.10) is resolved into its real-(x) and imaginary-(y) components, the direct-axis flux model equation of the saturated induction machine in the rotor -oriented reference frame is obtained.

$$T_r^{\bullet} \frac{d|i_{mr}|}{dt} + |i_{mr}| = i_{sd} \tag{3.11}$$

$$w_{mr} = wr + \frac{i_{sq}}{Tr|\bar{i}_{mr}|} \tag{3.12}$$

The equations (3.11,3.12) are in the rotor flux reference frame, involving only rotor voltage equations. Similarly, the saturated voltage model, in the stator reference frame can be derived form equation (3.8) and is expressed as following:

$$\begin{bmatrix} V_{sa} \\ V_{sb} \\ V_{ra} \\ V_{rb} \end{bmatrix} = \begin{bmatrix} R_s + L_{sa}P & L_{sa}P & L_{ma}P & L_{ab}P \\ L_{ab}P & R_s + L_{sb}P & L_{ab}P & L_{mb}P \\ L_{ma}P & \omega_r.L_m + L_{ab}P & R_r + L_{rd}P & \omega_r.L_m + L_{ab} \\ -\omega_r.L_m + L_{ab}P & L_{mb}P & -\omega_r.L_m + L_{ab}P & R_r + L_{rq}P \end{bmatrix} . \begin{bmatrix} i_{sa} \\ i_{sb} \\ i_{ra} \\ i_{rb} \end{bmatrix} \tag{3.13}$$

3.4 MAGNETIC SATURATION

It is well known that, as the flux in the machine increases, the iron paths begin to saturate. Saturation prevents the machine from reaching the torque levels predicted by the linear magnetic model. Hence, it is desired to have a dynamic model of the induction motor, which includes saturation, in order for the controller to accommodate such effects. However, the modeling of saturation is by no means obvious and is still an active area of research. Recent progress in this area has been reported [6,23,26,27]. In a unique approach to modeling saturation, the π -model of the magnetic circuit is used rather than the standard T-model [23]. However, the determination of the saturation curves for this model requires the measurement of the rotor currents, which is not possible on the squirrel cage induction machine. In [26] saturation is modeled using air gap length that varies as a function of both position and level of the air gap flux, and by the addition of some fictitious winding to generate third harmonic components. Experimental results are given showing the model predicts spatial saturation effects with good accuracy. However, this model is somewhat complex; this complexity in turn also makes the resulting nonlinear input-output linearization controller complex. In [8] Vas developed a model for magnetic saturation by making the mutual inductance a function of rotor magnetization current. The resulting model is complex but more practical and is used for this thesis.

For constant speed applications, the flux is typically set to a constant value. For demanding speed trajectories, the flux reference must vary with the time. In particular, as the speed of the motor increases, the flux must be decreased (field-weakening). This is done because the inverter has current and voltage limit constraints. The standard method employed for field weakening is to decrease the flux as $1/\omega$ after some base speed is reached. However, it is not clear how to choose this speed, nor is it clear that this is the best possible method to accomplish field-weakening, moreover, the $1/\omega$ scaling does not include saturation effects.

3.5 SPLINE INTERPOLATION

For simulation process, the magnetization saturation curve for the induction motor is obtained from the unsaturated model by using a spline interpolation. The spline interpolation is a piece-wise polynomial interpolation. This means that if a function f(x) is given on an interval $a \le x \le b$. An approximate f(x) on this interval by a function g(x) that is obtained as follows: We partition $a \leq x \leq b$; that is, we divide it into intervals with common endpoints, $x_o \ldots x_n$, called nodes,

$$a = x_o < x_1 < \ldots < x_n = b$$

$$g(x_o) = f(x_o), \ldots g_{n-1}(x_n) = f(x_n)$$

where $g_i(x_o)$-are polynomials, one polynomial per subinterval, so that at the nodes, g(x) is several time continuously differentiable on the entire $a \leq x \leq b$; f(x) is approximated by *n* polynomials. Hence an approximating polynomial function $g(x_o)$, called spline, is obtained for interpolation and approximation of ψ from the estimated value of i_m . For this thesis the cubic spline is used for interpolation and extrapolation of the magnetizing rotor flux. Figure 6.1 the effect of saturation on the motor magnetizing inductances. The spline program was written for the Matlab simulation program to estimate the tangent inductance and the chord inductances.

Chapter 4

FLUX ESTIMATION BASED ON SATURATION EFFECT

4.1 INTRODUCTION

The process of calculating the flux space phasor position, the direct and indirect methods by using estimators for the stator voltages, currents and speed measured with known parameters. At low speeds (and low frequencies) direct methods are susceptible to noise, and DC offset and are better suited for high-speed applications. Indirect methods based on current models are sensitive to changes in the rotor time constant, and otherwise are appropriate at low speeds but still susceptible to noise while requiring position sensing.

To overcome the problem stated above, a different approach was proposed by F. Blaschke, J. Van der Burgt and A. Vandenput [3]. This technique is free of integration methods. In this method an additional high frequency test current component induces a rotor current component that can be sensed in the stator voltage. The induced rotor current components depend on the angle difference between the estimated and the real rotor flux vector. In this way the position of the rotor flux of the induction machine can be obtained from only the stator voltage, even at zero frequency.

The method is based upon an angle difference between the test stator current and the induced test rotor current. The effect of this difference appears only in the region of magnetic saturation. This algorithm provides the basis. It utilizes high frequency magnetizing current injection, without modification of the induction machine design. This effect has to do with the way in which motions of the stator current vector are transformed into corresponding motions of the rotor current vector. The transfer properties can be derived from the equations of a current fed induction machine taking saturation into account. Assuming relatively fast and small motions of the stator current vector, an approximate, but very simple, transfer function concerning the injected test currents (indicated by Δi) can be derived as shown in figure 4.1. The transfer from the stator currents to the (negative) rotor currents is described in the rotor flux reference frame by the transfer gains k_1 and k_2.

The transformation of the currents from the stator coordinates to rotor flux coordinates and vice versa is done by the rotation over the (negative) rotor flux angle (- or + ρ) with the rotator $e^{\pm j\rho}$. The factors k_1 and k_2 depend on the saturation condition of the machine. This is shown with the help of saturation curve of the of the induction machine, in figure 4.2, where the magnitude of the air gap flux, ψ_r, is drawn against the rotor magnetizing current, i_m.

Each operating point has two characteristic values: the angle σ with respect to the origin of the curve and the angle β of the tangent at the operating point under consideration. The factors $k_1 = \dfrac{1}{1+\dfrac{L_{rl}}{L}}$ and $k_2 = \dfrac{1}{1+\dfrac{L_{rl}}{L_m}}$ strongly depend on the these angles, where $L=d\psi/di_m$ and $L=\psi/i_m$, also see figure 6.1.

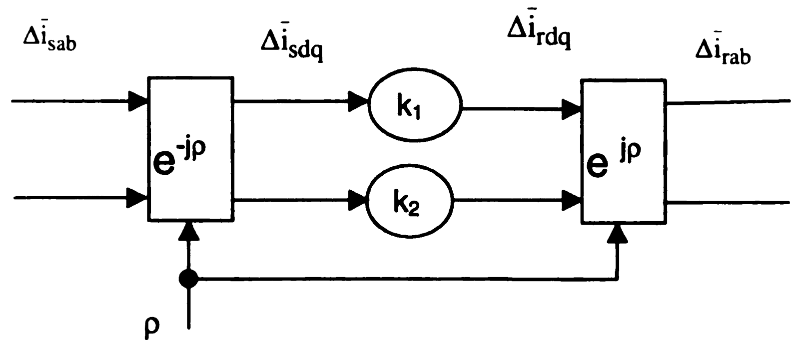

Figure 4.1 Model of the test current transfer function

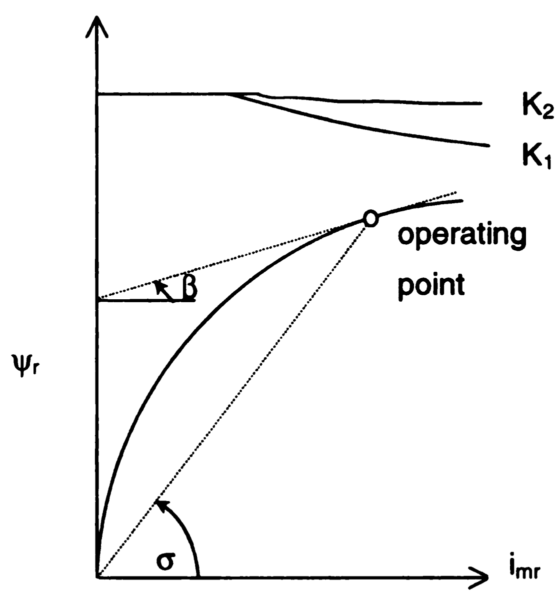

Figure 4.2 Saturation curve of the induction motor

4.2 LOCUS OF TEST VECTOR

The stator test current vector should have no net affect on the induction machine operation and it is desired to separate the rotor test current vector from the rotor current vector that is induced by the normal stator current command vector. For these reasons a pulsating stator test current vector 'a' with small amplitude and a relatively high frequency (compared to the flux frequency of the machine) is used. This stator test current vector is applied in the direction of the estimated rotor flux vector. This current is generated by taking the projection of a rotating auxiliary current vector 'a' on the estimated rotor flux vector axis see figure 4.3 and figure 4.5. Consequently, the test current equals:

$$\Delta i_{s\hat{d}\hat{q}} = \begin{bmatrix} [\Delta i_s]_T \\ 0 \end{bmatrix} = \begin{bmatrix} a \bullet \mathrm{Cos}\alpha \\ 0 \end{bmatrix}$$

Where α is the test angle in the estimated flux of reference. This means that the test current is a cosine signal that is added to the magnetizing component (in the estimated flux frame) of the stator current vector. This test current vector is in stator coordinates:

$$\Delta i_{sab} = \begin{bmatrix} [\Delta i_s]_T . \cos\hat{\rho} \\ [\Delta i_s]_T . \sin\hat{\rho} \end{bmatrix}$$

The construction of the test vector is shown in the diagram of figure 4.5. The applied pulsating stator test current vector is shown figure 4.3. It moves along the curve when the auxiliary vector a makes one revolution. The locus of the induced rotor test current vector $\Delta\bar{i}_r$ .is shown in figure 4.4 as a dotted line. If the rotor current is measured and transformed into the estimated rotor flux coordinate system and the high-frequency test current is separated by high-pass filter, the shifting angle γ is obtained. This shift angle can be used in a controller that changes the estimate of the rotor flux angle until γ becomes zero. Then $\hat{\rho} = \rho$, i.e. the real flux axis has been basically determined.

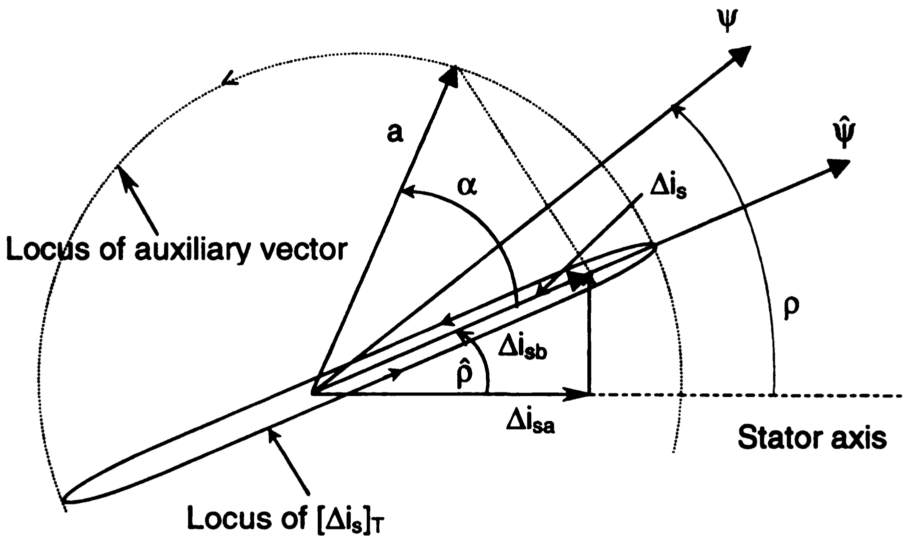

Figure 4.3 Locus of the stator current test vector

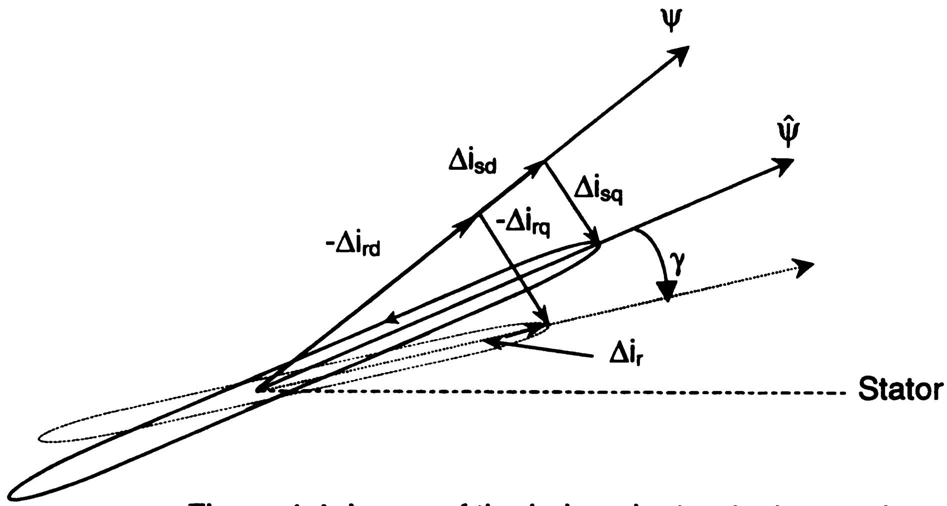

Figure 4.4 Locus of the induced rotor test current

An important property of this technique should be emphasized: in fully tuned operation, i.e. when the real flux has been found, the stator current test vector is pulsating in parallel with the rotor flux vector (magnetizing current injection) and consequently does not influence the torque producing stator current component. Because the test has a small amplitude and relatively high frequency, the rotor flux is not affected. This means that the electromagnetic torque, that is proportional with the rotor flux times the torque-producing stator current component, is not affected by this high-frequency magnetizing current injection method. These considerations clarify the reason why the perpendicular or torque-producing stator current component was not chosen as the test component. In that case the electromagnetic torque of the machine would have been influenced considerably.

A test current vector $\Delta\bar{i}_s$ that has a zero q-axis (i.e. torque-producing) component is generated. This means that $\Delta\bar{i}_s$ is parallel to the estimated rotor flux vector ψ_r (note that the real rotor vector is unknown).

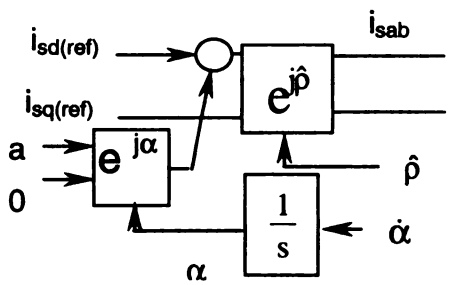

Figure 4.5 Construction of the stator current test vector.

4.3 USING ROTOR CURRENTS TO CORRECT FOR ROTOR FLUX POSITION

4.3.1 Case I Unsaturated Condition

Here real flux is in line with the estimated rotor flux: To analyze it let us first take a look at the effect of the test current when the motor is operated in unsaturated mode. Lets assume that the estimated rotor flux angle, $\hat{\rho}$, is not equal to the real rotor flux angle, ρ, see figure (4.6). The ratio of the projections $\Delta\bar{i}_s$ on the rotor flux and on an axis perpendicular to it is the same as the ratio of the corresponding components of the resulting $\Delta\bar{i}_r$ (see figure 4.6) since $k_1 = k_2$. In other words, even if the angle difference δ between the estimated rotor flux vector and the real rotor flux is not zero, then $\Delta\bar{i}_s$ and $\Delta\bar{i}_r$ are in line with each other. Hence it is not possible to use the angle difference between $\Delta\bar{i}_s$ and $\Delta\bar{i}_r$ to find the rotor flux position while the motor is operated in unsaturated condition.

4.3.2 Case II Saturated Condition Incorrect Estimation

The real flux is not in line with the estimated rotor flux: Figure 4.7 shows the basic consequences of the saturation effects: because k_1 is not equal to k_2 (see section 4.1, and figure 6.1), the induced rotor current vector does not have the same direction as the stator current vector and an angle difference γ between the rotor test current vector and the stator test current vector appears

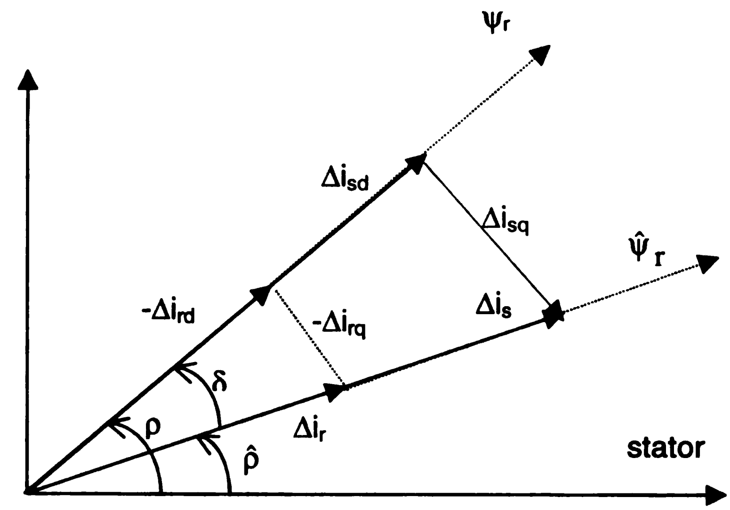

Figure 4.6 Real flux is in line with the estimated rotor flux

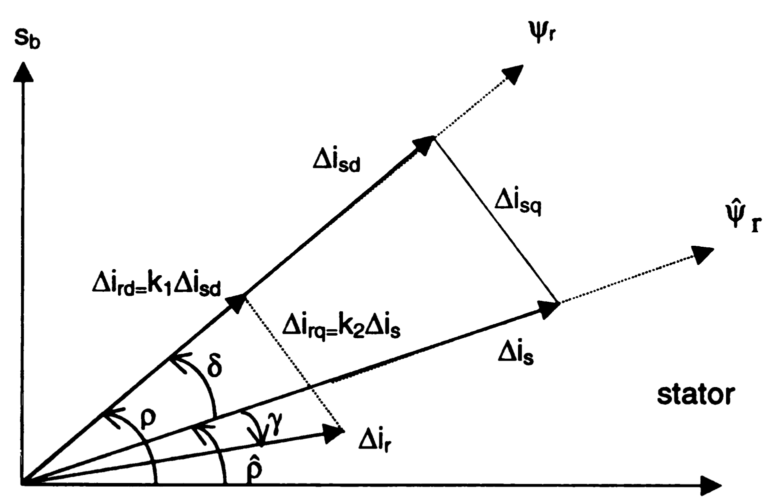

Figure 4.7 Real flux is not in line with the estimated rotor flux

As long as the estimated rotor flux angle, $\hat{\rho}$, is not equal to the real rotor flux angle ρ, the perpendicular component of the test stator current vector (with respect to the real rotor flux vector) is not equal to zero ($\Delta i_{sq} \neq 0$) and therefore $\gamma \neq 0$.

4.3.3 Case III - saturated condition correct estimation:

Here, real flux is in line with the estimated rotor flux and $\Delta i_{rq} = \Delta i_{sq} = 0$: The direction of $\Delta\bar{i}_s$ .and $\Delta\bar{i}_r$. will be the same (i.e. $\gamma=\delta=0$), only if $\Delta i_{sq}=0$ ($-\Delta i_{rq}=0$). That is if $\hat{\rho} = \rho$. then $\delta=\gamma = 0$, figure 4.8. It is due to the reason that the shifting angle γ and the difference angle the δ have opposite directions and that the shifting angle becomes zero when δ is zero.

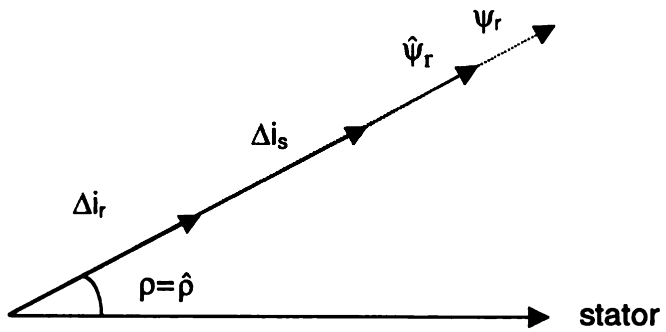

Figure 4.8 Real flux and estimated flux are in line

In summary, the angle difference δ between the estimated rotor flux vector and the actual rotor flux can be determined by measuring the angle γ between the stator test current vector (which is in parallel with estimated rotor flux vector) and the induced rotor test current vector.

4.4 ESTIMATING TEST ROTOR CURRENT FROM THE STATOR VOLTAGE

The induced test rotor current, described in the previous section can not be directly used for the flux determination, because the vector of the rotor current can not be measured. Normally this measurement cannot take place without modification of the machine. There is however a possibility to obtain the important information about the induced rotor test current vector from the stator voltage vector after the power frequency component has been filtered out. Figure 4.9 describes the method to isolate the rotor test current vector from the measured voltage.

The approximation is valid if the test frequency is sufficiently high and the operating frequency, $\dot{\rho}$ of the flux angle to be measured is not too high. These conditions are normally met in the low flux frequency range. There:

$$\Delta V_{s\hat{d}\hat{q}} = \Delta i_{s\hat{d}\hat{q}}.r_s + (-\Delta i_{r\hat{d}\hat{q}}.r_r) + \Delta i_{s\hat{d}\hat{q}}.L_{sl} + (-\Delta i_{r\hat{d}\hat{q}}.r_r).L_{rl} \qquad (4.1)$$

According to equation (4.1) the voltage vector consists of four terms, namely the ohmic and leakage inductive voltage drops of $\Delta i_{s\hat{d}\hat{q}}$ and $(-\Delta i_{r\hat{d}\hat{q}})$. The term that is presently in the fundamental measuring method can be found as term 2), multiplied however by r_r.

If the items 1), 3) and 4) were to be zero, the determination structure could be the same as the method with the rotor measurement. The terms 1), 3) and 4) could be reduced to zero by compensating actions on the stator voltage vector but this would require the knowledge of some machine parameters. The influence of these terms can be cancelled by enlarging the determination structure.

No action has to be taken to eliminate term 1) of equation (4.1), because the imposed $\Delta i_{s\hat{q}}$ is always equal to zero, so that the important second coordinate of the test voltage vector is not influenced by term 1).

Unfortunately, the terms 3) and 4) drastically change the test voltage vector, because these two inductive leakage voltage vectors are perpendicular to the previous ohmic ones 1) and 2). The final voltage vector, consisting of all terms, cannot therefore be used.

There is, however, a very effective countermeasure to this problem. The pulsating stator test current vector $\Delta i_{s\hat{d}\hat{q}}$ can be decomposed into two vectors with equal amplitude, which are rotating with respect to the estimated flux axis, in opposite directions: the positive-sequence vector, rotating with frequency $\hat{\alpha}$, and the negative-sequence vector with frequency $-\hat{\alpha}$. The positive-sequence vector is obtained by a rotation over $-\hat{\alpha}$, the negative sequence vector by a rotation over $+\hat{\alpha}$.

The decomposition of the voltage vector is used to obtain term 2) of equation (4.1). This is shown in figure 4.9 by $e^{\pm j\alpha}$ and the Low-pass filters (LPF), yielding f^a and g^a respectively. The ohmic terms of the voltage vector in the positive-sequence and the negative-sequence system are equal, but the directions of the leakage inductance terms are opposite. This means that the leakage inductance terms cancel each other out when the two systems are added and the resulting voltage (f^a+$g^{a'}$) only consists of terms 1)and 2) figure 4.10 of equation.4.1, multiplied by two. The second coordinate of this voltage vector, that is proportional to $-\Delta i_{s\hat{q}}$, is the signal that should be used to adapt the estimated rotor flux angle in the u/i-model. When this mean value is equal to zero, the shifting angle $\gamma = 0$ is equal to zero and the estimated rotor flux angle is equal to the real rotor flux angle for more detail see figures 4.11,4.12. Where vectors of f^a and $g^{a'}$.

In conclusion, the aforementioned measuring structure is able to determine the flux angle at small flux frequencies and particularly at zero frequency by only using stator voltages and stator currents.

The measuring structure, mentioned above, only functions satisfactorily if the machine is saturated. From the point of view of losses it is generally recommended to use such an operation condition when it is absolutely necessary. Besides, inadmissible voltages would result at high frequencies. Therefore, this measuring method is clearly an expedient which should help an already existing voltage/current model at low frequencies.

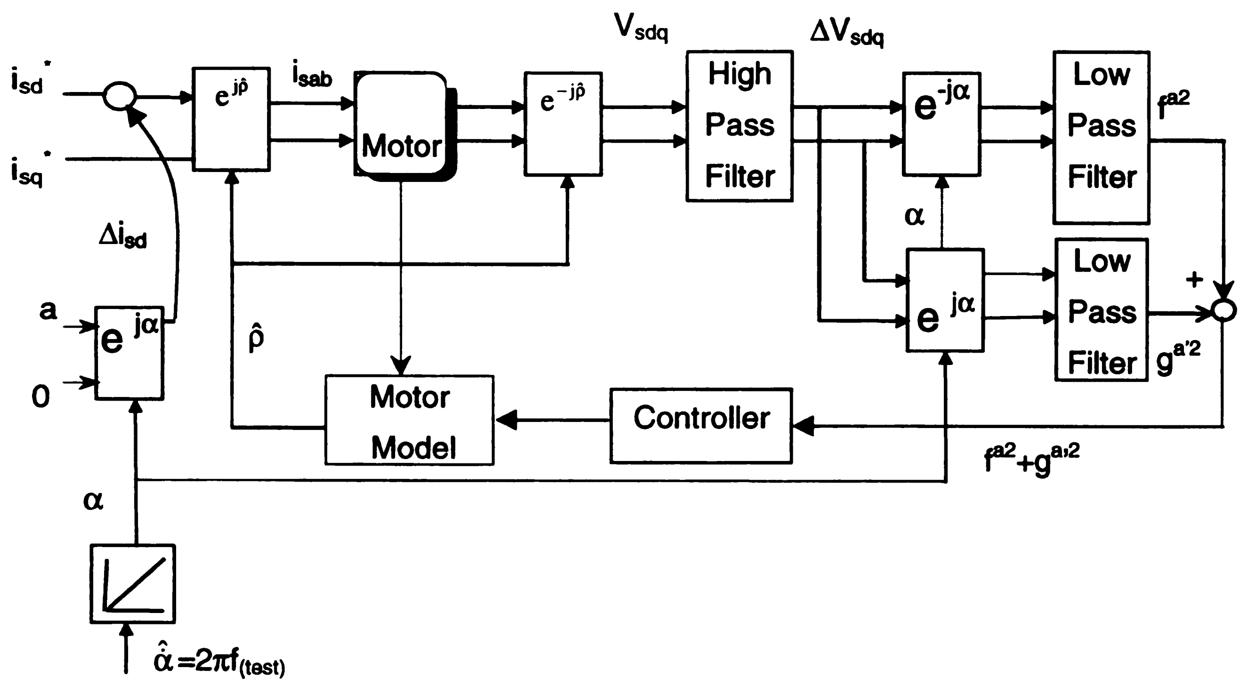

Figure 4.9 Block diagram of simulation/actual implementation

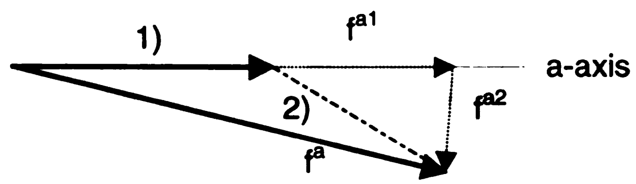

Figure 4.10 Construction of $f^{a'}$ when parts 1) and 2) are available

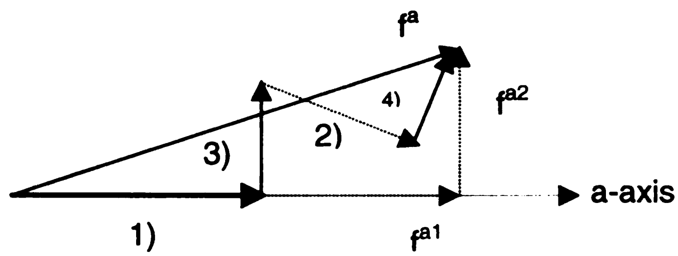

Figure 4.11 construction of f^{a} when parts 1) and 4) are available

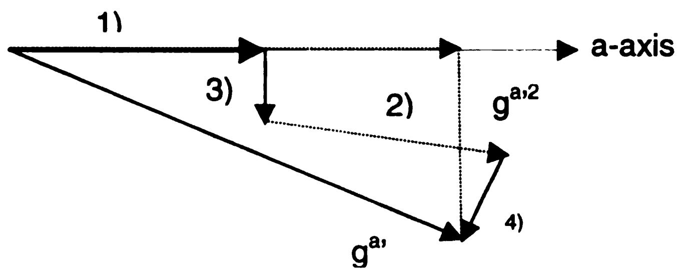

Figure 4.12 Construction of $g^{a'}$ when 1) and 4) are available

4.5 LIMITATIONS OF THE METHOD

The method described, although promising at low frequencies, has certain limitations.

a) Since it is based upon saturating a standard induction motor and by injecting a high frequency test-current, the power frequency has to be lower than the test frequency. This means the method is valid very close to the zero power frequency. An objective of this thesis is to investigate its accuracy as the power frequency is increased.

b) Another obvious limitation of the saturation-based approach is field weakening operation. Robust tracking of saturation-induced saliencies requires operation at flux levels that are considerably higher than normal or rated. The maximum operational speed is then limited by core loss and/or stator voltage. Obviously, field-weakening operation beyond base speed is not possible. Therefore, to obtain wide speed range operation, including field weakening, the high frequency injecting scheme must be combined with a scheme suitable for high-speed operation like direct field orientation (DFO).

c) The estimated rotor flux is sensitive to the angle difference between the estimated and the actual flux. When the difference angle is not too large, a value of the estimated magnetizing current would also result in large value of actual magnetizing current i_d, figure 4.13, thus maintaining saturation. If this angle is too large, it will result in loss of induction motor main-field saturation, due to the decrease in the excitation current i_d. Figure 4.14 shows that when the error angle is large, even a large value of estimated magnetizing current will result in small value of actual magnetizing current i_d, thus driving the motor out of saturation. Hence, a technique has to be developed to keep the flux constant, at an operating point around the zero power frequency operation. The injection of high frequency in the saturated induction machine promises to be a viable and potential attractive means of achieving transducer-less field oriented control in certain applications requiring sustained zero and low speed operation.

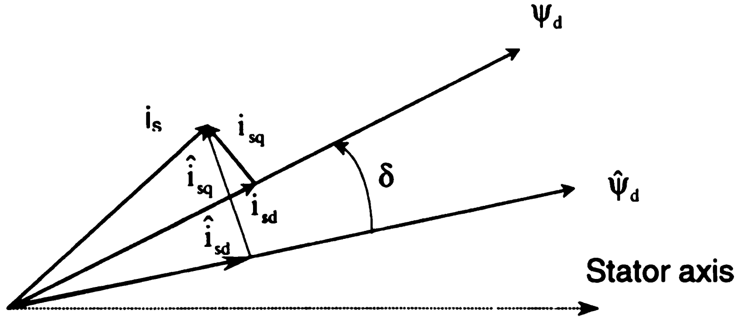

Figure 4.13 Saturated condition due to small estimated flux

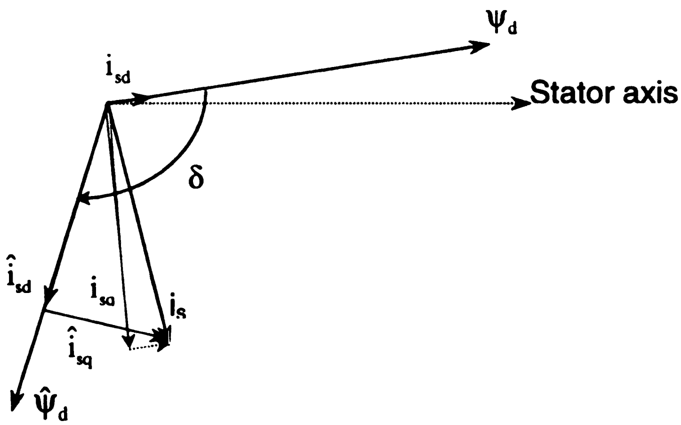

Figure 4.14 Loss of saturation due to large estimated flux error angle

Chapter 5

APPROXIMATED TEST SIGNAL VOLTAGE VECTOR

5.1 INTRODUCTION

From stator voltage equation of the induction machine it is possible to estimate the rotor test current. The stator voltage equation has to be transformed to the rotor flux reference frame. At low flux frequency an approximate expression of the approximated voltage vector at the output of high pass filter is obtained, which is derived in the next section. This approximation is valid if the frequency (test) is sufficiently high; in addition, the operating frequency $\dot{\rho}$ of the flux angle to be measured should be low. The well-known voltage equation for induction machine are expressed as follows:

$$\overline{V}_{sa} = R_s.\bar{i}_{sa} + \frac{d\overline{\Psi}_{sa}}{dt} \tag{5.1}$$

$$\overline{V}_{sb} = R_s.\bar{i}_{sb} + \frac{d\overline{\Psi}_{sb}}{dt} \tag{5.2}$$

$$\overline{V}_{r\alpha} = 0 = R_r.\bar{i}_{r\alpha} + \frac{d\overline{\Psi}_{r\alpha}}{dt} \tag{5.3}$$

$$\overline{V}_{r\beta} = 0 = R_r.\bar{i}_{r\beta} + \frac{d\overline{\Psi}_{r\beta}}{dt} \tag{5.4}$$

The stator flux linkages in the arbitrary reference frame x-y are:

$$\psi_{sx} = \psi_l + L_{ls} i_{sx} \tag{5.5}$$

$$\psi_{sy} = \psi_l + L_{ls} i_{sy} \tag{5.6}$$

where ψl is the leakage flux linkages.

Rotor flux linkages in the arbitrary reference frame are:-

$$\psi_{rx} = \psi_l + L_{lr} i_{rx} \tag{5.7}$$

$$\psi_{ry} = \psi_l + L_{lr} i_{sr} \tag{5.8}$$

The equations are given in the vector format. As shown, every vector variable has two components: the first component is parallel with the reference frame axis and the second component is perpendicular to the reference frame axis. The stator voltage equation is restricted to the stator reference frame because of the differential of the stator flux vector; the rotor current equation is however restricted to the rotor reference frame because of the differentiation. The flux equations are defined in the general reference frame. Before these equations are completed to obtain the approximated machine model in the rotor flux reference frame, the reference frame of the model has to be chosen. Some considerations about this are given in the next section.

5.2 CHOICE OF THE REFERENCE FRAME

The reference of the model must be a coordinate system in which quantities in a steady state are at rest, i.e. in which all quantities appear as DC quantities. The direction of the stator or rotor current vector and direction of any flux vector may be considered as reference axis, because these vectors are rotating at the same speed, i.e. synchronously, with respect to each other in a steady state. One should not choose the rotor axis or the stator axis as the reference axis, because all vectors are moving with respect each other to the rotor and stator in a general and also in the stationary operating condition.

The second consideration in choosing the reference frame is the desired decoupling of the rectangular (Cartesian) coordinates of the stator current vector. This decoupling of the stator current components means that the two components can be controlled separately and independently of each other. This way a control strategy similar to the DC machine control can be achieved. Figure 5.1 shows some of the different reference axes that can be chosen.

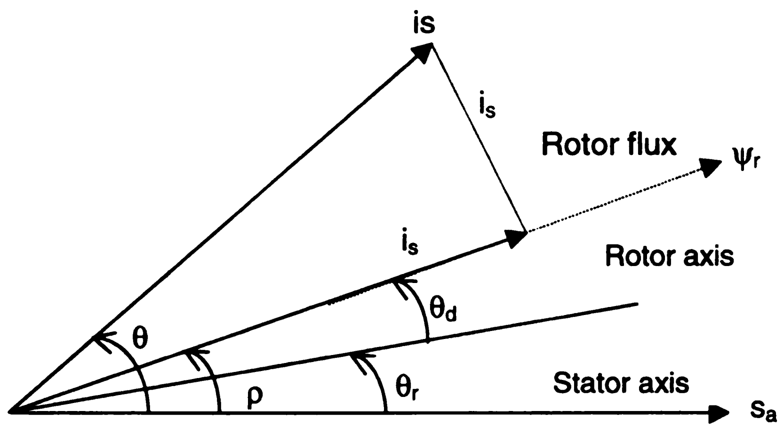

Figure 5.1 Different coordinates axes in AC machine modeling

The flux linkage of the rotor windings, or abbreviated rotor flux, can be considered a central quantity because this flux is responsible for producing the current in the rotor windings (rotor current) and for producing the electromagnetic torque which will be shown in the next section. Therefore it is reasonable to choose the flux axis as the reference coordinate axis.

In the rotor flux reference frame the two-stator components are completely decoupled. This is not the case when choosing the stator flux axis or the air gap flux axis as the reference axis (however, simple measures can overcome this problem). This simple decoupling strategy is another reason to choose the rotor flux reference frame.

5.3 APPROXIMATED TEST SIGNAL VOLTAGE VECTOR USING FLUX LINKAGES

The rotor flux appears in its own coordinates systems only with its value as its first coordinate; the second coordinate is zero. Therefore, the $\psi_{rd}=\psi_r$ ($\psi_{rq}=0$) and hence the rotor flux can be written as:

$$\psi_{rd} = \begin{bmatrix} \psi_{rd} \\ \psi_{rq} \end{bmatrix} = \begin{bmatrix} \psi_r \\ 0 \end{bmatrix}$$

The stator flux is $\psi_s = \begin{bmatrix} \psi_{sd} & \psi_{sq} \end{bmatrix}^T$

To emphasize the coordinates transformation to the rotor flux references frame, the Cartesian field-oriented coordinate, parallel with the rotor flux is called magnetizing coordinates and the one perpendicular to the rotor flux vector, the torque-producing. It must be stressed that these coordinates (with respect to the induced voltage of the machine) do not correspond to the generally known reactive and active power components of the stator current (with respect to the terminal voltage of the machine) which are used to determine the power factor at the machine terminals.

The inputs of the current-fed induction machine model are the stator currents. The three-stator currents of the three-phase induction machine are transformed into an orthogonal two-phase system connected with the fixed stator. Inside the model the two-phase stator currents are transformed from the stator reference frame to the rotor flux reference frame. This way the magnetizing component and the torque-producing component of the stator are obtained. These field-oriented stator currents are the input variables of the current-fed induction machine model. Output variables are the rotor flux inside the machine, the slip frequency of the rotor flux, the angle of the rotor flux with respect to the stator reference frame (the field orientation angle), the electromagnetic torque, the rotor frequency, and angle of the stator terminal voltages.

The equation system of the current-feed induction motor in a vector notation starts with the voltage equation (5.1-2) of the stator windings (in stator coordinates) and the voltage equation (5.3-4) of the rotor windings (in the rotor coordinates). The stator flux linkages and the rotor flux linkages are defined in equation (5.5-6) and (5.7-8).

The total magnetization current i_m is defined as the air gap flux divided by the main inductance Lm.

$$\psi_m = L_m I_m$$

$$i_m = i_s + i_r$$

With the help of equation (5.5-8) an alternative magnetization current is defined which is valid in any reference frame:

$\psi_{rm} = L_m i_{rm}$

$I_{rm} = i_s + (1+\sigma) i_r$

Where

$\sigma = L_{rl}/L_m$ is the rotor leakage factor.

The rotor vector becomes a scalar in its own reference frame:

$$\psi_r = \begin{bmatrix} \psi_r \\ 0 \end{bmatrix}$$

Transformation of the derivative of the rotor flux vector from rotor coordinates (equation 5.3-4) to rotor flux coordinates is done by rotating this vector over angle $\theta_d = \rho - \theta_r$ (see figure (5.1)). This leads to:

$$\dot{\psi}_{r(\alpha\beta)} = \frac{d}{dt}\begin{bmatrix} \cos\theta_d & -\sin\theta_d \\ \sin\theta_d & \cos\theta_d \end{bmatrix}\begin{bmatrix} \psi_{rd} \\ \psi_{rq} \end{bmatrix} = \frac{d}{dt}\left[e^{j\theta d}\begin{bmatrix} \psi_{rd} \\ \psi_{rq} \end{bmatrix}\right]$$

where $e^{j\theta d} = \begin{bmatrix} \cos\theta_d & -\sin\theta_d \\ \sin\theta_d & \cos\theta_d \end{bmatrix}$ and $\frac{d}{dt} e^{j\theta d} = \dot{\theta} e^{j\theta d} e^{j\left(\frac{\pi}{2}\right)}$

$$= e^{j\theta d}\begin{bmatrix} \dot{\psi}_r \\ 0 \end{bmatrix} + \dot{\theta}_d e^{j\theta d} . e^{j\left(\frac{\pi}{2}\right)} \psi_r$$

$$= e^{j\theta d}\begin{bmatrix} \dot{\psi}_r \\ 0 \end{bmatrix} + \dot{\theta}_d \, e^{j\theta d} . \begin{bmatrix} 0 \\ \psi_r \end{bmatrix}$$

$$= e^{j\theta d}\begin{bmatrix} \dot{\psi}_r \\ \dot{\theta}_d \, \psi_r \end{bmatrix}$$

with the help of the last equation, vector equation (3-4) yields in the field oriented coordinates:

$$e^{j\theta d}\begin{bmatrix} \dot{\psi}_r \\ \dot{\theta}_d \, \psi_r \end{bmatrix} = -R_r . i_{r(\alpha\beta)} = -R_r . e^{j\theta d} i_{r(dq)}$$

$$\dot{\psi}_r = -R_r i_{rd}$$
$$\dot{\theta}_d \, \psi_r = -R_r i_{rq}$$

This means that the magnetizing rotor current (i.e. the induced magnetizing current component in the vector windings) originates from the variation of the flux value and the torque-producing rotor current originates due to the rotation of the flux vector with respect to the rotor. The frequency $\dot{\theta}_d$ of the rotor flux with respect to the rotor is called the rotor flux slip frequency.

The rotor flux magnitude is calculated by integrating the $\dot{\psi}_r = -R_r i_{rd}$:

$$\psi_r = \int \dot{\psi}_r dt$$

The equations $\psi_{rm} = L_m i_{rm}$ and $I_{rm} = i_s + (1+\sigma) i_r$ yield the relation between the rotor current and the stator currents:

$$-i_{rd} = \frac{1}{1+\sigma_r}\left(i_{sd} - \frac{\psi_r}{L_m}\right)$$

$$-i_{rq} = \frac{1}{1+\sigma_r}\left(i_{sq}\right)$$

The above equations and in addition $\dot{\psi}_r = -R_r i_{rd}$ and $\dot{\theta}_d \psi_r = -R_r i_{rq}$ are the central equations of the current-feed induction motor model. When the rotor flux slip frequency is added to the rotor speed, the rotor flux frequency with respect to the stator is obtained:

$$\dot{\rho} + \dot{\theta}_d = \dot{\theta}_r$$

The frequency is integrated to obtain in the field orientation angle ρ:

$$\rho = \int \dot{\rho} \ \ dt$$

This angle is used to transform the input current vector from the stator frame to the rotor flux reference frame:

$$\begin{bmatrix} i_{sd} \\ i_{sq} \end{bmatrix} = e^{-j\rho} \begin{bmatrix} i_{sa} \\ i_{sb} \end{bmatrix}$$

where $e^{-j\rho} = \begin{bmatrix} \cos\theta_d & \sin\theta_d \\ -\sin\theta_d & \cos\theta_d \end{bmatrix}$

The equations mentioned above belong to the equation system of the current fed induction machine.

5.4 APPROXIMATED TEST SIGNAL VOLTAGE VECTOR USING ROTOR FLUX AND STATOR CURRENTS

The stator voltage vector is calculated from the estimated rotor flux and the measured stator currents in the field oriented coordinates. The calculation starts from the stator voltage equations.

The voltage equations $\overline{V}_{sa} = R_s.\bar{i}_{sa} + \frac{d\overline{\psi}_{sa}}{dt}$, $\overline{V}_{sb} = R_s.\bar{i}_{sb} + \frac{d\overline{\psi}_{sb}}{dt}$ the stator flux linkages in the arbitrary reference frame $\psi_{sx} = \psi_l + L_{ls}i_{sx}, \psi_{sy} = \psi_l + L_{ls}i_{sy}$ and the rotor flux linkages $\psi_{rx} = \psi_l + L_{lr}i_{rx}$, $\psi_{ry} = \psi_l + L_{lr}i_{sr}$ in the arbitrary reference frame yield the following equation:

$$\overline{V}_{s(ab)} = R_s.\bar{i}_{s(ab)} + \frac{d}{dt}\left(\overline{\psi}_{r(ab)} - L_{rl}.i_{r(ab)} + L_{ls}.i_{s(ab)}\right)$$

This equation is transformed to rotor flux coordinates:

$$R(\rho)\overline{V}_{s(dq)} = R_s.e^{j\rho}.\bar{i}_{s(dq)} + \frac{d}{dt}\left[e^{j\rho}.\left(\overline{\psi}_{r(dq)} - L_{rl}.i_{r(dq)} + L_{ls}.i_{s(dq)}\right)\right]$$

$$R(\rho)\overline{V}_{s(dq)} = R_s.e^{j\rho}.\bar{i}_{s(dq)} + e^{j\rho}.\left(\overline{\psi}_{r(dq)} - L_{rl}.i_{r(dq)} + L_{ls}.i_{s(dq)}\right) + \dot{\rho}.e^{j\rho}e^{j\frac{\pi}{2}}.\left(\overline{\psi}_{r(dq)} - L_{rl}.i_{r(dq)} + L_{ls}.i_{s(dq)}\right)$$

After rotation of -ρ, this yields:

$$\overline{V}_{s(dq)} = R_s.\bar{i}_{s(dq)} + \dot{\overline{\psi}}_r - L_{rl}.\dot{i}_{r(dq)} + L_{ls}.\dot{i}_{s(dq)} + \dot{\rho}.e^{j\frac{\pi}{2}}\left[\overline{\psi}_r - L_{rl}.i_{r(dq)} + L_{ls}.\dot{i}_{s(dq)}\right]$$

Split into real and imaginary components, this equation yields:

$$\overline{V}_{sd} = R_s.\bar{i}_{sd} + \dot{\overline{\psi}}_r - L_{rl}.\frac{d}{dt}i_{rd} + L_{ls}\frac{d}{dt}.i_{sd} - \dot{\rho}.\left[-L_{rl}.i_{rq} + L_{ls}.\dot{i}_{sq}\right]$$

$$\overline{V}_{sq} = R_s.\bar{i}_{sq} - L_{rl}.\frac{d}{dt}i_{rq} + L_{ls}\frac{d}{dt}.i_{sq} + \dot{\rho}.\left[\psi_r - L_{rl}.i_{rd} + L_{ls}.\dot{i}_{sd}\right]$$

The above equation can be analyzed from a different prospective:

The well-known voltage equations for induction machine are expressed as follows:

$$\overline{V}_{sd} = R_s.\bar{i}_{sd} + \frac{d\overline{\Psi}_{sd}}{dt} - j\omega\overline{\Psi}_{sd}$$

$$\overline{V}_{sq} = R_s.\bar{i}_{sq} + \frac{d\overline{\Psi}_{sq}}{dt} + j\omega\overline{\Psi}_{sq}$$

$$\overline{V}_{rd} = 0 = R_r.\bar{i}_{rd} + \frac{d\overline{\Psi}_{rd}}{dt} - j(\omega - \omega_r)\overline{\Psi}_{rd}$$

$$\overline{V}_{rq} = 0 = R_r . \bar{i}_{rq} + \frac{d\overline{\psi}_{rq}}{dt} + j(\omega - \omega_r)\overline{\psi}_{rq}$$

Stator flux linkages:

$$\psi_{sd} = L_s i_{sd} + L_m i_{rd}$$

$$\psi_{sq} = L_s i_{sq} + L_m i_{rq}$$

Rotor flux linkages:

$$\psi_{rd} = L_m i_{sd} + L_r i_{rd}$$

$$\psi_{rq} = L_m i_{sq} + L_r i_{rq}$$

Considering the stator and rotor flux linkages for the rotor flux oriented model, that is ψ_{qr}=0 the stator equations can be expressed as:

$$i_{sd} = -\frac{R_r + L_r}{\frac{d}{dt} L_m} P i_{rd}$$

$$i_{sq} = -\frac{L_r}{L_m} i_{rq}$$

$$V_{sd} = \{R_s + (\sigma L_s)P\}\, i_{sd} + \frac{R_r L_m^2 P}{L_r(R_r + L_r P)} i_{sd} - \omega\ \psi_{sq}$$

$$V_{sq} = \{R_s + (\sigma L_s)P\}\, i_{sq} - \omega\ \psi_{sd}$$

Where P is the derivative operator and σL_s is the transient inductance. At zero or low stator frequency, where the magnitude of ω is quite small, $\omega\psi_{sq}(<<V_{sd})$ and $\omega\psi_{sd}(<<V_{sq})$, hence these terms can be neglected.

$$V_{sd} \approx \{R_s + (\sigma L_s)P\} i_{sd} + \frac{R_r L_m^2 P}{L_r\left(R_r + \frac{d}{dt} L_r\right)} i_{sd}$$

$$V_{sq} \approx \left\{R_s + \frac{d}{dt}(\sigma L_s)\right\} i_{sq}$$

For the high frequency components of the voltage the above equation can be written as:

$$\Delta V_{sd} \approx \{R_s + j\omega_i(\sigma L_s)\} \Delta i_{sd} + j\omega_i \frac{R_r L_m^2}{L_r(R_r + j\omega_i . L_r)} \Delta i_{sd}$$

$$\Delta V_{sq} \approx \{R_s + j\omega_i(\sigma L_s)\} \Delta i_{sq}$$

The value of the transient inductance becomes smaller at test frequency than that at zero or low fundamental frequency. Moreover, at test frequency L_m >>L_{sl} & L_{rl}, hence L_m at test frequency can be neglected. Hence σL_s can be further simplified as:

$$\sigma L_s = L_{sl} + L_{rl}\left(\frac{L_m}{L_m + L_{rl}}\right) \approx L_{sl} + L_{rl}$$

Similarly considering the rotor equations the induction motor, a dq-axis impedance diagram can be presented in per phase equivalent circuit as:

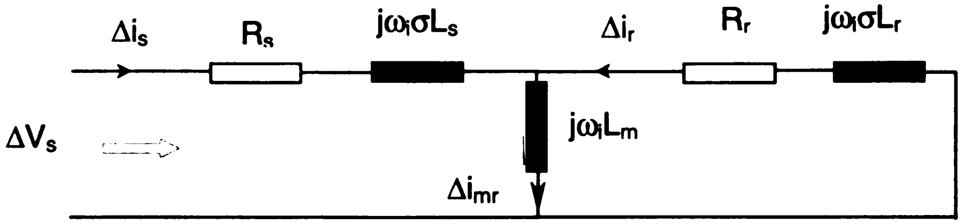

At zero stator-rotor frequency and magnetizing type conditions L_m is very high and can be neglected. Therefore the per phase induction motor machine equivalent circuit can be redrawn without L_m at the test frequency.

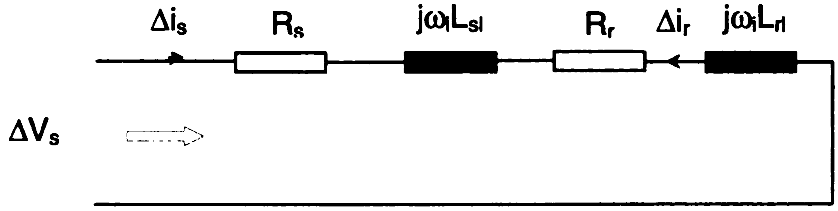

The diagram leads us to the following stator per phase equation, with ΔV_s as the applied two phase stator voltage and Δi_s is the stator test current and Δi_r is the induced test current in the rotor windings.

$$\Delta V_S \approx \Delta i_S.R_S + (-\Delta i_r).R_r + L_{sl}\frac{d}{dt}\Delta i_S + L_{rl}\frac{d}{dt}(-\Delta i_r)$$

Moreover, in a mirror image of the test signal synchronous frame of reference about estimated the d-axis, the voltage equation is

$$\Delta V_S' \approx \Delta i_S.R_S - \Delta i_r R_r - L_{sl}\frac{d}{dt}\Delta i_S + L_{rl}\frac{d}{dt}\Delta i_r$$

Subtracting the two voltages

$$\Delta V_S - \Delta V_S' \approx 2\Delta i_S.R_S - 2\Delta i_r R_r$$

As evident, the component on the right-hand side ($\Delta i_r R_r$) of the above equation can be used to directly give information conceming the displacement angle γ. The above equation approximation is valid if the test frequency is sufficiently high and the operating frequency $\dot{\rho}$ (ω_m) of the flux angle to be measured is not too high. These conditions are normally met in the low flux frequency range.

5.5 APPROXIMATED TEST SIGNAL VOLTAGE VECTOR USING VOLTAGE MODEL

$$\begin{bmatrix} V_{sa} \\ V_{sb} \\ V_{ra} \\ V_{rb} \end{bmatrix} = \begin{bmatrix} R_s + L_{sa}P & L_{ab}P & L_{ma}P & L_{ab}P \\ L_{ab}P & R_s + L_{sb}P & L_{ab}P & L_{mb}P \\ L_{ma}P & \omega_r L_m + L_{ab}P & R_r + L_{ra}P & \omega_r L_r + L_{ab}P \\ -\omega_r L_m + L_{ab}P & L_{mb}P & -\omega_r L_r + L_{ab}P & R_r + L_{rb}P \end{bmatrix} \cdot \begin{bmatrix} i_{sa} \\ i_{sb} \\ i_{ra} \\ i_{rb} \end{bmatrix} \quad (5.9)$$

The above equation 5.9 parameters are derived and explained in chapter 3. In this section the given derivation is used for simulating the approximated test signal voltage vector. The model was simulated but has coupling effects and assumptions that can not be realized in real time applications. To overcome this problem the equation needed to be de-coupled to make the simulation compatible to the real time application. The vector components in equation 5.9 are detailed in chapter 3.

$L_{sa}=L_{sl}+L_{ma}$

$L_{sb}=L_{sl}+L_{mb}$

$L_{ma}=L_0+L_2\cos(2\mu)$

$L_{mb}=L_0-L_2 \cos(2\mu)$

$L_{ab}=L_2*\sin(2\mu)$

Where $L_0=(L+L_m)/2$; $L_2=(L-L_m)/2$; and

$$L = \frac{d|\overline{\psi}r|}{d|\bar{i}_{mr}|}$$

$$L_m = \frac{|\overline{\psi}_r|}{|\bar{i}_{mr}|}$$

$$L_{ma} = L\cos(2\mu) + L_m\sin(2\mu)$$

$$L_{mb} = L.\cos(2\mu) + L_m\sin(2\mu)$$

$$L_{rd} = L_{rl} + L_{ma}$$

$$L_{rq} = L_{rl} + L_{mb}$$

$$L_r = L_{rl} + L_m$$

$$L_s = L_{sl} + L_m$$

Then the voltage equation become:

$$\begin{bmatrix} V_{sa} \\ V_{sb} \\ V_{ra} \\ V_{rb} \end{bmatrix} = \begin{bmatrix} R_s & 0 & 0 & 0 \\ 0 & R_s & 0 & 0 \\ 0 & \omega_r.L_m & R_r & \omega_r.L_r \\ -\omega_r.L_m & 0 & -\omega_r.L_r & R_r \end{bmatrix} \cdot \begin{bmatrix} i_{sa} \\ i_{sb} \\ i_{ra} \\ i_{rb} \end{bmatrix} + \begin{bmatrix} L_{sa} & L_{ab} & L_{ma} & L_{ab} \\ L_{ab} & L_{sb} & L_{ab} & L_{mb} \\ L_{ma} & L_{ab} & L_{ra} & L_{ab} \\ L_{ab} & L_{mb} & L_{ab} & L_{rb} \end{bmatrix} \cdot \overset{\bullet}{\begin{bmatrix} i_{sa} \\ i_{sb} \\ i_{ra} \\ i_{rb} \end{bmatrix}}$$

Splitting them in stator and rotor equations:

$$\begin{bmatrix} V_{sa} \\ V_{sb} \end{bmatrix} = \begin{bmatrix} R_s & 0 & 0 & 0 \\ 0 & R_s & 0 & 0 \end{bmatrix} \cdot \begin{bmatrix} i_{sa} \\ i_{sb} \\ i_{ra} \\ i_{rb} \end{bmatrix} + \begin{bmatrix} L_{sa} & L_{ab} & L_{ma} & L_{ab} \\ L_{ab} & L_{sb} & L_{ab} & L_{mb} \end{bmatrix} \cdot \overset{\bullet}{\begin{bmatrix} i_{sa} \\ i_{sb} \\ i_{ra} \\ i_{rb} \end{bmatrix}}$$

$$0 = \begin{bmatrix} 0 & \omega_r L_m & R_r & \omega_r L_r \\ -\omega_r L_m & 0 & -\omega_r L_r & R_r \end{bmatrix} \cdot \begin{bmatrix} i_{sa} \\ i_{sb} \\ i_{ra} \\ i_{rb} \end{bmatrix} + \begin{bmatrix} L_{sa} & L_{ab} \\ L_{ab} & L_{mb} \end{bmatrix} \cdot \overset{\bullet}{\begin{bmatrix} i_{sa} \\ i_{sb} \end{bmatrix}} + \begin{bmatrix} L_{ra} & L_{ab} \\ L_{ab} & L_{rb} \end{bmatrix} \cdot \overset{\bullet}{\begin{bmatrix} i_{ra} \\ i_{rb} \end{bmatrix}}$$

In
th
st
ec
fre

which gives:

$$\begin{bmatrix} V_{sa} \\ V_{sb} \end{bmatrix} = \begin{bmatrix} R_s & 0 & 0 & 0 \\ 0 & R_s & 0 & 0 \end{bmatrix} \cdot \begin{bmatrix} i_{sa} \\ i_{sb} \\ i_{ra} \\ i_{rb} \end{bmatrix} + \begin{bmatrix} L_{sa} & L_{ab} \\ L_{ab} & L_{sb} \end{bmatrix} \cdot \begin{bmatrix} \dot{i}_{sa} \\ i_{sb} \end{bmatrix} + \begin{bmatrix} L_{ma} & L_{ab} \\ L_{ab} & L_{mb} \end{bmatrix} \cdot \begin{bmatrix} \dot{i}_{ra} \\ i_{rb} \end{bmatrix}$$

$$\begin{bmatrix} \dot{i}_{ra} \\ i_{rb} \end{bmatrix} = \begin{bmatrix} L_{ra} & L_{ab} \\ L_{ab} & L_{rb} \end{bmatrix}^{-1} \left\{ \begin{bmatrix} 0 & \omega_r L_m & R_r & \omega_r L_r \\ -\omega_r L_m & 0 & -\omega_r L_r & R_r \end{bmatrix} \cdot \begin{bmatrix} i_{sa} \\ i_{sb} \\ i_{ra} \\ i_{rb} \end{bmatrix} + \begin{bmatrix} L_{ma} & L_{ab} \\ L_{ab} & L_{mb} \end{bmatrix} \cdot \begin{bmatrix} \dot{i}_{sa} \\ i_{sb} \end{bmatrix} \right\}$$

In the above model the states are the rotor currents. The rotor currents (i_{sd}, i_{sq}) in the rotor flux reference frame are the inputs, and are then transformed to the stator reference frame (i_{sa}, i_{sb}). Using the Matlab-simulink the stator voltage equation is estimated and was used for calculating the test signal at very low flux frequency, see figure 4.9.

Chapter 6

SATURATED MODEL PARAMETERS-SIMULATION

Computer programs were developed to simulate the limitations of the scheme used for the project. Basically there are two methods in computing the transient performance of a.c. machines; either the currents or the flux linkages can be taken as state variables. When currents are chosen for the saturated model, differentiation of inductance with respect to magnetizing current arises, and when flux linkages are chosen it does not.

To simulate the control response of the field-oriented control drive systems at zero or near zero fundamental frequency. We Inject a high frequency test current in the estimated d-axis of the saturated induction motor model. The machine parameters used for the simulation were different from the machine to be used for the real time application.

To simulate the phenomena in the induction motor which take place due to saturation, a large magnetizing current is used to create flux levels significantly larger than the nominal rated flux. The saturation magnetizing current graph, figure 6.1, indicates that in order to obtain values in excess of 1.3 to 1.5 times the rated flux requires magnetizing currents of more than two times the rated current. Hence, for the project analysis the flux obtained with i_{ds} approximately 150% o f the rated current was used.

6.1 INCREMENTING OF INDUCTANCE IN SATURATED MODEL

Including of the saturation of induction motor model in the field oriented induction machine modeling requires of knowledge of the motor saturation curve. Therefore, the saturation curve was first plotted by simulation of unsaturated model. Figure 6.1 illustrates typical magnetization characteristic for the induction machine, showing the nonlinear relationship between the rotor magnetization current and the magnetization flux linkages Ψ_{mr} used for this project. This magnetization curve was obtained by using the parameters of induction machine given in [13-14]. The unsaturated area was approximated to match the linear parts of the machine model. The same parameters of the machine were used for simulation.

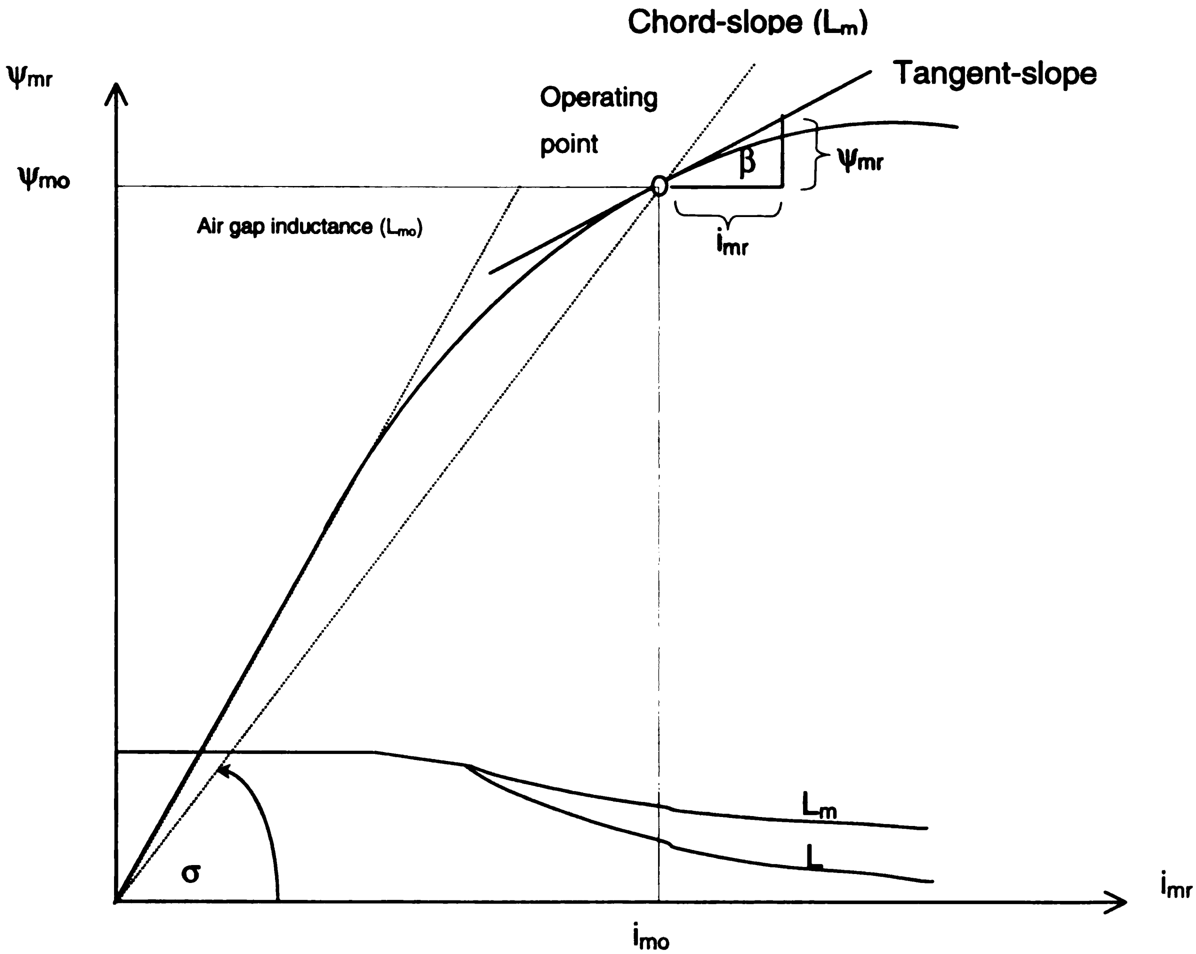

Figure 6.1 Magnetization curve

In a current fed field oriented induction motor, i_{sd} (at steady state equal to i_{mr}) is the magnetizing current and is a known variable. Figure 6.1 clearly shows that the high flux levels predicted by the unsaturated model cannot be achieved when the motor is saturated, i.e. operated well above the knee of the curve.

The variation in magnetizing inductance $L_m = \frac{|\psi_{mr}|}{|i_{mr}|}$ (also called cord inductance) and the variation of the dynamic inductance $L = \frac{d|\psi_{mr}|}{d|i_{mr}|}$ (also called tangent inductance and is the first derivative of the magnetizing curve) and, also the air gap inductance L_{mo} (unsaturated model inductance) are plotted in figure 6.1. These inductances can be treated as the known parameters derived from the magnetization curve. It can be seen from the figure 6.1 that in the linear part of the magnetizing curve, $L=L_m=L_{mo}$. The two inductances L_m and L take into account the fact that in general i_{mr} is continuously changing due to injected test frequency.

For saturation induction motor model, Lm and i_{dr} become functions of the d-axis magnetizing currents, i_{ds} and i_{dr}. The field orientated motor model aligns the rotor flux with the d-axis. Thus to a first approximation, saturation will occur in d-axis, but not in q-axis. To reflect this in the model, the saturation value L_m was only used in the q-axis calculations.

The reason for choosing L and L_m, for the saturated motor model can be further elaborated. From figure 6.1 it seems clear if we consider an incremental change which results in a change in the amplitude of the mmf wave. The resulting flux wave amplitude is a nonlinear function of the total mmf (steady state plus incremental change) and the chord slope reactance will not correctly express the change. Instead, the tangent slope to the magnetizing curve, identified as the "transient saturated inductance" gives the appropriate relation between the change in flux amplitude and the change in mmf amplitude. Therefore, in the saturated model of this thesis, for incremental current variations which result in change of saturation level, the tangent slope inductance or "transient saturated inductance" is employed. For incremental current changes which effects only the phase of the flux as well as for terms proportional to the operating point flux (speed voltages), the chord slope steady state inductance is used.

Moreover, in case of the d-axis, the flux Ψ_{mdis} is equal to Ψ_{mr} the instantaneous amplitude flux. In general, this component of the flux will be in the vicinity of or above the "knee" of the magnetizing characteristic, where saturation becomes important. The magnetizing inductance is effectively the transient saturated inductance, the slope of the tangent of the magnetizing characteristic at the operating point. It can be imagined that the operating point continuously moves along the saturated region of the magnetizing characteristic during the dynamic process. The corresponding tangent at the operating point continuously changes its slope as well. Therefore it is simply necessary to incorporate the non-linear magnetizing characteristic itself into the d-axis portion of the dq-model.

The above statement can be summarized as: that the component in line with the flux (y-axis) tends to change the saturation level and its analysis requires use of the tangent slope inductance. The other component (x-axis) and all steady state terms use the normal chord slope inductance.

6.2 SATURATED FLUX MODEL

From the discussion in the previous section, it is clear that due to the saturation of the main-flux paths the magnetizing inductances in the direct and quadratic axis are different, and thus the self-inductance of the stator windings are also different. Similarly, the self-inductances of rotor windings is also different.

For simulation, the system of this project is an indirect field orientation scheme, shown in figure 6 2. The main assumptions will be those used during the derivation of the space-vector equations for linear model. The magnetizing curve in figure 6.1 shows that the high flux levels predicted by the unsaturated model cannot be achieved when the motor is saturated. Hence the new flux model (saturated model) requires modifying the flux reference trajectory to also account for saturation. If this is not done, the control effort can easily command more voltage and current than the inverter can supply. The equations in the next page is the saturated model.

$$\tau_r^{*} \frac{d\left|i_{mr}\right|}{dt} + \left|i_{mr}\right| = i_{sd}$$

$$\omega_{mr} = \omega_r + \frac{i_{sq}}{\tau_r \left|\bar{i}_{mr}\right|}$$

where

$$\tau_r^{*} = \tau_r\left(\frac{L}{L_m}\right) = L\left(\frac{L_{rl} + L_m}{L_m R_r}\right)$$

$$\tau_r = \left(\frac{L_r}{R_r}\right) = \left(\frac{L_{rl} + L_m}{R_r}\right)$$

igure 6.

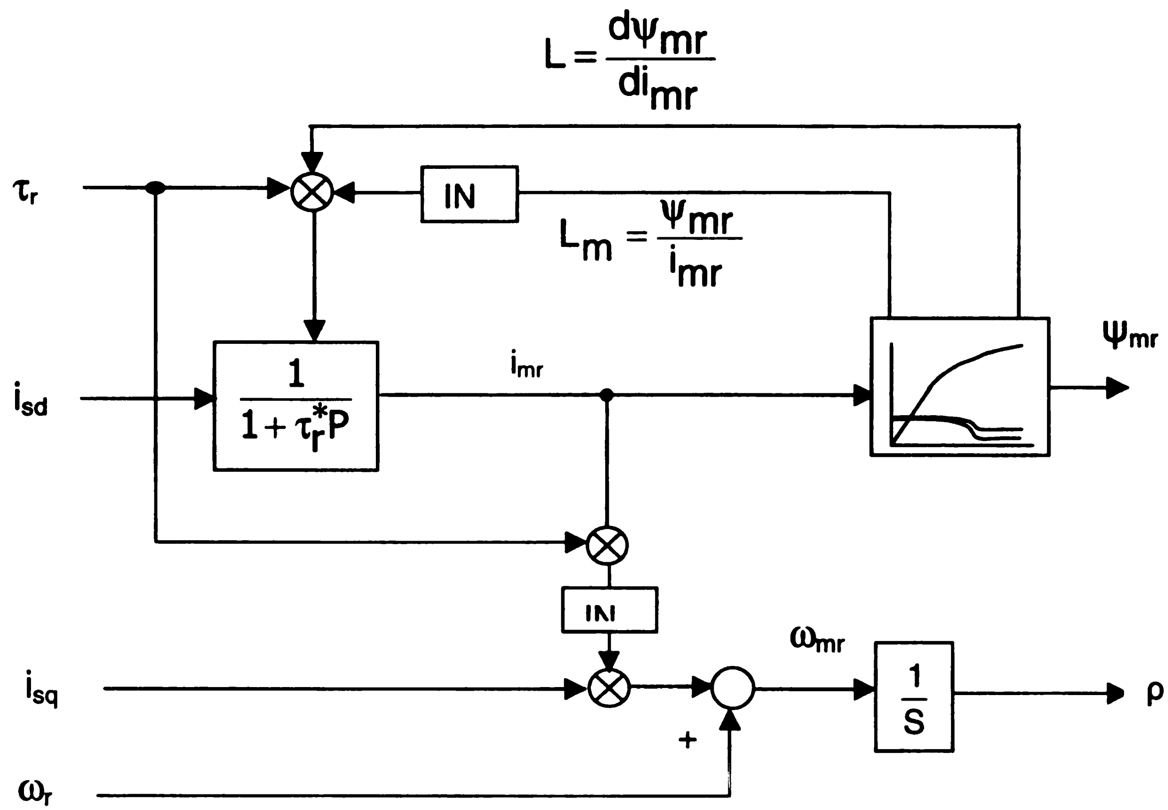

Figure 6.2 Field-Oriented Saturated Induction Motor Current-Fed Model

6.3 FLUX MODEL UNDER DYNAMIC AND STEADY STATE CONDITIONS

Since the flux is dynamically varying in amplitude, it must be accurately tracked to ensure that field orientation is achieved. The saturation model, which predicts the level of flux, is therefore important. In this section the saturation model is discussed, which is used for the simulation to study the limitation of the proposed scheme.

The assumptions on which field oriented flux model equations are based, are essentially the same as those for the unsaturated two axis model except that the main flux saturation in the flux axis (d-axis) is incorporated. As can be seen a subtle difference between the two models exists with respect to the division of the flux into leakage and magnetizing components. In the conventional model this division is actually quite arbitrary; any division whatsoever can be assumed and completely equivalent model results if the remaining parameters are properly evaluated. This is no longer true for the saturated model and, in principle, the division of leakage must be known to obtain an accurate representation. The effects of the saturation of the leakage flux paths are neglected and only the effects of the main flux saturation are incorporated in the analysis. In this thesis the correct calculated value of leakage inductance is treated as a constant value, both for stator and rotor leakage inductance, which has secondary effect and has not shown much effect on the simulation results. Also, it's clear from figure 6.3 that the flux linkages in the saturated model are not much different from each other. Moreover, the stator leakage inductance (L_{sl}) and the rotor leakage inc

[22

inc

tra

an

sig

6.4

i_{sq} i

of

wh

ass

is u

inductance (L_{rl}) are small (less than 5 percent of the magnetizing inductance) [22]. Since $L_s=L_{sl}+L_m$; $L_r=L_{rl}+L_m$; and $L_{sl}<<L_m$; $L_{rl}<<L_m$ the magnetizing inductance dominate during steady state operation. However, during a large transient, because of saturation there is not a large change in the flux component and the difference between the three flux components, shown in figure 6.3 is not significant.

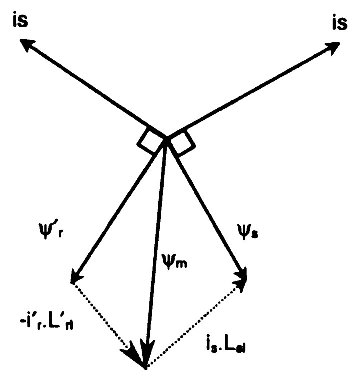

Figure 6.3 Induction machine flux linkages space phasors

6.4 ALIGNMENT OF SATURATED MODEL

When the saturated properties of the motor are included, the ratio of i_{sd} to i_{sq} is altered by the nonlinear relationship between i_{sd} and Ψ_{dr} and hence the ratio of i_{sq}/i_{sdq} increases in the unsaturated case. This difference occurs because, when saturated, increasing i_{sd} produces proportionally smaller flux Ψ_{rd}.

Since field orientation control provides flux only in the d-axis, it can be assumed that saturation only occurs in the d-axis. Hence, only d-axis saturation is used to track the amplitude and angle of the test current in the actual and estimated rotor flux reference frame. As a result, the q-axis parameters in the slip frequency $\omega_s = L_{mq} i_{qs}/(\tau_{rq}\ \Psi_{dr})$ do not vary with $\Psi_{dr.}$ However, d-axis parameter $L_{md} = L_m$ and τ_{rq} in the rotor flux equation $\Psi_{dr}=(L_{md}\ i_{ds})/(1+\tau_{rd})$ will be a function of the flux.

6.4.1 The Rotor Current Equations

To examine the effects of stator and rotor mmf on the resultant rotor flux under field-orientation, the relationship between the induced rotor currents and the impressed stator currents are formulated by using equation:

$$i_{rd} = -\frac{L_m}{L_r}\frac{\tau_r p}{R_r + \tau_r p} i_{sd} = (i_{mr} - i_{sd})\frac{L_m}{L_r}$$

$$i_{rq} = -\frac{L_m}{L_r} i_{sq}$$

Where, $A=L_m i_{sdq}$, $A'=L_m i'_{sdq}$, $B'=L_r i'_{dq}$ and $B=L_r i_{rdq}$ Also in the model of the induction motor: $i'_m=i_{mx}+i_{my}=i_m+j0=i'_s+i''_r=i_{mx}+j0=i_{sx}+i_{rx}+j(i_{sy}+i_{ry})$ It follows that the quadrature-axis magnetizing components is zero; $i_{my}=i_{sy}+i_{ry}=0$.

6.4.2 Steady State:

Steady state rotor flux is given by $\Psi_{dr}=L_m i_{sd}$, where i_{sd} is the total magnetizing current (i_m) of the d-axis. It can be seen from the rotor current equations and figure 6.5 that the d-axis component of rotor current is zero under constant flux operation. Therefore, the rotor current vector will align with the q-axis which is orthogonal to the rotor flux vector, see figure 6.6. From the rotor q-axis current equation the induced q-axis rotor current is linearly proportional to the impressed q-axis stator current. The Phasor diagram in figure 6.4 illustrates the current component of a field-oriented induction motor under variation in q-axis stator current from i_{qs} to $i'_{qs'}$ under constant i_{ds}. The resultant flux is composed of two components contributed by the stator and rotor currents as shown in figure 6.4 denoted by A and B respectively.

6.4.3 Transient Conditions

In the transient case, the rotor winding of the induction motor carries induced currents that combine with i_{ds} to form i_m and produce Ψ_{dr}. During (torque) transients (increased torque), the associated flux component ($L_m i_{qs}$) due to i_{qs} is exactly cancelled by opposing flux ($L_r i_{qr}$) produced by the induced q-component rotor current (since $L_r i_{qr}=-L_m i_{qs}$). In short, dynamically i_{dr} is proportional to the rate of change of i_{sd}. Therefore, is in response to change in i_{sd}, an opposing i_{rd} is induced to oppose that change and the total flux is unaffected. Hence, by injecting high frequency test current in the d-axis a continuosly dynamic condition is created. The resulted phenomena lead to the deviation angle between the test stator and induced test rotor currents. This phenomena allows to tracking of the actual rotor flux path.

As stated above, the relationship between d-axis current and rotor flux is a first order low pass function. This prohibits fast flux changes. As a result, it can be stated that the torque response to change of current i_{qs} is instantaneous, the response of rotor flux Ψ_{rd} to change of current is inertial with time constant τ_r.

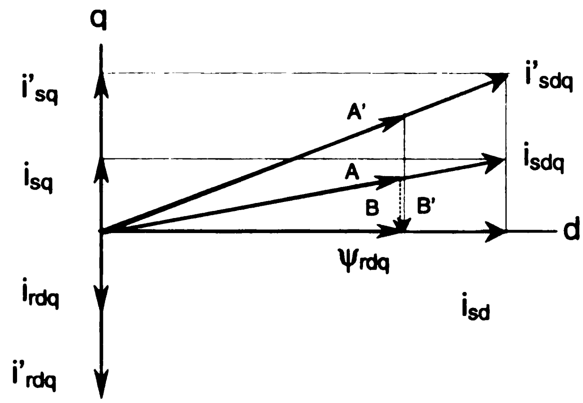

Figure 6.4 Vector components under field orientation

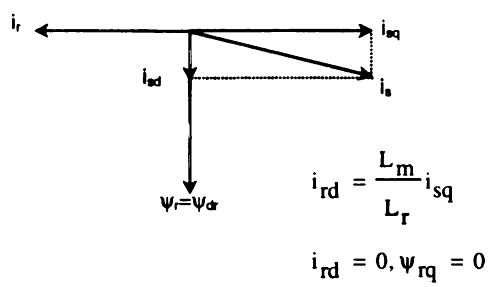

Figure 6.5 Fundamental Component current and flux vectors in the rotor flux field oriented under steady state loaded condition

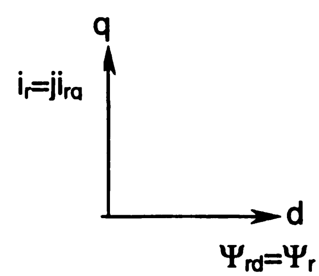

Figure 6.6 Vector of rotor current and flux in a field-oriented induction motor.

6.5 CONCLUSION:

Field orientation control provides flux only in the d-axis, it can be assumed that saturation only occurs in the d-axis. Hence only d-axis saturation is used for the flux model and for calculating the fundamental rotor current components for further processing or calculating the rotor

The motor flux saturated model includes both L_m (chord inductance) and L (tangent inductance). Due to saturation, the fundamental rotor current uses L_m (chord inductance) for both d and q-axis of the rotor current components.

By injecting a high frequency test current in the d-axis a continuous dynamic condition is created, which leads to the determination of the rotor flux position. Test rotor currents, due the saturation effects, produces different factors k_1 and k_2 as given below. These factors are independent of the test frequency and are valid at around zero fundamental power frequency:

$$\Delta i_{rd} = -k_1 i_{sd}$$

$$\Delta i_{rq} = -k_2 i_{sq}$$

where

$$k_1 = \frac{L}{L_r} = \frac{L}{L_{rl} + L} = \frac{1}{1 + \frac{L_{rl}}{L}} = \frac{1}{1 + \frac{L_{rl}}{\tan\beta}}$$

$$k_2 = \frac{L_m}{L_r} = \frac{L_m}{L_{rl} + L_m} = \frac{1}{1 + \frac{L_{rl}}{L_m}} = \frac{1}{1 + \frac{L_{rl}}{\tan\sigma}}$$

Chapter 7

SIMULATION RESULTS

7.1 TRACKING THE DISPLACEMENT ANGLE (γ)

Two different sets of simulation were run in order to evaluate the motor performance under the proposed scheme:

a) It was assumed first that the motor rotor currents could be measured, and compared to the stator currents. A partial model of the proposed scheme was used, as shown in figure 7.1.

b) The estimator method was simulated as it is implemented in the experiment. This complete scheme has already been discussed and shown in figure 4.9.

Figure 7.2 presents the results of simulation and verified experimentally. For simulation and on line implementation different parameters motors were used. In both the cases, it verifies relationship between the errors in the flux position, $\rho - \hat{\rho}$, and the resulting displacement angle, γ, between the applied stator test current $\Delta\bar{i}_s$ and the corresponding rotor current $\Delta\bar{i}_r$. Except for a dc offset, there is proportionality that can be used for correction of the estimated rotor angle. Figure 7.3 presents the results of a simulation where this angle γ, is used to drive a PI controller that corrects the estimated rotor flux angle.

1/
tra
the

The same measurements on the actual experiment were conducted on a 1/12-hp induction machine. The experimental results demonstrate that a trackable signal of the shifting angle in the test frequency exits which can lead the rotor flux estimation at very low and zero frequency.

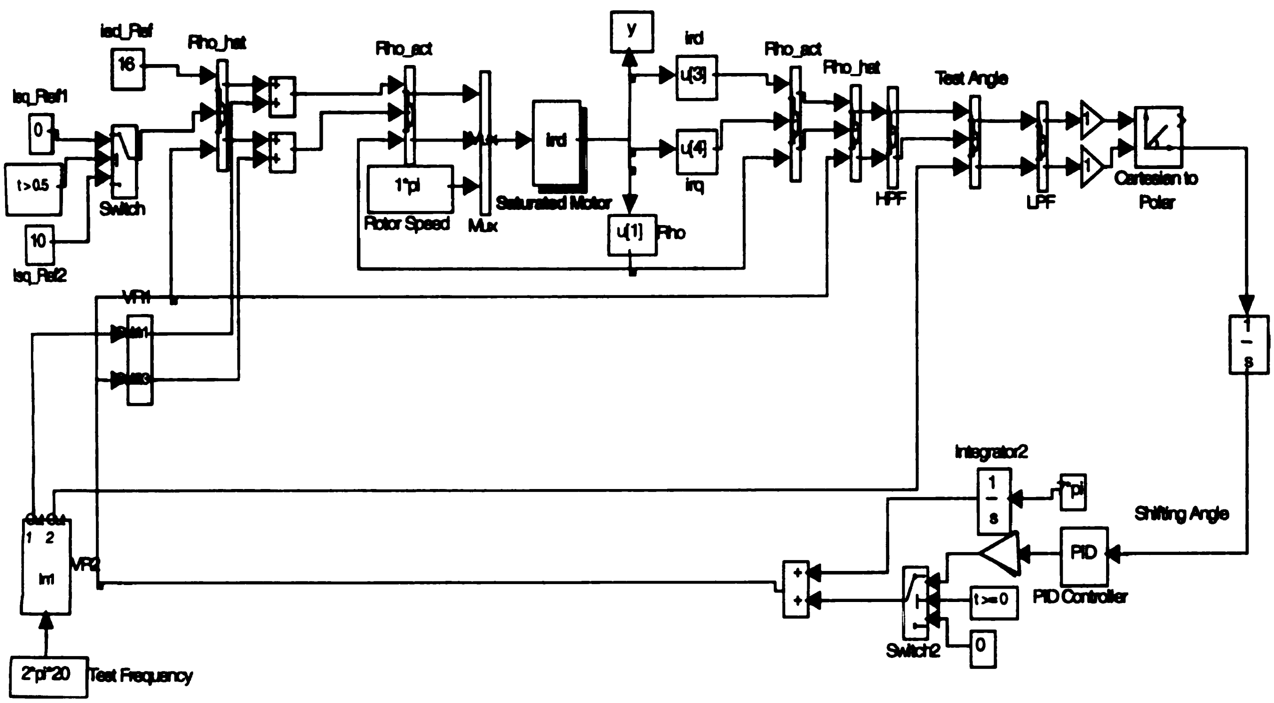

Figure 7.1 Simulation model for saturated Motor

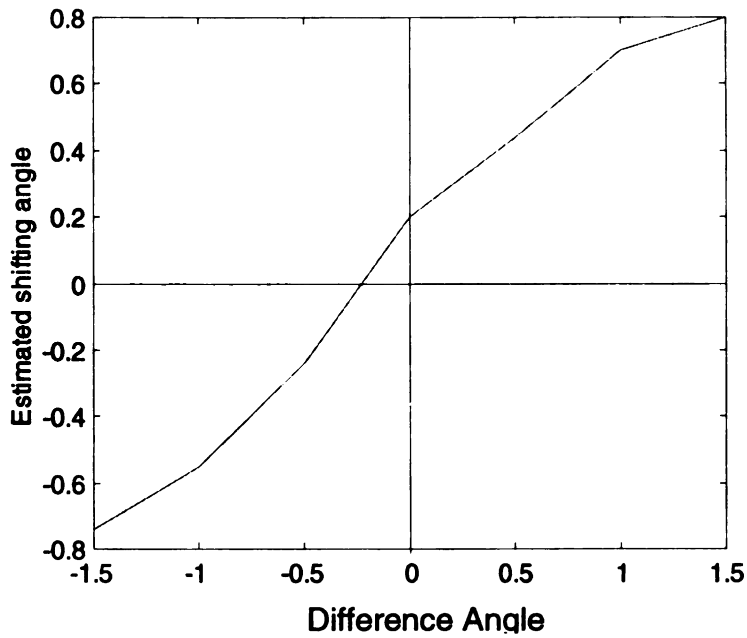

Figure 7.2 The Error Angle Vs the angle between actual and estimated flux

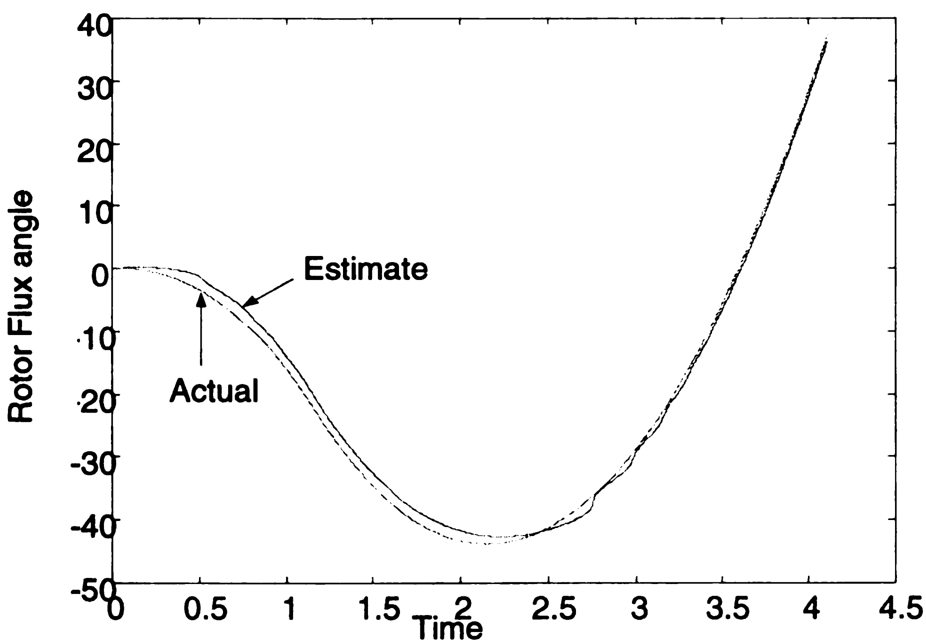

Figure 7.3 Using the angle γ to correct for rotor flux estimation

7.2

7.2.

orde

curr

q-axi

with

and t

This

betw

rotor

angle

one

shiftin

angle

wheth

estim

positio

7.2 LIMITATION OF THE PROPOSED METHOD

7.2.1 Loss Of Saturation

In the proposed method, magnetic saturation of the rotor is necessary in order to create saliency. This saturation can be accomplished by applying stator current component, $i_{sd,}$ that is on the same axis as the rotor flux. As a result, the q-axis parameters in the slip frequency do not vary much (small change in L_m) with Ψ_{dr}. However, the d-axis parameters i.e. the tangent inductance L ($Lm \neq L$) and the rotor time constants in the rotor flux equations are functions of the flux. This effect leads to the displacement angle in the rotor flux reference frame, between the stator test current and the induced rotor test current.

It is very important to understand that in the test magnetizing current in the rotor flux reference the shifting angle or displacement angle γ depends on the angle difference (error angle) δ between the real flux axis ρ and the estimated one $\hat{\rho}$. In other words the shifting angle is proportional to the error angle. The shifting angle and the difference angle have opposite directions and the shifting angle becomes zero when δ is zero. The shifting angle γ clearly indicates whether the estimated flux axis $\hat{\rho}$ corresponds with the real axis or whether the estimated one is leading or lagging the real one.

As explained in section 4.4, using the rotor current to construct rotor flux position shows basic consequences of the saturation effects. Due to saturation the chord inductance and the tangent inductance are not equal, hence, the induced rotor test current vector does not have the same direction as the test stator current vector. As result of the difference in these two currents, the shifting or displacement angle γ is generated. This angle will exist as long as the motor is operated well above the knee of the magnetization curve and the estimated flux axis $\hat{\rho}$ is not aligned with the real flux axis ρ (i.e. $\hat{\rho} \neq \rho$). The angle will not appear if the motor goes out of saturation, even if the $\hat{\rho} \neq \rho$. It is important to note that the scheme presented in this thesis is based on the conditions that the motor is fully saturated.

Simulation results revealed a limitation in the proposed scheme in that the estimated rotor flux is sensitive to the angle difference between the estimated and the actual flux. When the angle error is not too large, as in figure 7.4 a large value of estimated magnetizing current would also result in large value of actual magnetizing current i_d, thus maintaining saturation. If the angle error is big, it will result in loss of induction motor main-field saturation, due to the decrease in the actual excitation current $i_{d.}$ Figure 7.5. Then, when the error angle is large, even a large value of estimated magnetizing current will result in small value of actual magnetizing current i_d, thus driving the motor out of saturation. Hence, a technique has to be developed to keep the flux constant, at an operating point around the zero power frequency operation.

Figure 7.7 shows the variation of rotor magnetization current due to the increase in the displacement angle γ. The lower part of figure 7.6 shows the effect of the angle error, δ , on the shift angle, γ, that is used for correcting the estimation of the rotor flux position. When this angle error become large it was difficult to use the value of γ. Figure 7.7 shows how for a fixed value of i_{sd} command in the estimated flux frame, the values i_{sd}, i_{sq} and i_{mr} changed, leading to loss of saturation.

For simulation the commanded i_{sd} was kept at high value to keep the motor in saturation for larger difference value. In actual implementation keeping the value i^*_{sd} beyond two to three times the rated value may leads to excessive losses and high current demands from the inverter. Hence, adding the feed back can solve this limitation of the system and the stability can be obtained.

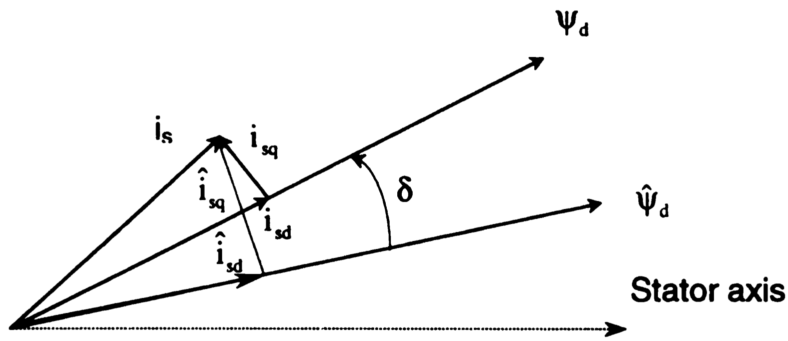

Figure 7.4 Saturated condition due to small estimated flux

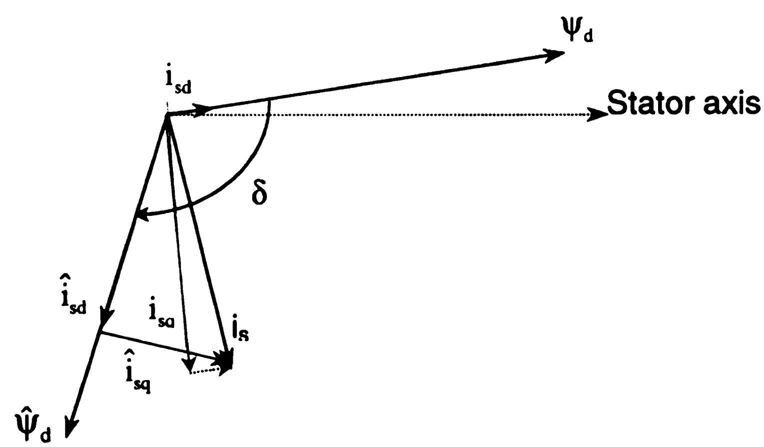

Figure 7.5 Loss of saturation due to large estimated flux

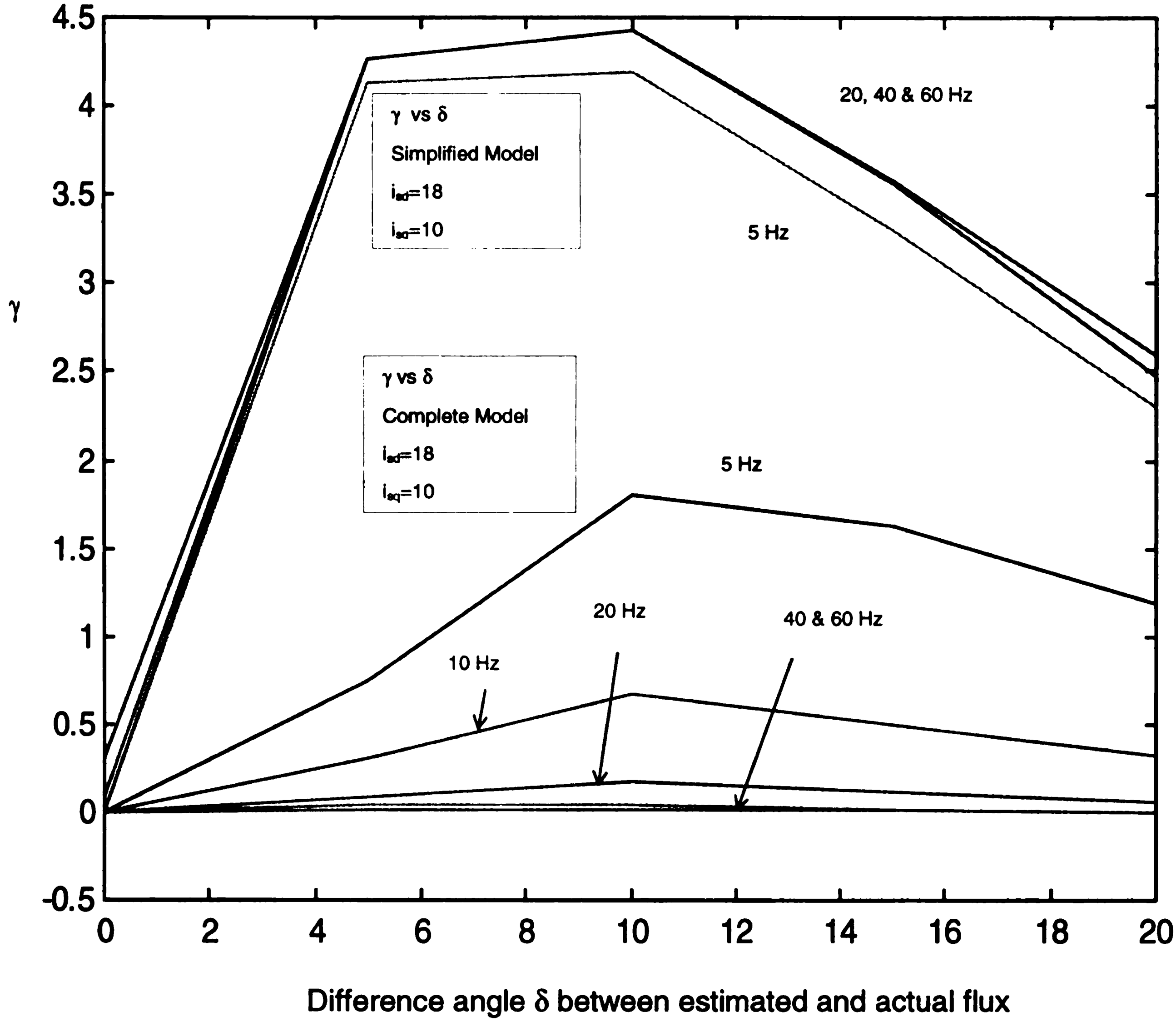

Figure 7.6 Effects of large angle error and increased test frequency on the shift angle, γ.

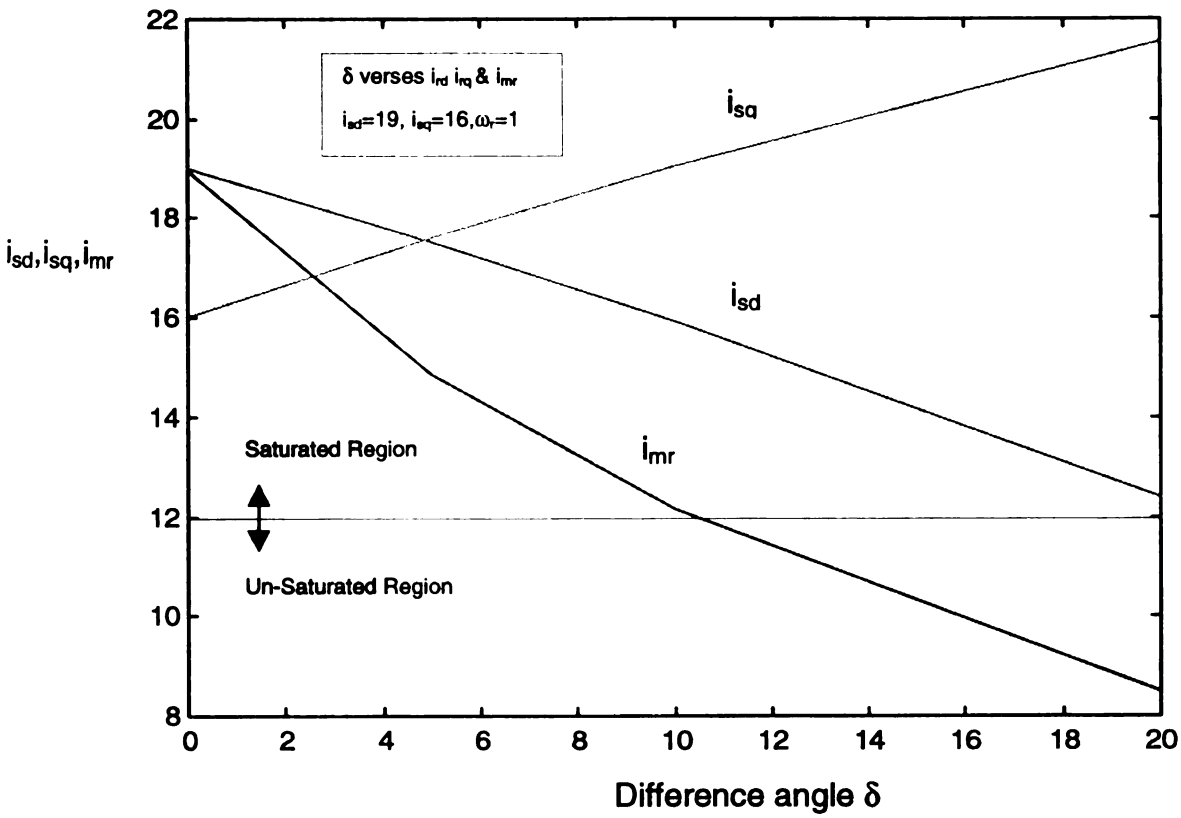

Figure 7.7 Variation in magnetizing parameters

7.2.2 Power Frequency Limits

Since in the realization of the proposed method it is impossible to use the rotor currents, we rely on the effect these currents have on the stator voltage. We consider the stator voltage equation in the rotor flux frame of reference:

$$\overline{V}_{s(dq)} = R_s.\bar{i}_{s(dq)} + \dot{\overline{\psi}}_r - L_{rl}.\dot{i}_{r(dq)} + L_{ls}.\dot{i}_{s(dq)} + \dot{\rho}.e^{j\frac{\pi}{2}}\left[\overline{\psi}_r - L_{rl}.i_{r(dq)} + L_{ls}.\dot{i}_{s(dq)}\right]$$

When operating at low power frequency, the rotor flux frequency $\dot{\rho}$ will be negligible and the values in the equation within the parentheses will have no effect on the stator voltage equation. Moreover, at test frequency $L_m >> L_{sl}$ & L_{rl}, hence L_m at test frequency can be neglected. This effect leads us to the following approximate equation:

$$\overline{V}_{s(dq)} = R_s.\bar{i}_{s(dq)} + \dot{\overline{\psi}}_r - L_{rl}.\dot{i}_{r(dq)} + L_{ls}.\dot{i}_{s(dq)}$$

This approximation is useful in extracting information about angle γ, and it is valid if the magnetizing test current frequency is sufficient high; in addition, the operating frequency $\dot{\rho}$ of the flux angle to be estimated has to be low. These conditions are met only in the region of small power frequencies. As explained in chapter 4, the quadrature component of the above-simplified equation directly gives information concerns the displacement angle γ.

7.2.3 Test Frequency Limits

The analysis presented in chapter 4 for the relationship between stator and rotor currents is valid when the test frequency is sufficiently low. The top curves in figure 7.6 show the effect of saturation for a variety of test frequencies, under the simplification that these test frequencies are adequately low. Indeed, the results show little effect of the test frequency on the angle γ.

On the other hand, when the complete model is used for simulation, the effect of test frequency is pronounced. As shown in the lower curves, obtained with the complete motor model, for the method to be valid the frequency of the injected test currents must be below 10 Hz.

Section 7.2.2 and 7.2.3 impose two contradictory requirements on the frequency of the test currents: it has to be sufficiently low so that the test stator current will be reflected on the corresponding rotor current, and sufficiently higher than the power frequency so that these rotor currents will have an effect on the stator voltage. The two requirements mean that the proposed method is feasible only in small region of power frequencies near DC, and the test frequencies should be between 5 and 10 Hz.

7.3 FIELD WEAKENING

Another limitation of the saturation-based approach is field weakening operation. Robust tracking of saturation-induced saliencies requires operation at flux levels that are considerably higher than normal or rated. The maximum operational speed is then limited by core loss and/or stator voltage. Obviously, field-weakening operation beyond base speed is not possible. Therefore, to obtain wide speed range operation, including field weakening, the high frequency injecting scheme has to be combined with a scheme suitable for high-speed operation. Suitable method were investigated that will provide a smooth transition to high power frequency operation. The rotor based direct field orientation (DFO) technique is used, explained in chapters 1 and 2.

7.3.1 Selection of Scheme for High Speed Operation.

The system analyzed in this thesis is capable of changing dynamically, i.e during operation of the drive, the reference frame of the test current injected controller without any change of the controller hardware opens new perspectives of the induction motor drives. Drives that have to operate over a wide speed range can combine now, with the test current injected controller, different control strategies. For instant, at low speed range or around zero frequency range the test current injected controller is set to saturated condition. At higher speeds and in the flux weakening area, DFO with rotor flux controller is preferable. In this way the best of the best schemes are implemented without additional hardware and software of the controller.

7.3.2 Rotor Based Direct Field Orientation

Figure 7.9 shows the diagram of a rotor based direct-filed orientation. In this system, the stator flux is estimated form the rotor voltages and phase currents in the stator reference frame:

$$\psi_s = \int (V_{as} + R_s i_s) dt$$

$$\psi r = \frac{L_r}{L_m}(\psi_s - \sigma L_s i_s)$$

$\rho = a\tan\frac{\psi_{rb}}{\psi_{ra}}$ is the rotor flux angle in the rotor flux reference frame.

The success of rotor based DFO depends on good estimation of the stator flux. The stator flux is obtained by integrating the phase voltage minus the voltage drop in the stator resistance. In the implementation of online system the dc offset in the voltage and current minimized by using the band pass filter and digitizing it using bi-linear transformation. Further, to maintain the accuracy of the estimated flux quantities, correct values of machine parameters are needed. In particular the stator resistance plays a crucial role in the stator flux estimation at low speeds, it is important to identify the correct value of this parameter.

7.3.3 Smooth Transition

From a saturated magnetization curve and vector diagram one can derive that a change of the reference vector also requires a change of the commanded value of the flux (i^*_{sd}). Otherwise the motor will be operating in saturated mode and this would lead to high losses in the system and inability of the inverter to provide the required voltage. To cope with this problem one can calculate the two different schemes every sampling cycle. Due to the high processing speed of the processor (see chapter 8) the two controllers can be operated sequentially using the same routine for both schemes. Doing so, both reference frames of interest processor are in stand-by. The input command of the controller for the slow speed and the higher speed value can be calculated from the rotor flux speed or comparing the torque producing current components. However, the two routines have

smo

figur

this

The

of th

the

have to be provided in order switch from one reference to another. This way the smooth transition in simulation and on line implementation can be achieved see figures 7.8. The matlab simulink block diagram is shown in figure 7.9 used for this thesis for smooth transition from the saturated model to the rotor based DFO. The smooth transition could not be achieved properly and requires more analysis of the transfer technique. The system transfer tested several time, in most cases the transfer process was not stable.

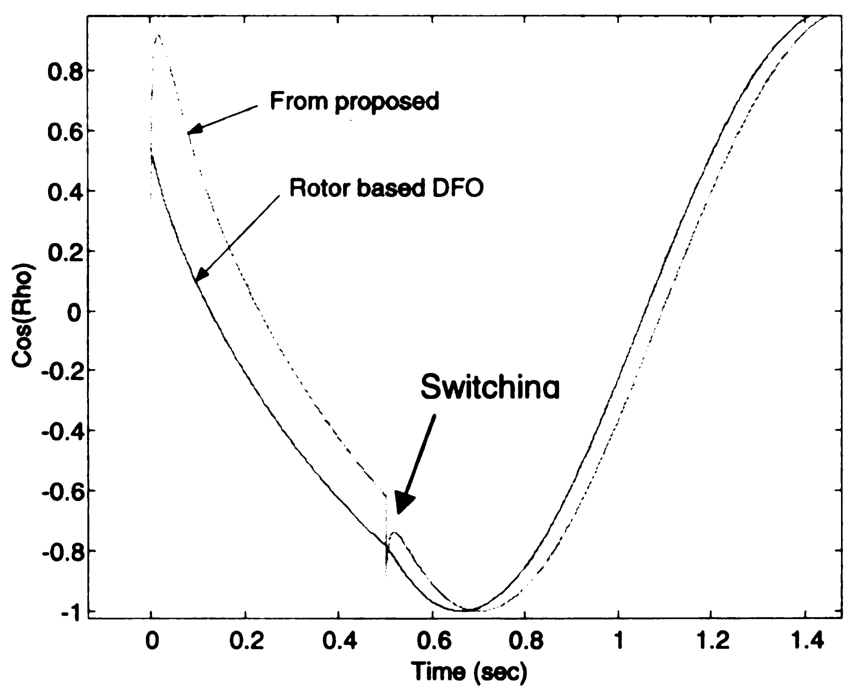

Figure 7.8 Transition from DFO to Estimated Error method

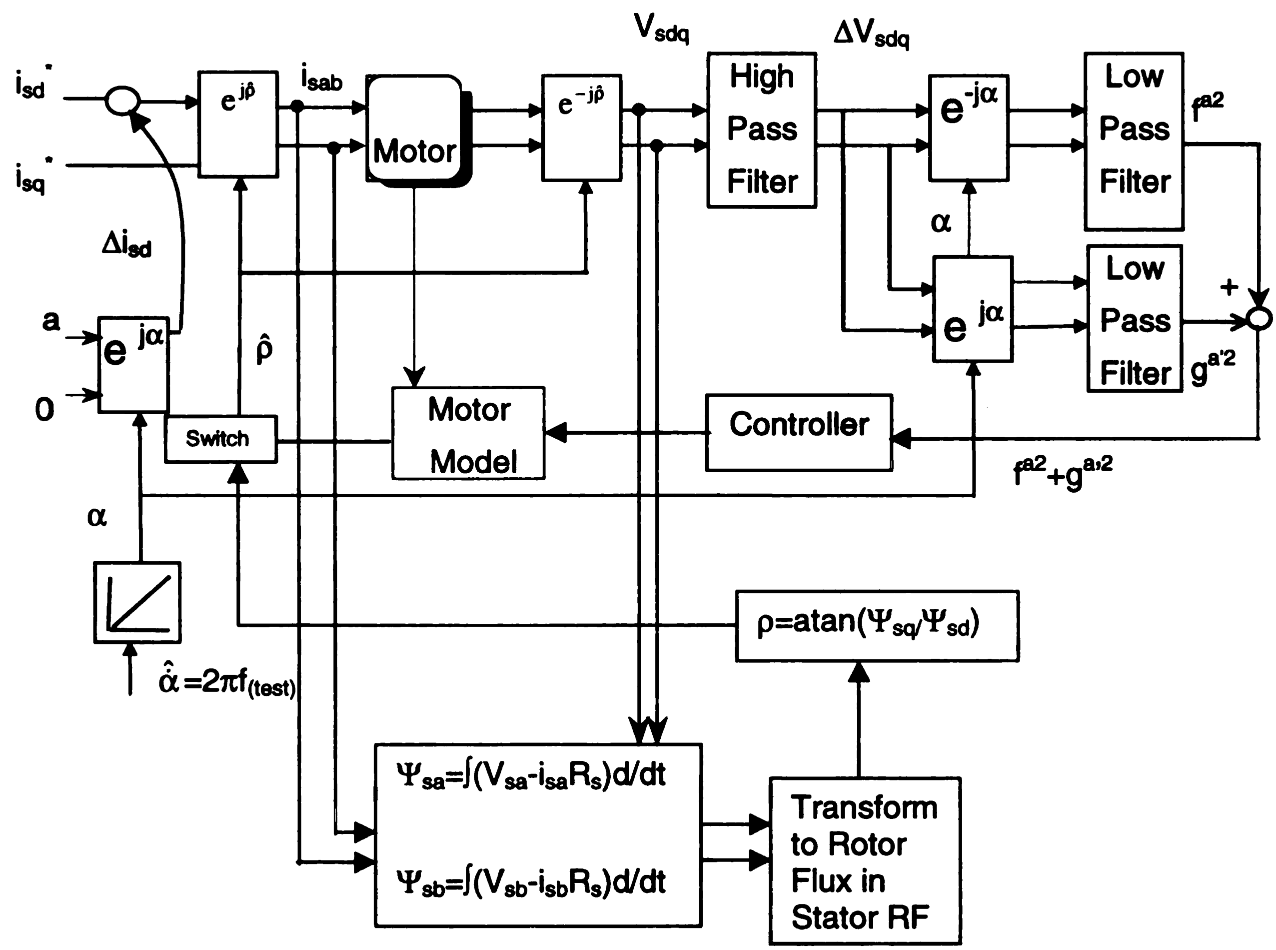

Figure 7.9 Switch from saturated model to DFO simu-link block

Chapter 8

EXPERIMENTAL SET-UP

8.1 INTRODUCTION

Real-time computing is an important area of computer engineering due to the fact that computer systems must interface and deal with the real world, where certain time constraints are often present. Real-time systems must generate the desired outputs from given inputs, but the time at which these results are produced and delivered is of equal importance. The computer processor handles this task.

Real Time Lunix is an extension to the Linux operating system, which allows for the execution of real-time tasks. It uses an ingenious technique to circumvent the apparently inherent non-real-time nature of the operating system. With RT-Linux we can take total control of the PC (we used PC because for the moment there is no implementation of RT-Linux for any other architecture) as for the case of MSDOS. During a real time task it is possible to access all the ports of the PC, install interrupt handlers, and temporally disable interrupts.

The advantages of using PC hardware in embedded systems are by now well known. In contrast to much hardware developed specifically for the embedded market, PC hardware is mass-produced, easily available, and cheap.

We can expect interface boards such as analog and digital I/O boards, network interfaces, and image acquisition and processing boards to cost more than twice as much when designed for the VME bus as for one of the PC buses.

When field orientation is used the induction machine can be controlled to provide high dynamic performance. To achieve this performance, flux angle has to be calculated both fast and accurate. During a short cycle time the complete set of real-time calculations has to be performed. This set of calculations can be very large when it embodies a model of the induction machine, the field-orientated control model, speed and/or torque controllers and parameter estimators. Until 15 years ago, a sampling time (which is also the real-time calculating time step) that was small enough was not possible with the real available microprocessors. For this reason until recently often analog controller were used for the field orientation control of AC drives.

The increasing use of PC hardware is one of the most important developments in high-end embedded systems in recent years. Hardware costs of high-end systems have dropped dramatically as a result of this trend, making feasible some projects which previously would not have been done because of the high cost of non-PC-based embedded hardware. But software choices for the embedded PC platform are not nearly as attractive as the hardware. One can choose DOS, with its well-known limitations; Microsoft Windows, with its lack of real-time capability; or one of the high-end real-time operating systems, which are expensive, proprietary, and mostly non-portable. The Linux operating system presents an attractive alternative to these options, having none of the above disadvantages. RT-Linux is used for this thesis.

Using pentium processors at 400 and 450 MHz and the RT-Linux environment the gap between simulation and experiment can be closed. The System is much faster, reliable and cheaper especially in data processing, than the DSP system. The necessary calculation and input/output speed of real time simulation can be achieved and the performance of the analog simulator can be matched. The analog part should consist of the interface between the PC-processor and analog signal from the machine (A/D converter for voltage and current measurement). The advantages of using RT-Linux in a PC processor in particular as opposed to DSP are:

- higher reliability, because no boards and wire connection is inside the computer.
- flexibility of models and control structure because of the high-level software implementation;
- no debugger and measured data transfer interface program are required. Data is directly stored for processing with MATLAB and printing.
- easy change of model parameters and inputs (software);
- output of any signal to media: hard disk, floppy drives; after saving the data all kinds of signal processing can be performed without designated software.

- no standard configuration files are created to perform initialization of the system software (timers, interrupt vectors, I/O cards, etc).

8.2 EXPERIMENTAL CURRENT CONTROL HARD WARE SET-UP

8.2.1 Experiment Drive Setup

The drive setup is shown in figures 8.1 to 8.3 are explained below. In case of simulation, part of figure 4.9 is used. In the experiment the same induction models are used to control the real drive system.

1. The experiment drive setup consists of a PC-based controller using Linux operating system with analog to digital (A/D) data accusation system, for induction motor control, as shown in figure 8.1.
2. A 3-phase, 1/12 HP, 60 Hz induction motor is connected through a voltage controlled current regulated hysteresis-PWM inverter. The three-phase hysteresis current control PWM inverter is composed of 3-phase, 60 Hz, 208 V_{LL}, AC/DC converter and a 10 kHz IGBTs switches.
4. The three-phase motor, stator voltage measurements and stator current measurements are done by using voltage transducers (VTs) and current transducers (CTs) as see figure 8.1.
5. The analog output signals from VTs and CTs are transformed to the digital signals are obtained by using a 12 bit A/D converter. The 12-bit AD 7874 converter has 8-μsec/channel conversion time and has

four-channel simultaneous sampling capacity. These characteristics are ideally suited for use in the induction motor vector control.

6. Six digital signals from the PC-based controller are fed to the inverter IGBTs switches, through the switching control board. These digital signals are produced after comparing the estimated current values with the reference current signals.

7. Matlab is used to display the measured or simulated voltage, currents, flux, in a rotating or stationary coordinate frame. Magnetic current sensors do the three-phase current measurement.

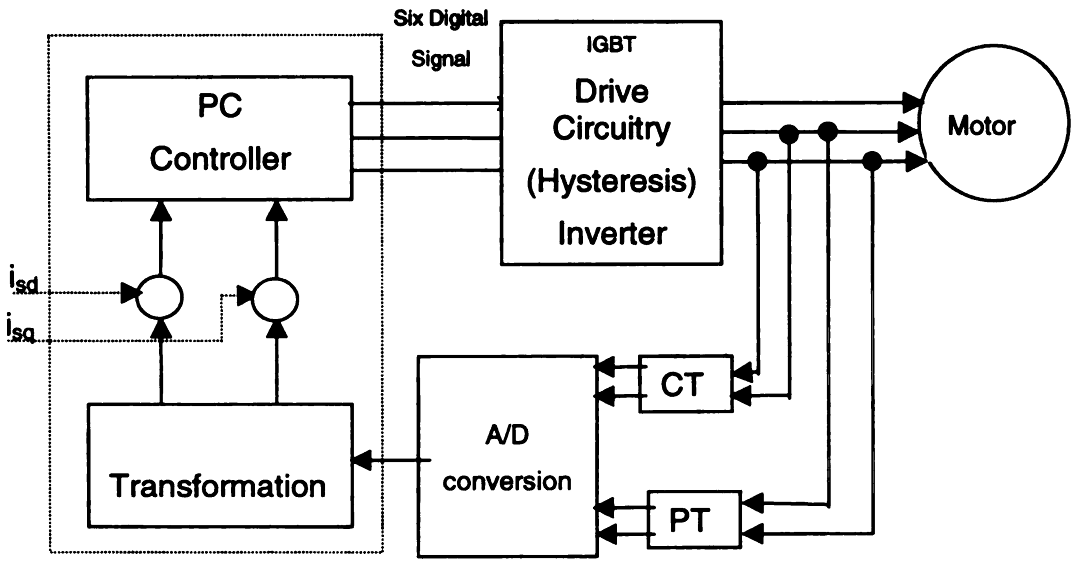

Figure 8.1 Experimental set-up

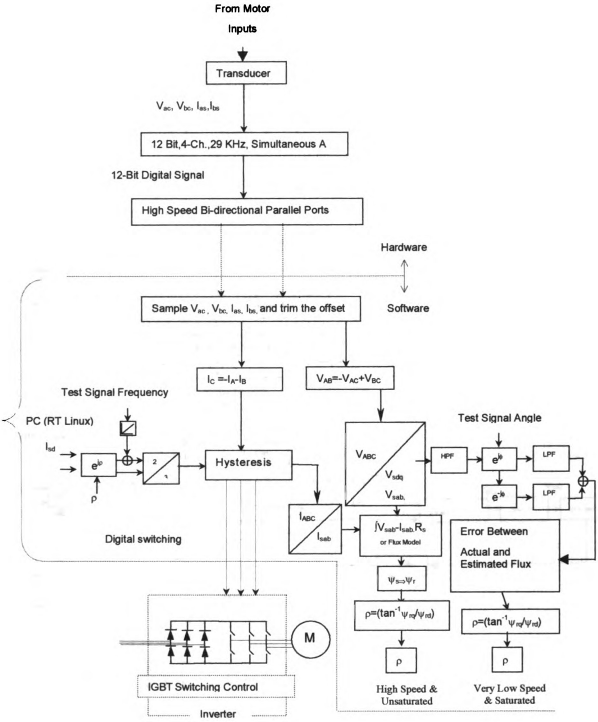

Figure 8.2 Hardware and software schematic of the experimental set up

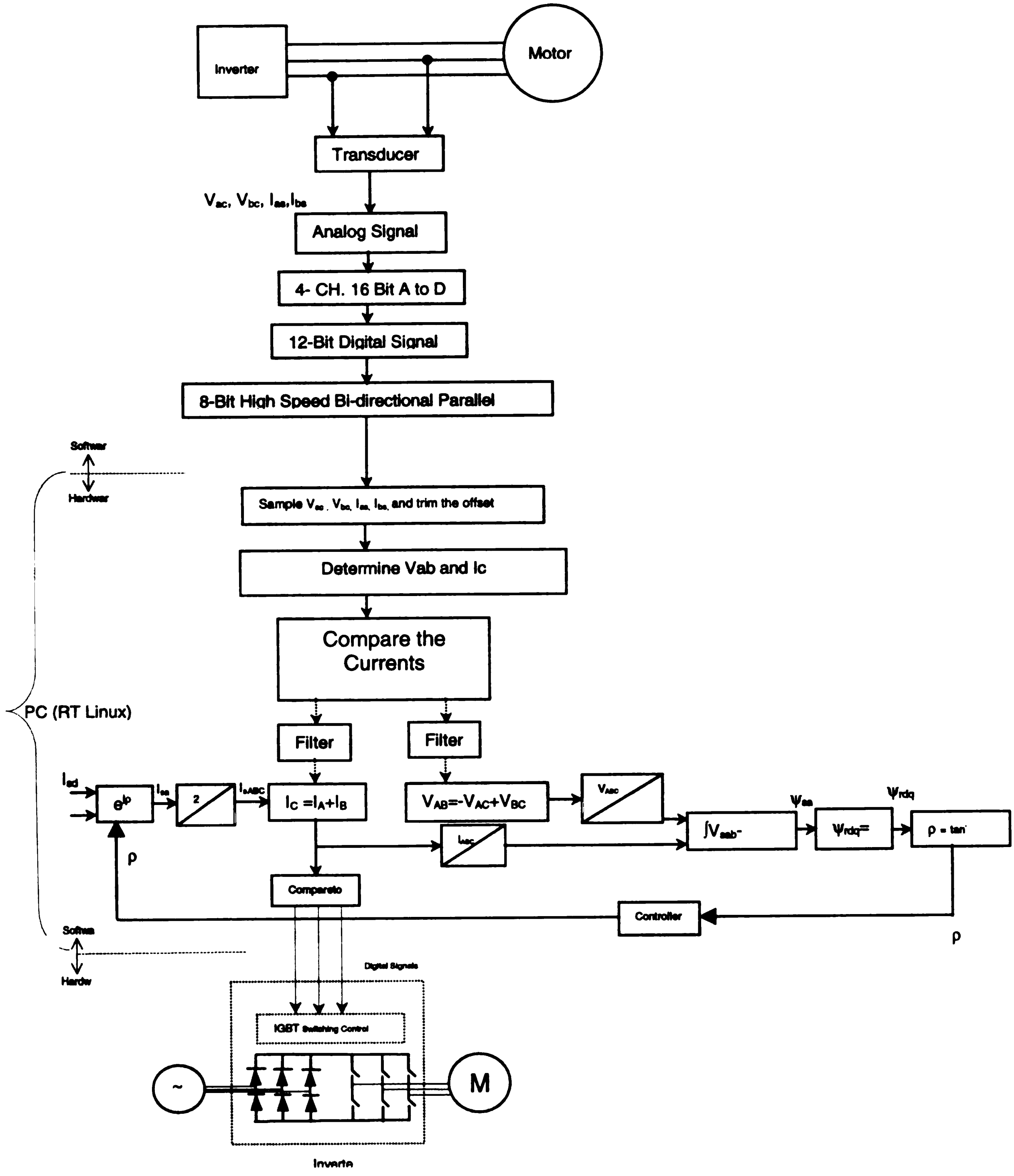

Figure 8.3 Signal flow in the experimental setup

8.3 HYSTERESIS CURRENT CONTROL

The current source can be a voltage inverter hysteresis or PWM controller. In the hysteresis the current controller upper and lower band levels are defined relative to the reference value of the current (see figure 8.4) and the inverter is used to ensure that the actual stator current is limited to between the hysterisis bands. By defining narrow hysteresis bands, it is possible to ensure tight control, but this demands a high switching frequency from the inverter. The actual current contains harmonics, which produce high-frequency torque ripples. These are filtered out by the inertia of the machine so the speed of the machine can almost be free from the effects of these ripples. Compared to the PWM current controller, the hysteresis current controller reacts almost instantaneously to changes in the reference values of the current, and thus the time lag is very small, whereas in the PWM current controller the switching frequency of the inverter is preset and it is easy to determine the time delay between the time the reference changes and when corrective switching action is performed by the current controller.

Impressed stator currents supply the stator windings of the induction machine. The currents are obtained from a current-controlled switching transistor inverter with a high switching frequency. This application is similar to the application of armature current control in a converter-fed d.c. drive. The main advantages of this type of operation is that because of the impressed stator currents, the effects of stator resistance and leakage inductance on the drive dynamics are eliminated and the motor interaction is simplified.

A time delay of 7µs was introduced in the hardware of the inverter used for this thesis. This delay is sufficient to avoid the short circuit in the inverter, while keeping the high switching frequency as demanded by the upper and lower current limits.

The signal flow diagram in figure 8.4 shows three hysteresis controllers, one for each phase. Each controller determines the switching-state of one inverter leg such that the error of the corresponding phase current is maintained within the hysteresis band. The width of the hysteresis is $\pm\Delta i$. The control method is simple to implement, and its dynamic performance is excellent. There are some inherent drawbacks which are not in the scope of this thesis.

Encoder was also connected to find the actual flux angle for estimating the error difference between the actual flux and the created angle difference.

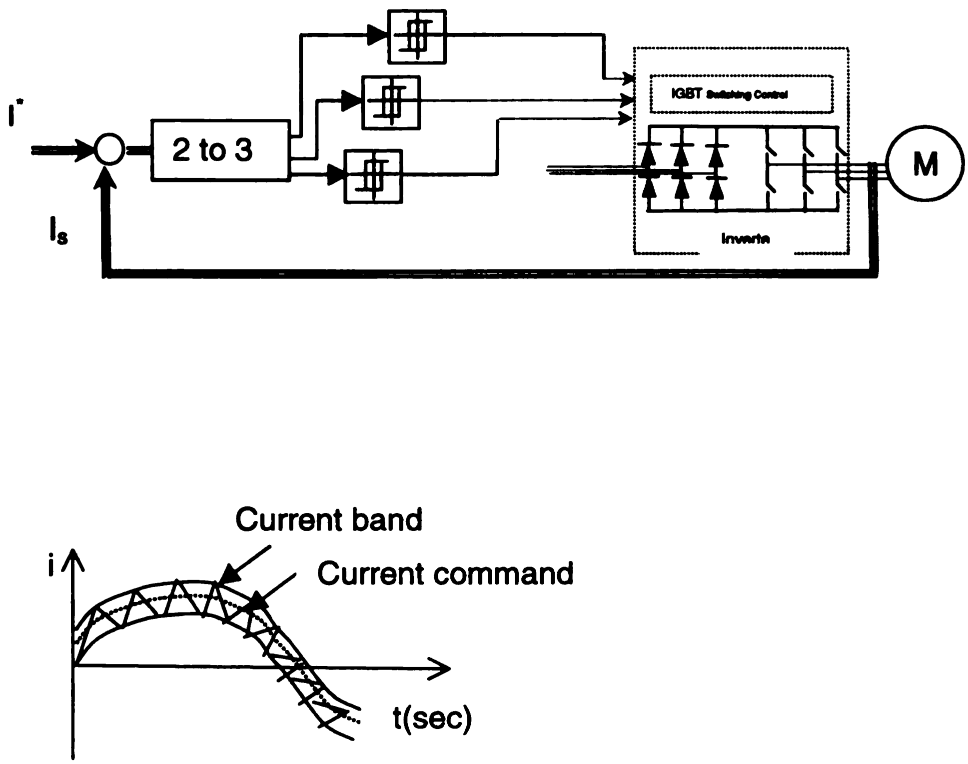

Figure 8. 4 Hysteresis current control: (a) signal flow diagram; (b) basic current waveform.

8.4 DIGITAL TO ANALOG CONVERSION

A very important issue when using digital PC based processor OS is the analog to digital conversion of the measured signals, e.g the induction machine voltages and currents. The A/D converter used in this thesis is AD7874 a four-channel simultaneous sampling, 12-bit data acquisition system. The part contains a high speed 12-bit ADC, on chip reference, on-chip clock and four track/hold amplifiers. This latter feature allows the four input channels to be sampled simultaneously, thus preserving the relative phase information of the four input channels, which is not possible if all four channels share a single track/hold amplifier. This also, makes the AD7874 ideal to sample multiple input channels simultaneously without incurring phase errors between signals connected to several devices. The AD7874 is also fully specified for dynamic performance parameters including distortion and signal-to-noise ratio.

8.4.1 I/O Board

One bi-directional parallel port on-board with options to upgrade to 3 ports and support IRQs, which eliminates system conflicts.

The PC processor used in the control system of this thesis is the Pentium II 400 MHz. It is a 32-bit floating-point unit, a 16-/24-bit fixed-point unit, on-chip memory, and flexible serial and parallel input/out ports. It has the capability of to support wide variety of computation-intensive large numbers of repetitive mathematical operation applications. The arithmetic unit, allows the device to perform up to 25 million floating point operations per second (with clock rate of

400 MHz). This performance was sufficient to satisfy many of the real time algorithms used in my thesis.

8.4.2 Software:

In order to perform real-time simulation and control in an accurate way, it is necessary to calculate the complete machine control process with small time steps. In this thesis the interrupt frequency was high. Hence it was preferred to program the RT-Linux in the C language. A library contains programs for analog and digital inputs and output, as well as C language program to generate a MATLAB data files are given in appendix B-1 and B-2.

Figure 8.1 verify the experimentally the relationship between γ vs δ which leads to the estimation of the rotor flux angle. The encoder was used to find the flux angle using indirect field orientation.

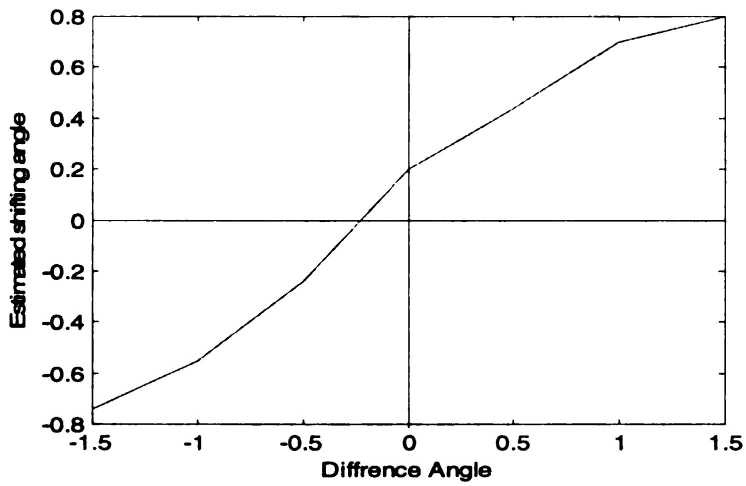

Figure 8.1 The Error Angle Vs the angle between actual and estimated flux

Chapter 9

CONCLUSION

In this work we presented a promising solution to one of the fundamental problem in the induction machine speed control at zero flux frequency, with some limitations. The zero flux frequency is not stable with derivative feedback nor with flux magnitude estimation. Chapter 4 introduced an alternative method that does not replace the existing voltage-current model, but supports it

At zero (or around zero) rotor flux frequency, the stator based DFO and IDFO using voltage-model and current-model are at the stability boundary. The risk of a steady-state flux angle and magnitude error exists if the flux value is not accurate in comparison with the flux command value. This is explained in chapter 1, for the case of a de-tuned but constant main inductance L_m (unsaturated). An improvement of this situation is the operation of induction machine in the saturated condition. This is only necessary in the zero frequency or very low frequency area. It should be restricted to the area to minimize the extra losses caused by the saturation. The low flux frequency is a small operation area to be solved: the operation area around zero flux frequency where saturation could leads to a solution. The scheme presented in section 2.5 indicates that the induction motor speed control scheme at zero frequency is devised in this work can be successfully implemented to solve the problem in the AC machines.

The derivation of the saturated model and assumption of simplified induction motor voltage equations in Chapter 3 and chapter 5 and are the major equations used for the simulation of this thesis. A sensor-less method, which is based upon saturation effect of the induction machine, is used to enable a stable flux determination near zero frequency. Our scheme does not suffer from the integration problem at low frequency.

We investigated the theoretical aspects of the scheme. The algorithm of high frequency injection presented in section 2.5 is applied. However, our design procedure and analysis are fundamentally different from those of [3] due to the use of a rotor flux model and not at the stator flux oriented model.

The algorithm used to control the induction motor at zero frequency is to inject high frequency test current in the d-axis of the saturated stator current. This technique is mostly machine oriented and is now gaining momentum for using it for controlling the AC motors. This high-high frequency magnetizing current injection method is meant to support, but not to replace the stator based DFO and IDFO techniques. It is due to the reason that the DFO and IDFO suffers from the integration problems at low frequency. In proposed scheme the high frequency test current passes through integration process. Its frequency remains high and constant during the filtering process, and hence does not suffer from the integration problem.

Chapter 3 & Chapter 4 deal with saturated motor model control by injecting high frequency test current. Many important contributions have been made in [4]. However, integrating the motor design with high-test frequency, make all of such attempts for special design motors and cannot be applied to any off shelf induction motors.

In this thesis several techniques for estimating the rotor flux at higher speed operation and their performance at low frequency were reviewed. The Direct Stator Flux orientation (DFO) control system rather than the rotor flux (used only at low or around zero frequency) offers the additional advantages of more robust estimation of the flux and direct control of the stator voltage in speed below rated and above i.e. the filed-weakening region. In general, DFO requires more computing power to implement than Indirect Field Orientation, used for the zero or near zero frequency operation.

As a result of the above study we laid the foundation or the development of the extension of our scheme to higher speeds. In this work we identified a direct stator based technique by using the DSFO, which is feasible for both below the low and high-speed operation of the induction motor. In conjunction with that we presented the high frequency limitations of the test injection scheme and the low frequency limitation of the DSFO. The hybrid system used is good from zero to high speed.

The deviation of the main inductance L_m causes a steady-state flux angle and magnitude error due to saturation, as a result of additional inductance (tangent and chord), as explained in Chapter 3. However, in the case of saturation, with proper saturation curve this L-detuning is no longer problematic, as expected. The detuning of the leakage inductance L_l has a very small effect on the stability of the system: the simulation analysis with L_l and analysis without L_l yielded similar results with negligible differences.

More over, the experimental results show the versatile digital control/data acquisition system based on RT-Linux with PC 400 MHz processor and A/D converter presented a good performance for both low and high-speed, filed weakened operation, which needed more computational time. This would bring a a very high speed operation and reduction in the price of on line embedded data acquisition system.

FURTHER RESEARCH

- The proposed system and the transition between this and the DRFO as the speed changes, has to be further investigated both theoretically and experimentally.
- An interesting open question is to extend these results to more general class of AC motors. Also, the results and the technique used in this thesis can bring some ideas to control of electromagnetic operated devices, like linear motors, friction less bearing, etc.
- A further important issue that is not fully studied in this thesis is the effect of parameter detuning. In this thesis almost all contributions are based on the assumption that the system parameters are accurately known. In general, it seems that the operation of the machine in saturation has a positive effect on the parameter sensitivity of the field-orientated control system, especially at low flux frequencies. This appears to be caused by the fact that magnetizing current

variations cause relatively smaller flux variations in case of saturation. The positive effects of saturation (and its extra losses) are still to be analyzed.

- It would be interesting to find adaptive extension of the contributions given in, especially for the most difficult problem of tracking control of the actual excitation current (i_{sd}). To keep the track of the flux angle at very low speed, the magnetization current has to be sufficient in order to keep the motor in saturation condition, irrespective of the angle between the actual flux and estimated flux.

- Further research on the same subject should contain more details of the complete theoretical background of the high-frequency magnetizing-current injection method. Moreover, would be useful to optimize its practical utilization.

- The rotor resistance Rr however has an important effect on the steady state, because the slip frequency is proportional to Rr, and on the dynamic behavior, because Rr is a parameter of its effects. That influence needs to be understood fully and examined for the saturated condition.

- Stator resistance detuning has an effect on the steady state of the field-orientated induction machine. This effect is negligible at high frequency test current. The detuning effect on the stability is still a very important subject to be examined under the saturated condition.

- The problems of using the DSP constraints of using the assembly language led to the use of an on-line system using PC based processor-using RT-Linux. This system can be further improved with high-speed PC processors and using high speed parallel I/O ports for data acquisition and transfers. Improvements to the RT-Linux system can lead to more efficient and fast controllers.

APPENDICES

APPENDIX A

A-1 FLOWCHART OF RT-LINUX WITH INTERRUPT ROUTINE

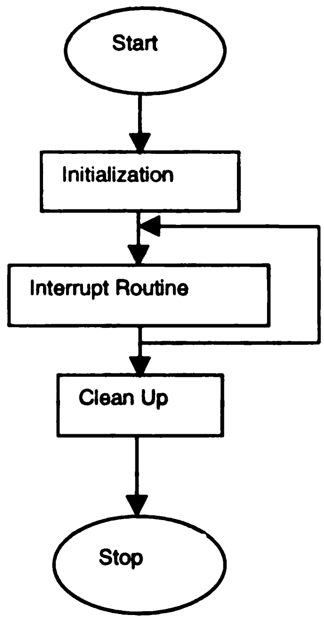

Flowchart of RT-Linux Based System with interrupt routine

A-2 INTERRUPT SERVICE ROUTINE

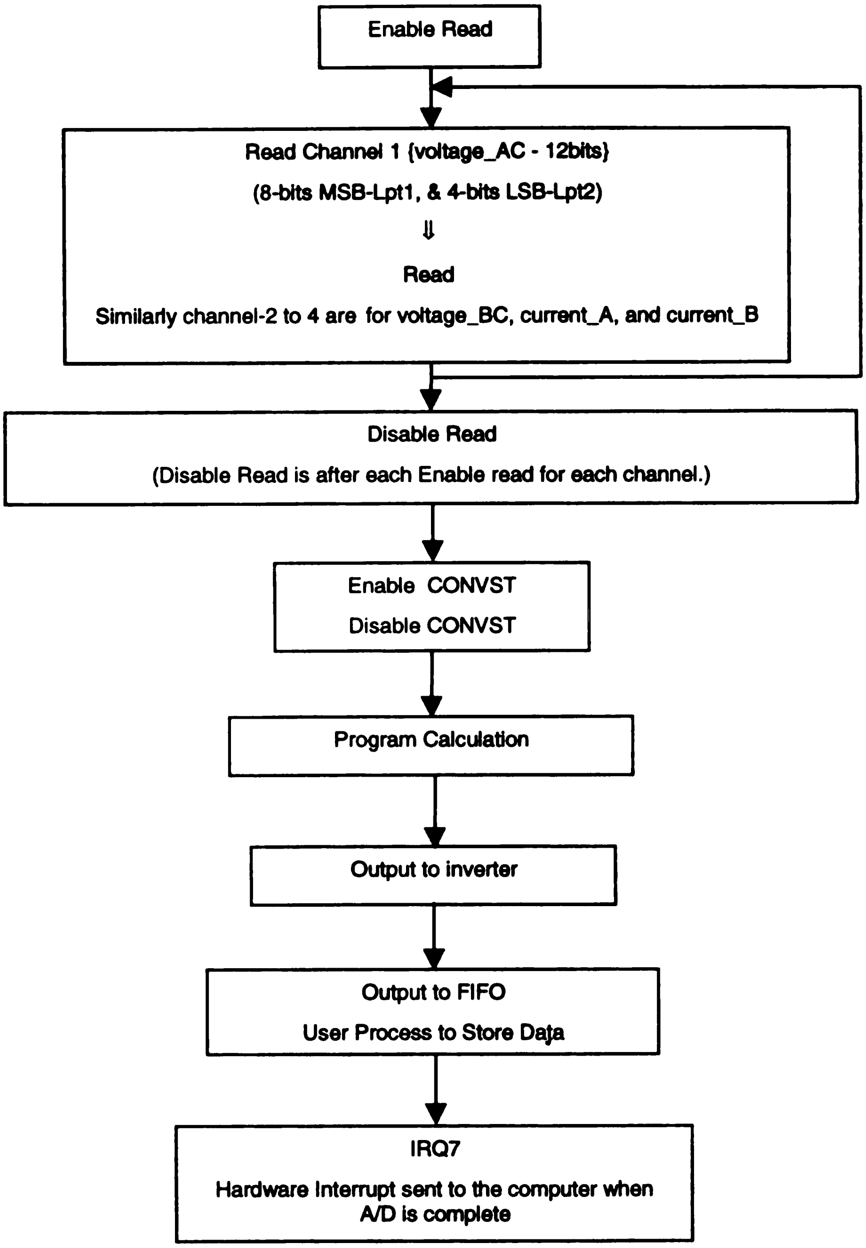

Interrupt service routine

A-3 RT-LINUX INTERRUPT TIMINGS

Table: Breakdown of time spent during one interrupt cycle using A/D converter with RT-Linux

4µs A/D Communication	5.1µs CPU Calculations	1.4µs Inverter Command	29.9µs CPU Free Time
	33.4µs A/D Conversion Time		5µs INT Pulse-width Delay

Total Interrupt Time = 50.4µs

Note: Other minor delays in the A/D are introduced by pulse-width of I/O commands.

APPENDIX B

B-1 RT-LINUX C-LANGUAGE PROGRAM FOR ON LINE SYSTEM

The program is used for the Direct and indirect rotor flux orientation control program and the user data writing program (Appendix B-2). This program compiled by "make" and run by "mods" and stop by "umods" commands.

```
#define MODULE
#define BASE_ADDRESS (127*0x100000)
#include <linux/module.h>
#include <linux/kernel.h>
#include <linux/version.h>
#include <linux/errno.h>
#include <linux/rt_sched.h>
#include <linux/rtf.h>
#include <asm/io.h>
#include <asm/rt_irq.h>
#include <math.h>
#define LPT 0x378
#define LPTS LPT+1
#define LPTC LPT+2
#define LPT2 0x268
#define LPT2S LPT2+1
#define LPT2C LPT2+2
#define LPT3 0x280
#define LPT3S LPT3+1
#define LPT3C LPT3+2
#define LPT4 0x288
#define LPT4S LPT4+1
#define LPT4C LPT4+2
int ;                                  //Define motor int variables constants and parameters
double ;                               //Define motor double variables constants and
parameters
void intr_handler(void)
{
 control=controll0x01;                 // Pulse RD
 outb(control,LPTC);                   // Pulse RD
 current_msb_a=inb(LPT);               // Read 8-bit MSB current_a from LPT
 current_lsb_a=inb(LPT2);              // Read 8-bit LSB current_a from LPT2
 control=control&0xFE;                 // Un-Pulse RD
 outb(control,LPTC);                   // Un-Pulse RD
 control=controll0x01;                 // Pulse RD
 outb(control,LPTC);                   // Pulse RD
 current_msb_b=inb(LPT);               // Read 8-bit MSB current_b from LPT
 current_lsb_b=inb(LPT2);              // Read 8-bit LSB current_b from LPT2
 control=control&0xFE;                 // Un-Pulse RD
```

```
outb(control,LPTC);                   // Un-Pulse RD
control=control|0x01;                  // Pulse RD
outb(control,LPTC);                   // Pulse RD
voltage_msb_a=inb(LPT);               // Read 8-bit MSB voltage_a from LPT
voltage_lsb_a=inb(LPT2);              // Read 8-bit LSB voltage_a from LPT2
control=control&0xFE;                 // Un-Pulse RD
outb(control,LPTC);                   // Un-Pulse RD
control=control|0x01;                 // Pulse RD
outb(control,LPTC);                    // Pulse RD
voltage_msb_b=inb(LPT);               // Read 8-bit MSB voltage_b from LPT
voltage_lsb_b=inb(LPT2);              // Read 8-bit LSB voltage_b from LPT2
control=control&0xFE;                 // Un-Pulse RD
outb(control,LPTC);                   // Un-Pulse RD
control=control|0x02;                 // Enable CONVST
outb(control,LPTC);                   // Enable CONVST
control=control&0xFD;                 // Disable CONVST
outb(control,LPTC);                   // Disable CONVST
ticks=rt_get_time()-zero_ticks;       // Get time in ticks
seconds=(double)ticks/1193180;       // Convert ticks to seconds
// Multiply the current MSB by 16 and add on the least sig. 4 bits of the LSB value
current_dig_a=(16*current_msb_a)+(current_lsb_a&0x0F);
if ((current_dig_a&0x800)==0x800)
current_dig_a=-(current_dig_a^0xFFF)-1;
current_A=( (offset triming factor)*(double)current_dig_a);
current_dig_b=(16*current_msb_b)+(current_lsb_b&0x0F);
if ((current_dig_b&0x800)==0x800)
current_dig_b=-(current_dig_b^0xFFF)-1;
current_B=((offset triming factor)*(double)current_dig_b);

// Multiply the voltage MSB by 16 and add on the least sig. 4 bits of the LSB value
  voltage_dig_a=(16*voltage_msb_a)+(voltage_lsb_a&0x0F);
  if ((voltage_dig_a&0x800)==0x800)
  voltage_dig_a=-(voltage_dig_a^0xFFF)-1;
  voltage_AC=(offset trimming factor)*(double)voltage_dig_a+0.294138077413;
  voltage_dig_b=(16*voltage_msb_b)+(voltage_lsb_b&0x0F);
  if ((voltage_dig_b&0x800)==0x800)
  voltage_dig_b=-(voltage_dig_b^0xFFF)-1;
  voltage_BC=(offset trimming factor)*(double)voltage_dig_b-0.449866251504;

            {      System Equations      }

// Current comparison Hysterisis
  if (current_A>(current_A_ref+band))
    inverter=inverter&0xFE;
  else if (current_A<(current_A_ref-band))
    inverter=inverter|0x01;
  if (current_B>(current_B_ref+band))
    inverter=inverter&0xFD;
  else if (current_B<(current_B_ref-band))
    inverter=inverter|0x02;
  if (current_C>(current_C_ref+band))
   inverter=inverter&0xFB;
```

```
  else if (current_C<(current_C_ref-band))
    inverter=inverter|0x04;
  outb(inverter,LPT3);
// Ten out put data parameters name can be added. This number can be icreased.
  rtf_put(1,&seconds,sizeof(double));              // Push seconds into fifo        // can be used as
standard
  rtf_put(2,&output parameter,sizeof(double));  // Push 12-bitvar_2 into fifo
  rtf_put(3,&output parameter,sizeof(double));  // Push 12-bitvar_3 into fifo
  rtf_put(4,&output parameter,sizeof(double));  // Push 12-bitvar_4 into fifo
  rtf_put(5,&output parameter,sizeof(double));  // Push 12-bitvar_5 into fifo
  rtf_put(6,&output parameter,sizeof(double)) ; // Push 12-bitvar_6 into fifo
  rtf_put(7,&output parameter,sizeof(double));  // Push 12-bitvar_7 into fifo
  rtf_put(8,&output parameter,sizeof(double));  // Push 12-bitvar_8 into fifo
  rtf_put(9,&output parameter,sizeof(double));  // Push 12-bitvar_9 into fifo
  rtf_put(10,&output parameter,sizeof(double)); // Push 12-bitvar_10 into fifo
}
int init_module(void)
{
 rtf_create(1,16*sizeof(double));          // Create fifo for seconds
 rtf_create(2,16*sizeof(double));            // Create fifo for current_a
 rtf_create(3,16*sizeof(double));            // Create fifo for current_b
 rtf_create(4,16*sizeof(double));            // Create fifo for voltage_a
 rtf_create(5,16*sizeof(double));            // Create fifo for voltage_b
 rtf_create(6,16*sizeof(double));            //Create fifo for var_a
 rtf_create(7,16*sizeof(double));            // Create fifo for var_b
 rtf_create(8,16*sizeof(double));            // Create fifo for var_c
 rtf_create(9,16*sizeof(double));            // Create fifo for var_d
 rtf_create(10,16*sizeof(double));           // Create fifo for var_e
 request_RTirq(7, intr_handler);             //Install interrupt handler
 outb(inb(0x21)&(~0x80),0x21);               //irq7 setup: set the mask and read pending irq
 outb(0x20,0x20);
 control=control_default=inb(LPTC);          //Store initial values
 control=control|0x10;                       //Enable irq7
 outb(control,LPTC);                         //Enable irq7
 control=control|0x20;                       //Enable input direction on LPT
 outb(control,LPTC);                         //Enable input direction on LPT
 outb(inb(LPT2C)|0x20,LPT2C);                //Enable input direction on LPT2
 control=control&0xF0;
 outb(control,LPTC);                         //Clear control bits
 for (i=0;i<20000;i++)                       //Reset interrupt bit by pulsing
 {
  control=control|0x01;                      //RD bit
  outb(control,LPTC);                        //RD bit
 }
 for (i=0;i<20000;i++)
 {
  control=control&0xFE;
  outb(control,LPTC);
 }
 control=control|0x02;                       //Enable CONVST
 outb(control,LPTC);                         //Enable CONVST
 control=control&0xFD;                       //Disable CONVST
 outb(control,LPTC);                         //Disable CONVST
 zero_ticks=rt_get_time();                   //Get time in ticks
 return 0;
}
```

```
void cleanup_module(void)
{
 rtf_destroy(10);                    //Destroy fifo
 rtf_destroy(9);                     //Destroy fifo
 rtf_destroy(8);                     //Destroy fifo
 rtf_destroy(7);                     //Destroy fifo
 rtf_destroy(6);                     //Destroy fifo
 rtf_destroy(5);                     //Destroy fifo
 rtf_destroy(4);                     //Destroy fifo
 rtf_destroy(3);                     //Destroy fifo
 rtf_destroy(2);                     // Destroy fifo
 rtf_destroy(1);                     //Destroy fifo
 control=control&(~0x10);            //Disable irq7
 outb(control,LPTC);                 //Disable irq7
 outb(control_default,LPTC);         //Replace initial values
 free_RTirq(7);                      //Uninstall interrupt handler
}
```

B-2 OUTPUT DATA PROGRAME FOR ANALYSIS

user.c – this program is run by typing "user" will prompt for file name. The output data is used for analysis of on line results. In this thesis Matlab is used for analyses of data.

```
#define NUM_SAMPLES 40016
#define MODULE
#define BASE_ADDRESS (127*0x100000)
#include <linux/module.h>
#include <linux/kernel.h>
#include <linux/version.h>
#include <linux/errno.h>
#include <linux/rtf.h>
#include <sys/types.h>
#include <sys/stat.h>
#include <fcntl.h>
#include <unistd.h>
#include <stdio.h>
#include <sys/time.h>
#include <sys/resource.h>
int main(void)
{
  int rt_to_user_1,rt_to_user_2,rt_to_user_3,rt_to_user_4,rt_to_user_5;
  int
rt_to_user_6,rt_to_user_7,rt_to_user_8,rt_to_user_9,rt_to_user_10;
  int i;
  double stor_seconds[NUM_SAMPLES];
  double stor_current_a[NUM_SAMPLES];
  double stor_current_b[NUM_SAMPLES];
  double stor_voltage_a[NUM_SAMPLES];
  double stor_voltage_b[NUM_SAMPLES];
  double stor_var_a[NUM_SAMPLES];
  double stor_var_b[NUM_SAMPLES];
  double stor_var_c[NUM_SAMPLES];
  double stor_var_d[NUM_SAMPLES];
  double stor_var_e[NUM_SAMPLES];
  FILE *fp;
  char datafile_name[20];
  double current_a,current_b,voltage_a,voltage_b,seconds;
  double var_a,var_b,var_c,var_d,var_e;
  setpriority(PRIO_PROCESS,0,-20);          // Increase priority

  // Open fifo
  if ((rt_to_user_1 = open("/dev/rtf1", O_RDONLY)) < 0)
  {
    fprintf(stderr, "Error opening /dev/rtf1\n");
    exit(1);
  }
```

```
// Open fifo
if ((rt_to_user_2 = open("/dev/rtf2", O_RDONLY)) < 0)
{
  fprintf(stderr, "Error opening /dev/rtf2\n");
  exit(1);
}

// Open fifo
if ((rt_to_user_3 = open("/dev/rtf3", O_RDONLY)) < 0)
{
  fprintf(stderr, "Error opening /dev/rtf3\n");
  exit(1);
}

// Open fifo
if ((rt_to_user_4 = open("/dev/rtf4", O_RDONLY)) < 0)
{
  fprintf(stderr, "Error opening /dev/rtf4\n");
  exit(1);
}

// Open fifo
if ((rt_to_user_5 = open("/dev/rtf5", O_RDONLY)) < 0)
{
  fprintf(stderr, "Error opening /dev/rtf5\n");
  exit(1);
}

// Open fifo
if ((rt_to_user_6 = open("/dev/rtf6", O_RDONLY)) < 0)
{
  fprintf(stderr, "Error opening /dev/rtf6\n");
  exit(1);
}

// Open fifo
if ((rt_to_user_7 = open("/dev/rtf7", O_RDONLY)) < 0)
{
  fprintf(stderr, "Error opening /dev/rtf7\n");
  exit(1);
}

// Open fifo
if ((rt_to_user_8 = open("/dev/rtf8", O_RDONLY)) < 0)
{
  fprintf(stderr, "Error opening /dev/rtf8\n");
  exit(1);
}

// Open fifo
if ((rt_to_user_9 = open("/dev/rtf9", O_RDONLY)) < 0)
{
  fprintf(stderr, "Error opening /dev/rtf9\n");
  exit(1);
}
```

```
  // Open fifo
  if ((rt_to_user_10 = open("/dev/rtf10", O_RDONLY)) < 0)
  {
    fprintf(stderr, "Error opening /dev/rtf10\n");
    exit(1);
  }

  for (i=0;i<NUM_SAMPLES;i++)
  {
    // Read seconds from fifo
    while(read(rt_to_user_1,&seconds,sizeof(double))==0);
    stor_seconds[i]=seconds;                // Store seconds in vector
    // Read 12-bit current_a from fifo
    while(read(rt_to_user_2,&current_a,sizeof(double))==0);
    stor_current_a[i]=current_a;            // Store 12-bit current_a
in vector
    // Read 12-bit current_b from fifo
    while(read(rt_to_user_3,&current_b,sizeof(double))==0);
    stor_current_b[i]=current_b;            // Store 12-bit current_b
in vector
    // Read 12-bit voltage_a from fifo
    while(read(rt_to_user_4,&voltage_a,sizeof(double))==0);
    stor_voltage_a[i]=voltage_a;            // Store 12-bit voltage_a
in vector
    // Read 12-bit voltage_b from fifo
    while(read(rt_to_user_5,&voltage_b,sizeof(double))==0);
    stor_voltage_b[i]=voltage_b;            // Store 12-bit voltage_b
in vector
    // Read var_a from fifo
    while(read(rt_to_user_6,&var_a,sizeof(double))==0);
    stor_var_a[i]=var_a;                    // Store var_a in vector
    // Read var_b from fifo
    while(read(rt_to_user_7,&var_b,sizeof(double))==0);
    stor_var_b[i]=var_b;                    // Store var_b in vector
    // Read var_c from fifo
    while(read(rt_to_user_8,&var_c,sizeof(double))==0);
    stor_var_c[i]=var_c;                    // Store var_c in vector
    // Read 12-bit var_d from fifo
    while(read(rt_to_user_9,&var_d,sizeof(double))==0);
    stor_var_d[i]=var_d;                    // Store var_d in vector
    // Read 12-bit var_e from fifo
    while(read(rt_to_user_10,&var_e,sizeof(double))==0);
    stor_var_e[i]=var_e;                    // Store var_e in vector
  }

  close(rt_to_user_10);                     // Close fifo 10
  close(rt_to_user_9);                      // Close fifo 9
  close(rt_to_user_8);                      // Close fifo 8
  close(rt_to_user_7);                      // Close fifo 7
  close(rt_to_user_6);                      // Close fifo 6
  close(rt_to_user_5);                      // Close fifo 5
  close(rt_to_user_4);                      // Close fifo 4
  close(rt_to_user_3);                      // Close fifo 3
  close(rt_to_user_2);                      // Close fifo 2
  close(rt_to_user_1);                      // Close fifo 1

  // Get name for datafile
```

```
  printf("Enter the name for the datafile: ");
  scanf("%s",datafile_name);

  while (fopen(datafile_name,"r")!=NULL)
  {
    printf("Already Exists!  Enter a new name for the datafile: ");
    scanf("%s",datafile_name);
  }

  fp=fopen(datafile_name,"w");              // Open datafile

  // Write seconds, current_a, current_b, voltage_a, var_a, var_b,
var_c, var_d and var_e to file
  for (i=16;i<NUM_SAMPLES;i++)
  {
    seconds=stor_seconds[i];
    current_a=stor_current_a[i];
    current_b=stor_current_b[i];
    voltage_a=stor_voltage_a[i];
    voltage_b=stor_voltage_b[i];
    var_a=stor_var_a[i];
    var_b=stor_var_b[i];
    var_c=stor_var_c[i];
    var_d=stor_var_d[i];
    var_e=stor_var_e[i];

fprintf(fp,"%f\t%f\t%f\t%f\t%f\t%f\t%f\t%f\t%f\t%f\n",seconds,current_a
,current_b,voltage_a,voltage_b,var_a,var_b,var_c,var_d,var_e);
  }

  fclose(fp);                               // Close datafile

  return 0;
}
```

BIBLIOGRAPHY

BIBLIOGRAPHY

[1] P.L. Jansen, R.D. Lorenze. "Accuracy Limitation of velocity and flux estimation in direct field orientated induction machines". *The European Power Electronics Association",* pp. 312-318, 1993

[2] Seog-Joo Kang, Jan-Mok Kim and Seung-ki Sul. " Position Sensorless Control of Synchronous Reluctance Motor Using High Frequency Current Injection", *IEEE Industry Application Society.,* pp. TB1-3.1-3.

[3] F.Blashke, T. Vander Burgt and A. Vandenput. "Sensorless Direct Field Orientation at Zero Flux Frequency, " *Conference. Record IEEE IAS Annual Meeting,* pp. 189-196, 1996.

[4] P.L Jansen, R.D. Lorenz. " Transducer-less Field Orientation Concepts Employing Saturation-Induced Saliencies in Induction Machines". *IEEE Industry Application Society Annual Metting,* pp. 174-181,1995.

[5] Jung-Ik Ha and Seung-ki Sul. " Sensorless Filed Oreinted Control of an Induction Machine by High Frequency Signal Injection". *IEEE Industry Application Society Annual Metting* New Oreleans, Lousiana, October 5-9, 1997" Page 426-432

[6] Peter Vas. " Sensorless Vector And Direct Torque Control ". 1998 *Oxford Science Publication*

[7] P.L Jansen, R.D. Lorenz. " Transducer-less Position and Velocity Estimation in induction and Salient AC Machines.". *IEEE Industry Application Society Annual Metting,* pp. 240-247, 1995

[8] Peter Vas. " Vector Control of AC Machines ". 1990, *Oxford Science Publication.*

[9] Boldea, S.A. Nasar. "Vector Control of AC Drives" 1992, *CRC Press.*

[10] A. Ferraf, K.J. Bradley. .P. J Hogben, M.S. Woolfson and G. M. Asher, "A transputer-based speed identifier for induction motor drives using real-time adaptive filtering," *IEEE IAS Conference. Record,* 1997, pp394-400..

[11] X. Xu and D. W. Novotny. "Implementation of direct stator flux orientation control on a versatile DSP based system," *in proc. IEEE-IAS Annual. Meeting.,* Oct. 1990

[12] B. Aloliwi, H.K Khalil, E.G Strangas. "Robust speed controller of induction motors " *In Proc. American Control Conference.,* Albuquerque, NM, June 1997. WP16:4

[13] H.K Khalil and E.G Strangas. "A robust speed controller of induction motors using position and current measurement." *IEEE Transaction Automatic Control.,* 41:1216-1220, 1996

[14] H.K Khalil and E.G Strangas. " A Speed Control of Induction Motors Using Adaptive Observer " A*CC* ,1998.

[15] Riccardo Marino, Segei Peresada, and Paolo Valigi. "Adaptive input-output linearizing control of induction motors"., *IEEE Transactions on Automatic Control,* 38(2): 208-221, February 1993.

[16] Luenberger, D.G. "An introduction to observers", *IEEE-Transaction on Automatic Control 16,* 1971, pp.596-602.

17 Kim, Y.R., Sul, S.k., and Park, M.H. "Speed Sensorless vector control of Induction Motor Using Extended Kalman Filter", *Proceedings . IEEE-IAS Annual Meeting,* 1992,pp.594-599.

[18] Ferra,A., Bradley, K.J., and Asher, G.M. "Sensor-Less Speed detection of inverter fed Induction Motor using rotor slots harmonics and Fast Fourier transformation",. *Proceedings IEEE-PES Meeting,* 1992, pp.279-86.

[19] Hurst, K.D., Habetler, T. G., Griva, G., and Profumo, F. " Speed sensorless field oriented control of induction machines using current harmonics spectral estimation." *IEEE-IAS Annual Meeting,* 1994, pp.601-7

[20] M. Ishida and K. Iwata. " a new slip frequency detector of an induction motor utilizing motor slot harmonics," *IEEE Trans. Indusrtial . Applications.* Vol. IA-20, No. 3, pp. 575-582, 1984..

[21] Zinger, D.S., Lipo, T.A., and Novotony, D.W. "Using Induction Motor Stator Windings to Extract Speed Information", *Proceedings IEEE-IAS Annual Meeting,* 1989, pp.213-218

[22] Cuzner, R., Lorenz, R.D., and Novotony, D.W. "Application of Non-Linear Observer for Rotor Position Detection on an Induction Motor Using the Machines Voltage and Current", *Proceedings IEEE-IAS Annual Meeting,* 1990, pp.416-421.

[23] Robert T. Novotnak, John Chiasson, and Marc Bodson. " High performance Motion Control of an Induction Motor with Magnetic Saturation;. *IEEE proc. of the 34th Conference on Decision & Control,* New Orleans, LA. Dec. 1995.

[24] Kreindler, L., Moreira, J. C., Testa, A., and Lipo, T. A. "Direct Field orientation controller using the stator phase voltage third harmonics", *Proceedings IEEE-IAS Annual Meeting,* 1994, pp.441-7.

[25] Paul C. Krause. " Analysis of Electric Machinery " *IEEE Press,*1995

[26] J. Robert, D.K. Tran. " Modelling and Simulation of Electrical Machines and Power Systems " *Proceedings of the Second International Symposium on Modeling and Simulation of Electrical Machines and Power Systems,* Quebec, Canada, 24-25 August, 1987.

[27] J.A.A. Melkebeek, Dr. Ir. " Magnetizing-field saturation and dynamic behavior of induction machines part 1: Improved calculation method for induction-machine dynamics " *IEE Proc. Vol.130, Pt B,* No, 1, pp. 1-9,January 1983.